Kiel University

Faculty of Computer Science

The application of agent-based modeling and fuzzy-logic controllers for the study of magnesium biomaterials

DISSERTATION

submitted to obtain the degree of

DOCTOR OF ENGINEERING (DR.-ING.)

Author:

Jalil Nourisa

From:

Iran

Supervisor:

Prof. Dr.-Ing. Sven Tomforde

Hamburg 2023

Examination:

The defense was held at the Institute of Informatics, Kiel University, on Monday, September 11, 2023, at 14:00.

Chair: Prof. Dirk Nowotka

Supervisor: Prof. Sven Tomforde

Examiners:

- Prof. Regine Willumeit-Römer
- Prof. Ralf Krestel

Declaration and Submission of Doctoral Thesis

I hereby confirm that, apart from my supervisor's guidance, the content and design of the thesis are entirely my own work. The research was conducted using only the sources listed in the bibliography, and all external materials have been properly cited and acknowledged. I declare that the submitted thesis has not been previously submitted either partially or wholly as part of a doctoral examination procedure to another examining body. Furthermore, the thesis has not been published or submitted for publication elsewhere. I affirm that the thesis has been prepared in compliance with the Rules of Good Scientific Practice of the German Research Foundation. All research and writing were conducted ethically, and the principles of integrity, honesty, and objectivity were maintained throughout the study. I confirm that no academic degree has ever been withdrawn from me.

Jalil Nourisa

Hamburg,

20/4/2023

Abstract

Agent-based modeling (ABM) is a powerful approach for studying complex systems and their underlying properties by explicitly modeling the actions and interactions of individual agents. This approach has been widely adopted in computational biology for modeling cellular systems, where agents are represented as cells. To simulate agents' responses to micro-environmental signals, various algorithms have been employed in ABM, including fuzzy-logic controllers (FLCs). FLCs offer a particularly appealing solution in computational biology due to their use of simple language in their formulation, which allows for the participation of domain experts in the model-building process. Furthermore, FLCs enable the creation of models using qualitative information, which is appropriate for the type of data commonly available in biological systems.

Over the past decade, numerous software programs have been developed to address the needs of the agent-based modeling (ABM) community. However, these solutions often suffer from limitations in design, a lack of comprehensive documentation, or poor performance. To tackle these issues, we introduce CppyABM - a general-purpose software for ABM that aims to enhance current state-of-the-art techniques. CppyABM provides well-documented simulation tools that are available in both Python and C++, allowing users to choose the programming language best suited to their background and simulation needs. Additionally, CppyABM enables ABM development using a combination of C++ and Python, taking advantage of the computational performance of C++ and the data analysis and visualization tools of Python. We demonstrate the capabilities of CppyABM through its application to various problems in ecology, virology, and computational biology. Our performance comparison shows that CppyABM is suitable for ABM requirements with different natures, and that using C++ or a combination of languages provides significant performance improvements compared to using Python alone.

In this thesie, we utilize CppyABM to explore the impact of magnesium (Mg^{2+}) ions on osteogenesis, a crucial process in bone tissue regeneration. Mg-based materials have emerged as the next generation of biomaterials that degrade in the body after implantation and eliminate the need for secondary surgery. The degradation products of these materials, such as Mg^{2+} ions, are bioactive and have been shown to stimulate various biological processes, including osteogenesis. To capture the behavior of mesenchymal stem cells (MSCs) in response to Mg^{2+} ions and other important signals such as growth factors and cytokines, we employ Fuzzy-Logic Controllers (FLCs) as the key components of our ABM. Our FLCs are based on qualitative and quantitative information from over 50 scientific reports, and incorporate fuzzy rules that describe the behavior of MSCs under varying levels of stimulatory signals. We calibrate our ABM using empirical data obtained from multiple cell culture experiments. The results show that the optimal concentration of Mg^{2+} ions for osteogenesis is between 3-6 mM to maximize the MSC population, and between 6-8 mM to drive MSC differentiation towards the osteoblast lineage. Furthermore, the model provides insight into the potential causes of discrepancies in

empirical findings, such as varying sensitivity of cells to stimulatory signals in different experiments.

In conclusion, this dissertation has made significant contributions to the field of systems biology from a computer science perspective. Specifically, it has introduced CppyABM as a novel agent-based modeling software that surpasses existing solutions in terms of functionality and versatility. Additionally, it has presented a holistic approach to computational biomodeling by combining fuzzy logic controllers and ABM to simulate complex biological systems that are influenced by multiple factors. Lastly, this dissertation has provided valuable insights into the biological role of magnesium ions in promoting osteogenesis through the use of this integrated approach, thus advancing our understanding of Mg-based biomaterials.

Zusammenfassung

Die agentenbasierte Modellierung (ABM) ist ein leistungsfähiger Ansatz zur Untersuchung komplexer Systeme und der ihnen zugrundeliegenden Eigenschaften, durch die explizite Modellierung der Aktionen und Interaktionen einzelner Agenten. Dieser Ansatz ist in der Computerbiologie zur Modellierung zellulärer Systeme, bei denen die Zellen als Agenten als dargestellt werden, weit verbreitet. Zur Simulation der Reaktionen von Agenten auf kleinste Umgebungssignale wurden in ABM verschiedene Algorithmen eingesetzt, darunter auch Fuzzy-Logic-Controller (FLC). FLCs bieten eine besonders attraktive Lösung für die Computerbiologie, da sie eine einfache Sprache für ihre Formulierung verwenden, was die Beteiligung von Biologieexperten an der Modellerstellung ermöglicht. Darüber hinaus ermöglichen FLCs die Erstellung von Modellen unter Verwendung qualitativer Informationen, was für die Art von Daten, die in biologischen Systemen üblicherweise verfügbar sind, angemessen ist.

In den letzten zehn Jahren wurden zahlreiche Softwareprogramme entwickelt, um den Anforderungen der agentenbasierten Modellierung (ABM) gerecht zu werden. Diese Lösungen leiden jedoch oft unter Einschränkungen im Design, einem Mangel an umfassender Dokumentation oder schlechter Leistungsfähigkeit. Um diese Probleme zu beheben, haben wir CppyABM eingeführt. Dies ist eine Allzweck-Software für ABM, die darauf abzielt, den Stand der Technik zu verbessern. CppyABM bietet gut dokumentierte Simulationswerkzeuge, die sowohl in Python als auch in C++ verfügbar sind, sodass die Benutzer die Programmiersprache wählen können, die am besten zu ihrem Hintergrund und ihren Simulationsanforderungen passt. Darüber hinaus ermöglicht CppyABM die Entwicklung von ABM in einer Kombination aus C++ und Python, wobei die Vorteile der Rechenleistung von C++ und der Datenanalyse- und Visualisierungswerkzeuge von Python genutzt werden. Wir demonstrieren die Fähigkeiten von CppyABM in der Anwendung auf verschiedene Probleme der Ökologie, Virologie und Computerbiologie. Unser Leistungsvergleich zeigt, dass CppyABM für ABM-Anforderungen unterschiedlicher Art geeignet ist und dass die Verwendung von C++ oder einer Kombination der Programmiersprachen im Vergleich zur alleinigen Verwendung von Python erhebliche Leistungsverbesserungen bietet.

Wir verwenden dann CppyABM, um die Auswirkungen von Magnesium (Mg^{2+})-Ionen auf die Osteogenese zu untersuchen, einen entscheidenden Prozess in der Regeneration von Knochengewebe. Materialien auf Basis von Magnesium haben sich als die nächste Generation von Biomaterialien herauskristallisiert, da sie sich nach der Implantation im Körper abbauen und eine zweite Operation überflüssig machen. Die Abbauprodukte dieser Materialien, wie beispielsweise Mg^{2+}-Ionen, sind bioaktiv und stimulieren nachweislich verschiedene biologische Prozesse, einschließlich der Osteogenese. Um das Verhalten von mesenchymalen Stammzellen (MSCs) als Reaktion auf Mg^{2+}-Ionen und andere wichtige Signale wie Wachstumsfaktoren und Zytokine zu erfassen, setzen wir FLCs als Schlüsselkomponenten unseres ABM ein. Unsere FLCs basieren auf qualitativen und quantitativen Informationen aus über 50 wissenschaftlichen Artikeln und enthalten Fuzzy-Regeln, die das Verhalten von MSC

für unterschiedliche Mengen an stimulierenden Signalen beschreiben. Wir kalibrieren unser ABM anhand empirischer Daten, die wir aus mehreren publizierten Zellkulturexperimenten gewonnen haben. Die Ergebnisse zeigen, dass die optimale Konzentration von Mg^{2+}-Ionen für die Osteogenese zwischen 3-6 mM liegt, um die MSC-Population zu maximieren, und zwischen 6-8 mM, um die MSC-Differenzierung in Richtung der Osteoblasten-Linie zu fördern. Darüber hinaus gibt das Modell Aufschluss über die möglichen Ursachen für Diskrepanzen in den empirischen Ergebnissen, wie z. B. die unterschiedliche Empfindlichkeit der Zellen auf stimulierende Signale in verschiedenen Experimenten.

Zusammenfassend lässt sich sagen, dass diese Dissertation einen bedeutenden Beitrag zum Gebiet der Systembiologie aus Sicht der Informatik geleistet hat. Insbesondere wurde mit CppyABM eine neuartige agentenbasierte Modellierungssoftware vorgestellt, die bestehende Lösungen in Bezug auf Funktionalität und Vielseitigkeit übertrifft. Außerdem wurde ein ganzheitlicher Ansatz für die computergestützte Biomodellierung vorgestellt, der Fuzzy-Logik-Controller und ABM kombiniert, um komplexe biologische Systeme zu simulieren, die von mehreren Faktoren beeinflusst werden. Schließlich hat diese Dissertation durch den Einsatz dieses integrierten Ansatzes wertvolle Einblicke in die biologische Rolle von Magnesiumionen bei der Unterstützung der Osteogenese geliefert und damit unser Verständnis von Mg-basierten Biomaterialien verbessert.

Content

Part I. Fundamentals

I.1. Introduction

Biological systems, including bone tissue repair, are inherently multiscale in time and dimension [1]. Biological tissues have hierarchical structures linking nanometers to centimeters [2]. Intracellular interactions of molecules on the scale of nanometers give rise to cellular response on micrometers [2]. Cellular responses in return form the shape and function of an organ [2]. Conversely, the conditions experienced on the tissue, such as mechanical load, are transmitted to cell and subcellular processes to guide cellular activities [1]. Defining experimental setups to capture the complexity of the biological processes occurring in multiple dimensional and temporal scales is impractical due to the measurement and cost limitations. Meanwhile, computational tools are able to provide quantitative information across multiple scales and capture key biological features at the population level, i.e. macroscale [3], [4]. To this end, the information obtained from different experiments is integrated in one platform and used to predict the system's response. Such platform can be utilized to investigate the underlying system by replicating the empirical observations or foreseeing the unseen experiments [5]. Computer models can assist in the investigation of the cellular mechanisms [6] or conducting *in silico* experiments to guide the design of biomaterials or drugs [7].

The choice of numerical techniques generally depends on the problem at hand, target measurements, availability of the empirical data, and the randomness in the system [8]. Amongst them, agent-based modeling (ABM) has gained special popularity in the simulation of heterogeneous systems with a focus on cellular behavior [9]–[11]. ABMs are bottom-up approaches where cells as agents interact with one another and with the environment, producing various behaviors such as cell migration, proliferation, and phenotypic change to other cells. The outcomes of ABM can be measured both on the single-cell scale as well as cumulatively at the population level. Detailed information regarding ABM is given in Section II.1.1. A crucial step in the modeling of cellular mechanisms is defining the algorithm that maps the cellular inputs to the cellular outputs [4], [12]. Different methods have been used in the literature for this purpose (see Section II.1.2). Amongst them, fuzzy logic controller (FLC) is an attractive approach for this purpose due to multiple reasons. FLC uses plain language in the formulation of the system, which enables model tractability as well as the contribution of the domain experts in model development [13]–[15]. In addition, FLC can define a system with qualitative information. This suits the nature of biological systems as quantitative information is scarce.

Osteogenesis is the key process in bone repair and revolves around three major cellular activities [16]–[18]. First, mesenchymal stem cells (MSCs) proliferation to increase the cell population. Second, MSCs commitment to osteoblastic lineage to produce bone cells. Third, bone cells activities to assure sufficient generation bone tissue (see Figure II-3 and Section II.2.1). Numerous factors can regulate these processes and determine the quality of bone healing process [17], [18]. Growth factors are amongst the most determinant factors [17], [18].

Throughout the healing, multiple cells produce growth factors to regulate themselves (paracrine effect) and other processes (autocrine) [16]. Inflammatory cells and, more importantly, macrophages are the significant contributors to this process [19]–[21]. The productions of macrophages such as tumor growth factor (TGF)-beta, bone morphological proteins (BMP), and different interleukins (IL) are the key regulators of osteogenesis [22]–[25]. More information regarding the regulators of osteogenesis is provided in Section II.2.2.

Magnesium (Mg)-based biomaterials are attractive choices in the orthopedic industry due to their multiple advantages over conventional metallic materials such as titanium [26][27]. Mg-based materials degrade in contact with body fluids, resulting in the resorption of the implant over time [26][28]. This mitigates the necessity for a second surgery for implant removal, saving cost and pain. Mg-based materials also offer superior physical properties compared to conventional metallic materials in terms of matching the physical properties of the local bone tissue [27]. In addition, the Mg degradation products such as Mg^{2+} ions are bioactive and can promote the tissue regeneration process [29]. More information regarding bone implants and Mg-based biomaterials is given in Section II.2.3.

Mg^{2+} ions are repeatedly shown to modulate a wide range of physiological activities, notably osteogenesis [27]. The bioregulatory effect of Mg^{2+} ions on osteogenesis can be evaluated in two main aspects. A direct influence by activating multiple signaling pathways of MSC [30]. And, an indirect influence by modulating macrophage productions, which in return influences MSC activities [30]. Multiple *in vitro* studies have reported the stimulatory role of Mg^{2+} ions on cellular metabolism and growth, resulting in a larger cell population [20], [31]. In addition, Mg^{2+} ions are shown to stimulate several signaling pathways associated with the osteoblastic differentiation of MSCs [27], [30] Different cell culture experiments have reported the stimulatory role of Mg^{2+} ions on osteoblastic differentiation, especially in the early differentiation process [29]. These observations signify the direct role of Mg^{2+} ions in MSCs activities through the engagement in metabolic activities as well as molecular signaling. The bioregulatory importance of Mg^{2+} ions in osteogenesis is further explained in Section II.2.4.

Although there is a general agreement over the osteoinductive properties of Mg^{2+} ions, several studies have shown their destructive effects on tissue regeneration [26], [32]. Fast degradation of Mg-based implants can release a high concentration of Mg^{2+} ions and results in a high alkaline condition, which can interfere with the natural process of bone repair [33]. A high concentration of Mg^{2+} ions, even in a controlled pH environment, has shown detrimental effects on various physiological processes such as cell viability and proliferation [34]. Furthermore, there are reports on the negative role of Mg^{2+} ions in the late stage of osteoblastic differentiation even in low concentrations [34]. These observations show the complex effects of Mg^{2+} ions on osteogenesis based on the applied dosage and the timing of the process. It is, therefore, paramount to thoroughly characterize the biological responses associated with the degradation products, particularly Mg^{2+} ions, before the clinical application of Mg as a bone implant.

So far, only experimental studies have evaluated the biological response of Mg-based materials. Empirical approaches can be expensive, pose ethical problems, and prolong the required

investigation time [35]. Even more so considering numerous candidate alloys for Mg biomaterials and the scores of biological reactions involved in the healing process [26], [32]. In addition, the inherent problems associated with the empirical approaches, such as noisy measurements or heterogeneous cellular response, can cause conflicting observations [36]. Computer models have shown significant capacity in assisting the characterization of biological systems [37]–[39]. They can formalize the current knowledge, objectively evaluate it against empirical observations, test new hypotheses, and foresee future experiments [37]–[39]. Several numerical approaches have been utilized in the study of biological characterization [40]–[42]. Amongst the simulation approaches, ABM and FLCs have been widely employed in the study of cellular mechanisms and biomaterials [43]–[46]. In the following, we provide several examples of the application of ABM and FLCs in biological systems.

Bayrak et al. [41] developed an ABM to study the effects of growth factors on MSCs cultured in biomaterial scaffold [41]. They showed that growth factors such as vascular endothelial growth factor (VEGF) and BMP-2 are crucial for cell survival and differentiation [41]. Kuehn and Checa [47] used ABM to quantitatively simulate the interaction of VEGFR1 and VEGFR2, as two receptors of VEGF-A. These receptors and their interaction are associated with the process of tip selection and sprouting during angiogenesis [47]. Their results showed the importance of VEGF-A receptors in the process of angiogenesis [47]. Lambert et al. [48] used ABM in the study of kidney uretic branching with a focus on the interactions of endothelial cells (ECs) and MSCs. They simulated early epithelial cell growth and branching as a switch-like mechanism regulated by growth factors [48]. They showed that cell division only occurs when the applied growth factors exceed a certain threshold [48]. Their findings indicate the crucial role of growth factors in cellular growth [48]. Ross et al. [10] used ABM to study cellular migration and the importance of cell-cell interaction in the population-level pattern development. They showed the importance of cell-cell interactions such as blind agent interaction (cells do not perceive surroundings) and adhesive/repulsive agent interactions (cells do perceive surroundings) on the pattern formation [10]. Aldridge et al [44] simulated intracellular pathways of human colon carcinoma cells using FLC. By association of the intracellular pathways with growth factors and insulin receptors, they successfully predicted pathways crosstalk and regulation and shed light on an unknown relationship between MK2 and ERK pathways [44]. Wang et al [49] and Niemeyer et al [50] used FLC to model the generation of different tissues during bone healing proccess. They have successfully demonstrated the impact of various mechanical environments on the patterns of bone tissue regeneration [49], [50].

Numerous software are available in the literature for ABM with different specialties, user experience, and processing capabilities [51], [52]. These software have been used for the simulation of real-world problems in different scientific domains [53], [54]. However, they still have several limitations such as being overly complex, lacking proper documentation, and inherent limitations in the design [51], [52]. A complete overview of ABM software with their capabilities and limitations can be found in [51], [52], [55], [56]. In ABM, rapid prototyping and the computational efficiency are two crucial factors. The former enables an early experimentation of the proposed model without dealing with the unnecessary complexities. The

latter assures the possibility of a large-scale real-world simulation. The current ABM libraries in the literature are either too complex for prototyping or lack the scalability features. To this end, Python as a programming language is a viable candidate with features such as ease-of-use and rich data analysis and visualization tools. However, current ABM libraries that provide the simulation tools in Python are limited in the design and cannot address the broad of ABM requirements, including those of this thesis. In addition, Python is less efficient in computational aspects, which hinders a large-scale simulation. Contrarily, C++ is computationally efficient and suitable for large scale models, but is too complex for prototyping. Therefore, a new ABM software is required to address the limitations of the current libraries.

I.2. Problem statement

The first goal of this thesis is to present a novel ABM platform to provide essential tools for the simulation of the target physiological processes associated with Mg biomaterials. This simulation platform, termed CppyABM, aims at improving on the state-of-the-art ABM software in multiple aspects. Notably, it aims at combining the power of C++ and Python in a single platform. CppyABM is an open-source project to ease model development for similar applications.

The second goal of this thesis is to employ different techniques to numerically study the bioregulatory effects of Mg^{2+} ions on osteogenesis. We address this goal in two steps. In the first step, by using CppyABM, we develop an ABM to simulate the MSCs cellular reactions of migration, mitosis, differentiation, and cellular death. In this model, the bio-regulatory effect Mg^{2+} ions together with pH, TGF-b, and BMP-2 are modeled. A fuzzy-logic controller is developed to simulate the decision-making center of cells and map the cellular inputs to outputs. Three sets of in-vitro cell culture experiments were used for the model calibration. These experiments report MSCs proliferation, mortality, and osteoblastic differentiation in response to different concentrations of Mg^{2+} ions.

In the second step, the previously proposed fuzzy-logic model is extended to study the process of osteoblastic differentiation in more detail. This study improves the previous model in three major aspects. Firstly, the non-linearity in the bioregulatory role of Mg^{2+} ions on osteogenesis is simulated in more detail. In addition, the regulatory effects of several inflammatory cytokines are included in the osteogenesis process in tandem with Mg^{2+} ions. Thus, the updated model represents the healing condition more accurately as the inflammatory cytokines are crucial players in the osteogenesis process. Moreover, five sets of cell culture data were used for model evaluation. These experiments are specifically focused on MSCs osteogenic activities and have reported multiple markers for early and late differentiation processes.

The computational platform proposed in this thesis facilitates the biological characterization of Mg-based implants, which is instrumental in safely commercializing these implants. The proposed computer models in this thesis shed light on the osteogenic response to Mg^{2+} ions. Considering that osteogenesis is the principal process during bone tissue regeneration, and Mg^{2+} ions are the primary productions of Mg-based implants' degradation, the contribution of this

study is significant. The findings of this study recommends the safe dosages of Mg^{2+} ions to optimize osteogenesis through the crucial cellular processes of MSC proliferation and osteogenic differentiation. Therefore, these findings can guide the design of future Mg-based implants and their degradation properties in order to optimize the outcome of bone healing response.

I.3. Organization of the thesis

The present document is a cumulative doctoral thesis and is organized as follows. In Part II, a general introduction into the relevant topics is provided. This includes an introduction to agent-based modeling, fuzzy logic controllers, and the biological processes targeted in this thesis such as osteogenesis process. In Part III, the publications generated in the scope of this thesis are presented, which are:

- Nourisa J, Zeller-Plumhoff B, Willumeit-Römer R. CppyABM: An open-source agent-based modeling library to integrate C++ and Python. Software: Practice and Experience. 2022. 52(6). 1337-51. DOI: 10.1002/spe.3067.
- Nourisa J, Zeller-Plumhoff B, Helmholz H, Luthringer-Feyerabend B, Ivannikov V, Willumeit-Römer R. Magnesium ions regulate mesenchymal stem cells population and osteogenic differentiation: A fuzzy agent-based modeling approach. Computational and structural biotechnology journal. 2021. 19. 4110-22. DOI: 10.1016/j.csbj.2021.07.005.
- Nourisa J, Zeller-Plumhoff B, Willumeit-Römer R. The osteogenetic activities of mesenchymal stem cells in response to Mg^{2+} ions and inflammatory cytokines: a numerical approach using fuzzy logic controllers. PLoS computational biology. 2022. 18(9). e1010482. DOI: 10.1371/journal.pcbi.1010482.

In Part IV, the main findings of the publications are restated, and the prospective view on the future work is given.

Part II. Theoretical Background

In this section, the important concepts used throughout the thesis are explained in two sections. First, an introduction to the concept of computational bio-modeling is given, with detailed explanation on ABMs and FLCs. After, an introduction to the topics related to the biological aspects of this thesis is provided such as the process of osteogenesis, Mg-based biomaterials, and the important regulatory factors.

II.1. Computational bio-modeling

Computational bio-modeling aims at understanding how cells and organism develop, function, and survive by employing computer simulations of biological systems. Mechanistic modeling is a subcategory of this field that aims at mechanistically simulating individual processes involved in the system's behavior [57], [58]. Continuum simulation and ABM are two approaches widely used for mechanistic modeling [57], [59]. In the continuum approach, the characteristics of the system are simulated as field variables, where a set of equations describe the aggregated behavior of the system in the course of time and space [59], [60]. For instance, the concentration of cells is simulated by partial differential equations, where different cellular activities such as cell migration, proliferation, and death are simulated by the evolution of cell density across the simulation domain over time [61]. Similarly, the formation of different tissue types, e.g. cartilage or bone tissue, are simulated by field variables, where their density changes depending on local cell activities. For instance, Jin et al [62] used a set of differential equations to describe the evolution of cell population in a scratch assay (a cell culture with an scratch in the middle, where the cells migrate the vacant area from surroundings). This simulation accounts for cell migration and proliferation by evolving the cell density in the course of time and dimension. They reported that logistic functions could correctly describe cell population growth in a scratch assay [62]. Although this approach is generally simpler to implement and requires lesser computation costs, the simulation of noise and heterogeneity in the system is impractical. ABM mitigates these issues by explicitly accounting for agents interactions. In the next section, ABM is explained in detail. Then, the algorithms used as decision-making center of ABM are elaborated with an attention to FLCs.

II.1.1. Agent-based modeling

ABM is a subcategory of agent-based computing and artificial intelligence with the aim of understanding emergent phenomena associated with complex adaptive systems [63], [64]. In ABM, the agent can take on various roles according to different applications; a car in city traffic, a human in social system, or a cell in biological environment are different forms of agents in ABM [57]. ABM differs from multi-agent systems (MAS) (another category of agent-based computing) as MAS mainly focuses on designing complex communication systems between agents, while ABM set rules and simpler communication protocols [64][65]. However, the distinguishing line between them has become blurred in the recent decade as many studies use

them interchangeably [65][56]. ABM is also referred by different keywords such as individual-based modeling or cell-based modeling, which are similar but somewhat different domains in agent-based computing [65].

ABM is a bottom-up computational approach to understand the system's behavior that emerges from the aggregation of individual agents' activities [66]. In contrary to most computational approaches that describe macroscale behavior of a system in equilibrium, ABM aims in describing the system in micro level by employing simple rules for agents [67]. This, nonetheless, is capable of describing complex phenomena emerging in macroscale and is repeatedly shown to be practical for real world problems [67]–[69] One of the earliest implementation of ABM was in Thomas Schelling's segregation model published in 1971 [70]. The basic concepts of ABM were successfully implemented in this model, where the interaction of independent agents in a shared environment resulted in observable emergent outcomes. More recently, a notable use case of ABM in addressing complex problems is in the domain of epidemiology to simulate the spread of COVID-19. Numerous studies have employed ABM to simulate the spread of this virus in response to different measurements and treatment protocols in order to inform public decisions for societies [71], [72]. ABM has found parallel applications in various disciplines such as biology and medicine, physics and chemistry, security, social and economic modeling, and supply network and transport optimization [66].

Object-oriented programming (OOP) is widely used to encapsulate agents' behavior in ABM [73]. In OOP, the static properties of objects are stored as object's data, i.e. fields, while functions define the procedure for objects behavior. According to the object's state, the defined procedure (methods) can update the object's attributes [74]. Different approaches are employed for OOP, notably defining classes to specify objects [74]. To this end, different classes can be defined to characterize different objects. Since agents are self-directed entities with the abilities to act autonomously, the use of class to describe agent is natural [75]. To this end, most of ABM software have adopted the concept of OOP is their design using different programming languages such as C++, Java, and Python [51], [52], [73].

ABM has been given an especial attention in systems biology [76], where agents represent cells, interacting with one another and with the environment. Cells in this approach receive mechanical and biochemical signals from their individual micro neighborhood and produce activities based on the defined algorithm. Cellular activities can contain various forms such as migration, proliferation, secretion of growth factors, and apoptosis/necrosis as different forms of cell death (see Figure II-1). The productions of individual cells are then aggregated in the system level, which can be evaluated against experiments. In ABM, uncertainty such as noise and randomness can be embedded in the cellular level, to give rise to heterogeneity in the system level [67], [68].

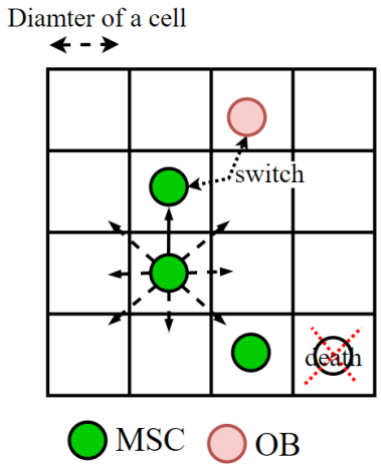

Figure II-1. In on-lattice ABM, cells are located inside the grids across the domain. They can migrate by moving to neighbor grids, differentiate to other cells by switching type, or undergo death by deactivation or disappearance from the domain.

ABM is multiscale by nature as entities operate in cell level with seconds or hours as timescale, while the outputs are aggregated in tissue level in hours or days [62], [68]. ABM can also be combined with other models in different scales to further address the multiscale nature of biological system. For instance, the integration of ABM with reaction-diffusion models of growth factors can increase the time resolution of the model in capturing the dynamics of the proteins down to milliseconds [77][78]. Cell models can also be integrated with continuum models such as finite-element models to take into account the factor of mechanical signals originated from tissue-level load bearing [61][49]. Moreover, in order to bridge the intracellular and the tissue scale together, ABM can be combined with the dynamical chemical models, which simulate intracellular processes [79]. These models explicitly simulate signaling pathways and interacting molecules, which offers a higher complexity and resolution to cellular responses [79].

ABMs are generally classified into two categories of on-lattice and off-lattice [80]. In the former, the simulation space is discretized into grids (also known as patches), where the movement and the interaction of agents are limited to the grids (see Figure II-1), while in the latter, the space is continuous with cells moving and interacting freely in the domain [81]. On-lattice approach has also its own subcategories depending on the specialty of the simulation [82]; for instance, the occupancy of a grid can be limited to one agent or more; or one agent can occupy one or multiple grids. On-lattice approach can be even simplified into the assumption that agents do not move and only interact with the environment. For instance, a specific quantity defined on a mesh can change depending on certain features of neighbor meshes. This method is called cellular automata and is widely used in pattern formation and game theories such as the famous Conway's game of life [4], [83].

On-lattice approach offers lesser complexity and computational costs compared to off-lattice method [84], [85]. However, they have several disadvantageous. Notably, the on-lattice approach assumes a spherical shape for cells, while in reality, cells can take on an elongated shape. Thus, direct comparison of the simulation to the experiments might face challenges,

especially for the models with a focus on the migration process. In addition, cell adhesion and repulsion are challenging to model in on-lattice approaches, as they require interfacial tension and internal pressure [84]–[86] Therefore, the choice of the model for a specific problem is a trade-off between ease of use, realistic outcomes, and computational efficiency. An extensive review of different ABM techniques can be found in [85].

The concept of time in ABM is simulated using discrete evolution of the system by an iterative approach [87]. At each iteration, the formulated equations and algorithm are executed, and the system is updated according to the outputs before running the next step. The choice of the time step heavily depends on the simulation target and the computational costs [85]. The time step is ideally chosen to capture the fastest biological process occurring in the system. For instance, to study cell proliferation, an ideal time step can be one day, while for cell migration, a fraction of a day is required to capture the details sufficiently [88]. Meantime, a smaller time step demands higher computations. Therefore, a trade-off between accuracy and computational feasibility determines time step [87], [88]

A large number ABM software have been developed in the last few decades [52], [89]. These software can be generally divided into two subcategories; those based on domain-specific languages (DSLs) [55], [89], [90]; and those based on public programming languages [8], [91]. The former ease the model development by providing a clear, high-level, and easy-to-read syntax, designed for specific applications. However, they are limited in multiple aspects. For instance, the integration of third-party libraries and frameworks is not practical [92]. Also, they have the disadvantage of learning a new scripting language. Arguably, Netlogo [90] is the most famous ABM software using DSLs, which has been widely used in numerous real word problems across multiple scientific domains [93], [93]. On the contrary, ABM libraries based on public programming languages are open-source and can mitigate the aforementioned problems. These libraries offer tools and functionalities that can be used or tailored based on the specialty of an ABM. Amongst the successful open-source ABM libraries are Mason [94] and Repast [91]. The major problem with these platforms is the complexity in the programming language or the design of ABM as well as the lack of sufficient documentation [92]. C++ and Java are widely used for these libraries thanks to their modular design and efficiency. However, these languages are less efficient for fast prototyping and visualization purposes. Therefore, a general-purpose ABM library that provides open-source tools and functions with ease of use and efficient performance has yet to be proposed. Refer to [51], [52] for further explanation regarding the merits and shortcomings of different ABM software.

II.1.2. Decision-making center of agents and fuzzy-logic controllers

One of the important steps in the development of ABMs in systems biology is defining an algorithm to correctly abstract cellular responses. The algorithm as the decision-making center of agents receives environmental cues as inputs and predicts cellular behavior as outputs. Different approaches have been used in the literature for this purpose such as simple rule definition, stochastic approach, artificial neural networks (NNs), and FLCs [4], [68], [95]–[98]. Deveaux et al [99] used simple rules in an ABM to simulate cell migration and proliferation for

cancer research. They reported the importance of cell movement for cancer proliferation. Browning et al [78] used simple rule definition and stochastic functions to describe cellular movement in an off-lattice ABM (cells can move freely on the simulation domain). The proposed model was able to realistically simulate collective cell migration and proliferation processes by calibrating against cell culture experiments. Jäger [98] used NNs embedded in ABM for the simulation of cellular migration. The proposed NNs receives environmental signals such as cell density and determines cell's choice whether to move to another location. They trained the algorithm using reinforcement learning and reported a successful training for Schelling's segregation problem.

Amongst the viable approaches, fuzzy logic-based solutions have demonstrated great potential due to multiple advantages [43], [44], [100], [101]. Firstly, the language used for FLCs is simple and readable by non-expert people in simulation. This is especially important in interdisciplinary fields such as systems biology, where the model developer has generally limited biological knowledge. Therefore, continuous collaboration with domain experts such as cell culture experimentalists is paramount for the successful creation of a numerical model. FLCs formulate the model in form of IF-THEN statements, where IF and THEN are conditions and results, respectively [102]. For instance, IF the-concentration-of-magnesium is low, THEN proliferation-rate-of-MSC is fast. This simple language has the potential to involve domain experts in the model development process and facilitate the creation of a successful digital replica.

In addition, FLCs enables the formulation of a system without precise mechanistic information [101]. In biological systems, information about the system in mostly qualitative or semi-qualitative due to noise in measurements or variations cellular responses. For instance, although Mg^{2+} ions have been reported to stimulate osteogenesis in low concentration, the precise value of such concertations differ from one experiment to another. Such qualitative information can be used in the formation of FLC by considering a range to the effect of a particular variable instead of a precise value. Modeling such a system with other simulation techniques, which require real-valued information, would be impossible if not difficult. Thus, the inherent capability of FLC in leveraging qualitative knowledge further implies their significance in biological simulations.

Another main advantage of FLCs is that the interactions among signaling factors are automatically defined during the definition of fuzzy rules [44], [101]. Since multiple signals affect the system's behavior both independently and in a combined format, it is important to correctly define how these signals interact in determining a particular cellular outcome. The rest of the methods in the literature define certain assumptions regarding the quality of the interactions, such as linear superimposition, in order to sum of the stimulatory effects [79], [103], [104]. Such approaches are idealized and pose scalability issues. Meanwhile, FLCs natively handles this issue as the available knowledge regarding the stimulatory effects also defines the possible interactions. Similarly, if information about an interaction is missing, the formulation of FLCs clarifies this shortcoming and potentially solves it through hypothesize

testing. However, FLCs are less powerful in modeling unknown relationships between signaling factors compared to state-of-the-art methods such as neural networks [105].

In order to model a system using FLC, the information regarding the bioregulatory effects of the signaling factors on cellular functions are compiled and turned into fuzzy sentences [44], [87], [100]. These information describe cellular functions as a function of different intensities of signaling factors. During this process, the missing information can be either simplified or defined as unknown parameters, which needs tuning in the calibration process. Then, the compiled knowledge is converted into a FLC in three processes; fuzzification, fuzzy rule definition, and defuzzification (see Figure II-2) [102]. The fuzzification process converts cellular inputs and outputs into fuzzy terms/levels such as low, medium, and high. The definition of these terms and their associated real values depend on the biological role. If a signaling factor has a complex concentration-dependent effect, it requires higher number of linguistic terms to sufficiently describe the regulatory effect in the whole spectrum. Similarly, if a cellular output occurs in different intensities depending on the different input conditions, a higher number of terms should be defined to sufficiently address the details. The conversion of real-valued variables into the fuzzy format is conducted using fuzzy membership functions (FMFs) [106]. Different FMFs are available such as rectangular, trapezoid, and Gaussian functions (see Figure II-2-A) [106]. The choice of a FMF depends on the biological role of a variable. For instance, if the stimulatory effect is expected to reach a maximum value at a certain concentration, rectangular membership functions are used, while trapezoid function assumes a range of values (instead of a single value) could induce the maximum effect.

Another essential step in the development of a FLC is defining fuzzy rules [102]. Fuzzy rules are the standardized form of the gathered information describing the system. Each fuzzy statement defines a particular cellular output as a function of a combination of certain inputs. Higher number of linguistic terms in cellular inputs and outputs requires more fuzzy statements to fully describe the system (Figure II-2-A). For instance, to describe the stimulatory role of two growth factors of G1 and G2 on the proliferation rate, the multivariate fuzzy statement can look like ”IF G1 is physiological and G2 is stimulatory, THEN proliferation is fast”. A complete set of fuzzy rules defined to describe MSC osteoblastic differentiation in response to Mg^{2+} ions and inflammatory cytokines can be found in Section III.3.

A set of cellular inputs can simultaneously trigger multiple fuzzy statements, each with different activation degrees. These multiple activations can occur due to the fact that a given real quantity of cellular input can fall into more than one category of fuzzy terms. For instance, Mg^{2+} ions concentration of 5mM can be partly within ‘low’ and partly ‘high’ levels. Thus, two or more fuzzy statements can fire for a given concentration of 5mM. The activation degree of each statement would depend on the attribution of the given concentration to each fuzzy level. In the diffuzification process, one final output is calculated from the activation of multiple statements.) [102]. Several approaches are available for this purpose such as centroid method and weighted average method [107]. In centroid method, the center of the mass/surface area due to the activation of each fuzzy level is calculated (see Figure II-2-C).

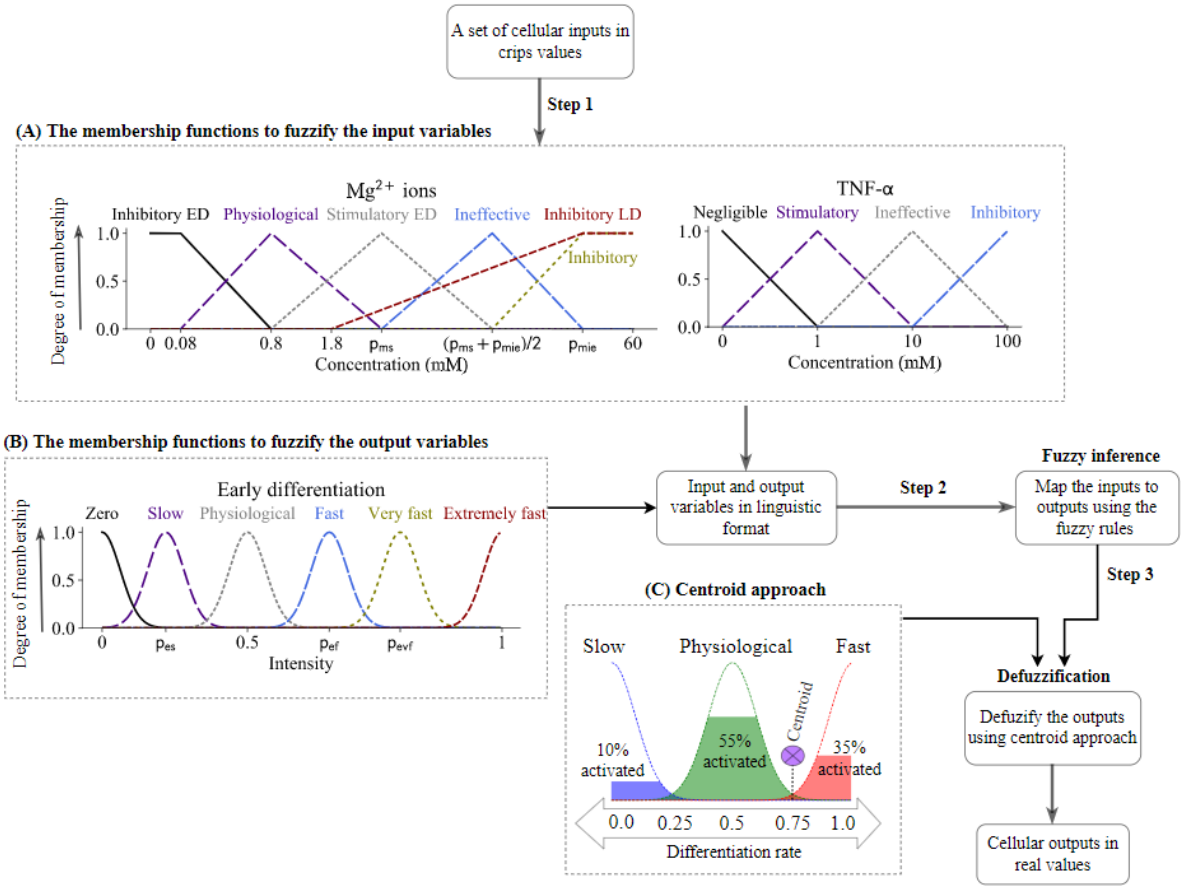

Figure II-2: Model development processes in fuzzy-logic controllers. In step 1, the set of real-valued variables for cell inputs and outputs are converted to fuzzy variables using fuzzy membership functions (A&B). Once the inputs are fuzzified, the set of rules derived from literature knowledge is used to predict cellular reactions in step 2. The controller generally activates multiple fuzzy outcomes at once. In order to create an outcome, an averaging algorithm, e.g. centroid approach, is used to defuzzify the outcomes. The image is adopted from [108].

II.2. Biological background

In this section, the introduction regarding the biological background of this thesis is provided. First, an introduction to the process of osteogenesis with the involved cellular activities is presented. After, the important regulatory factors of osteogenesis are explained. Next, an introduction to bone implant materials and the importance of magnesium in this field is given. Finally, the bioregulatory importance of magnesium in osteogenesis is explained.

II.2.1. Osteogenesis: MSC proliferation and osteoblastic differentiation

Bone fracture healing is a complex process and follows a series of coordinated events such as bleeding, inflammation, angiogenesis, and tissue production [16]. Inflammation occurs shortly after a fracture, where the inflammatory cells such as macrophages migrate into the fracture site, remove foreign material and damaged tissue, and promote the healing process by releasing a multitude of cytokines and growth factors [16]. The released chemicals diffuse to the neighbor region and attract the cells involved in the bone healing process, notably MSCs [16]. MSCs are multi-potent cells that migrate to the fracture site, increase cell population via proliferation process, and differentiate into different cell types such as fibroblasts, chondrocytes, and osteoblasts [16], [109]. The differentiation of MSCs into fibroblast and chondrocytes results in the production of fibrocartilage, also known as soft callus, which provides an early stability in the fracture sites [110]. The differentiation of MSCs into osteoblasts leads to the calcification of the callus and the stabilization of the fracture site, which is the fundamental step in the healing process [110].

Osteogenesis is a complex, multistep process that evolves around MSCs activities (see Figure II-3), notably the proliferation and osteoblastic differentiation, finely regulated by a multitude of cells and molecules. MSCs are the source of new cell production thanks to their unlimited self-renewal capacity [109]. MSCs can give birth to two daughter cells through cell division process without aging or losing their special characters as stem cells [109], [111]. Proliferation process can be divided into four major phases of G1 phase, S phase, G2 phase, and M phase [112]. In G1 phase, the cell decides whether to initiate a new division process. Once committed to a new cell cycle, in S and G2 phases, the cell replicates its DNA, grows, and prepares for mitosis (division) [112]. Finally, in M phase, the cell commits the actual division process and produces two daughter cells [112]. Each proliferation stage is a result of a complex network of cellular pathways, activated by plethora of signaling factors [112].

A decline in the proliferation capacity of MSCs is generally followed by the initiation of the differentiation process [16]. The coordination between the proliferation and differentiation is essential for a proper tissue repair upon injury [113]. Several studies have shown that MSCs perceive signals for differentiation specifically in G1 phase, whether to further proliferate or switch to differentiation [112]. Several factors can affect cell fate decision such as physical cues, cell population, oxygen density, pH, and growth factors [113], [114]. Throughout the healing process, the cross communication between inflammatory cells and MSCs plays a

significant role in the fate of the healing process [115]. However, the understanding of the regulatory network underlying cell fate decision is still incomplete [114].

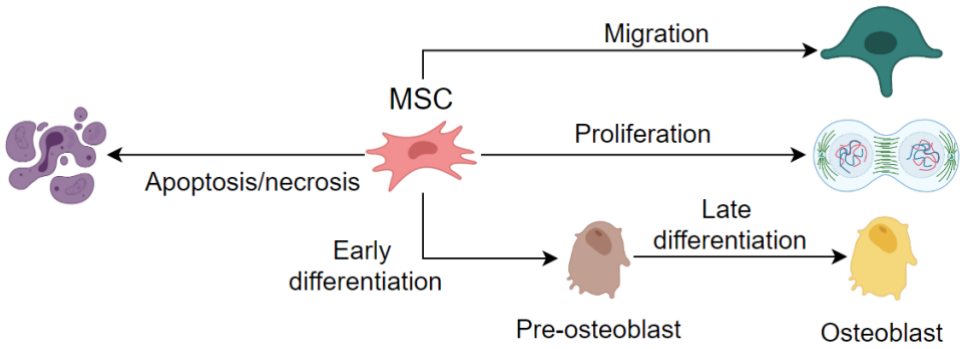

Figure II-3: Osteogenesis evolves around MSCs activities; MSCs migrate to the damage site in response to inflammatory conditions, increase cell population through proliferation process, differentiates to different cell types, notably osteoblasts in two steps of early and late processes, and undergo apoptosis (programmed death) or necrosis (death due to damage). Created with BioRender.com.

II.2.2. Osteogenesis: regulatory factors

Among the signaling factors, MSCs are particularly sensitive to the mechanical signals such as strain in their microenvironments [116], [117]. For instance, a higher magnitude of strain encourages the differentiation of MSCs into fibroblast and chondrocyte, resulting in fibrocartilage formation, while a lower strain causes osteoblastic differentiation and formation of bone [116], [118]. Therefore, the mechanical stability in the fracture site is crucial for osteogenesis. In addition, growth factors play an essential role in various MSCs activities such as proliferation and differentiation [112]. Inflammatory cells and, in particular, macrophages, are the primary producers of growth factors and cytokines in the repair process [19], [119]. Inflammatory cells release different profiles of proteins at different stages of healing process, directing the recruitment and controlled proliferation of MSCs as well as timely differentiation of MSCs into different cells including osteoblasts [19], [119]. In the past decade, a multitude of studies has specifically implied the importance of macrophage productions in directing osteogenic differentiation [19], [24], [119]. Macrophages are the major source of growth factors and cytokines throughout the healing process. Among them, TGF-b, BMP-2, IL10, IL1-b, and IL8 are especially significant in osteogenesis [120]. For more information regarding the bio regulatory factors of these growth factors on osteogenesis, refer to Sections 0 and III.3. Biomaterials are another category of substances that can significantly affect osteogenesis [121], which are further explained in the next session.

II.2.3. Bone implant materials and magnesium

Although bone has the capacity to restore itself after a fracture, a sufficient mechanical stability in the fracture site is required for the cells to survive and function properly [110]. Bone implants are designed to provide such mechanical stability. Physical and mechanical properties of the implant can significantly determine the success of a healing [122]. An excessively rigid implant

can result in a phenomena called stress shielding, which prevents the local cells to experience favorable mechanical signal, vital to their normal functioning [122], [123]. On the other hand, an excessively flexible implant can lead to an unstable healing site, causing cell death or resulting in a suboptimal healing progress [124].

Different types of materials have been used for bone implants in orthopedic industry, such as metals and polymers [121]. Metallic materials such as stainless steel, cobalt chromium, and titanium are the commonly used for bone implants [121]. These materials generally offer superior performance in terms of load-bearing capacity compared to polymers [121]. However, they might suffer from several disadvantageous. Firstly, stress-shielding phenomena [122], [123]. The young modulus of these materials are significantly higher than bone tissue, which hinders bone regeneration and leads to one resorption around the implant [122], [123]. In addition, the metallic materials undergo corrosion in contact with body environment, releasing ions and materials, which are generally toxic for the local cells [125]. Moreover, the conventional metallic bone implants require a second surgery to remove the implant after the successful bone reunion [121]. This process poses additional financial and health burdens.

Mg-based implant offer multiple advantageous offer conventional metallic materials [126]. Mg-based materials degrade in contact with body solution, which mitigates the necessity for the second surgery (see Figure II-4) [26]. Mg-based materials also offer a superior physical properties compared to the conventional metallic materials, in terms of matching with the local bone tissue to reduce the stress-shielding phenomenon [26]. Mg alloys have a Young's modulus of 41 to 45 GPa [127], while titanium allows, for instance, has a Young's modulus of 110 to 230 GPa [128]. Considering the Young's modulus of human bone tissue is 10 to 40 GPa [128], Mg alloys can physically align better with fractured bone. Moreover, the degraded Mg products such as Mg^{2+} ions are bioactive and promote tissue regeneration process [26]. Mg is an abundant metal in the body, which is also stored in skeleton and acts as a natural agonist of calcium [121]. Mg in the form of ion (Mg^{2+} ions) is crucial for bone metabolism [129]. In addition, Mg^{2+} ions are involved in different cellular pathway activation including osteogenesis, which is elaborated in Section II.2.4.

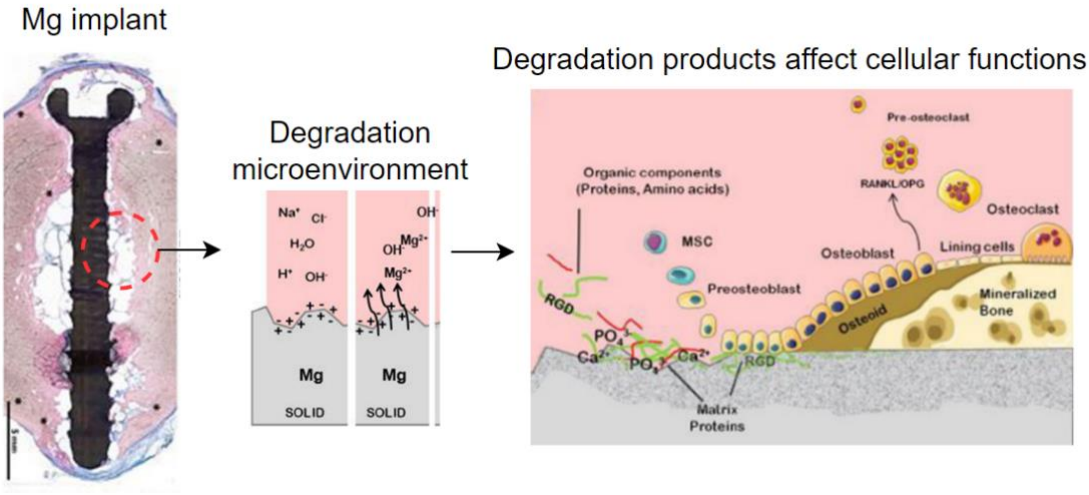

Figure II-4: Mg implant degrade shortly after implantation, producing a broad range of ions and materials, interfering with different biological reactions. The image was reproduced from [26].

Despite the several advantages offered by Mg-based materials, their usage in the orthopedic industry faces multiple challenges [26], [126], [130]. Firstly, a rapid degradation of Mg products could produce toxicity and instability in the fracture site, potentially leading to implant failure. An ideal implant should degrade with a pace proportional to the pace of the host tissue's renewal. In this way, the loss in the mechanical stability of the implant is compensated by the newly generated bone. In order to improve the degradation properties of Mg, different materials such as calcium, zinc, gadolinium, and silver are mixed with Mg in the form of alloys [26], [126], [130]. Although this process improves the early degradation properties of Mg, the degraded products of the alloy can be potentially harmful for the healing process [26], [126], [130]. This is in addition to the challenges in the manufacturing techniques of Mg alloys [26], [126], [130]. Thus, a thorough characterization of the degradation process as well as the biological reaction are prerequisites for the clinical application of Mg alloys.

II.2.4. Magnesium as a bio-regulatory factor

Mg as a natural substance of the body is essential for synthesis of proteins and is an important cofactor of a broad range of enzymes and transporters [131]. Intracellular Mg is a requirement of adenosine triphosphate (ATP) production, which is the universal currency of energy [131]. Mg also forms a complex with ATP to compose a biologically functional form, which regulate essential pathways in cellular functioning [132]. Mg deficiency is associated with hypertension, atherosclerosis, vasospasm, sudden cardiac death, stroke, and inflammatory conditions [131], [132].

The influence of Mg^{2+} ions on osteogenic activities can be evaluated in two aspects of direct and indirect (Figure II-5) [30]. Mg^{2+} ions have shown to directly interfere with MSCs intracellular signaling pathways and influence their phenotype change [31]. Wang et al has reported the association of Mg^{2+} ions with MAPK/ERK and Wnt/ β-catenin signaling pathways [31]. These pathways are involved in osteoblastic differentiation of MSCs [31]. Ni et al have shown MgCl2 activates p38/Osx/Runx2 and thereby promotes MSCs osteogenic differentiation in a mouse model [133]. Several studies have reported the stimulatory effect of Mg^{2+} ions on MSCs activities both in terms of phenotypic change [29], [34] and molecular response [27], [134]. Mg^{2+} ions has shown to affect cell population, mortality, and differentiation process on both concentration-dependent and phase-dependent fashion [29], [34], [135], [136]. While low concentration of Mg^{2+} ions is generally associated with an increased cell proliferation and faster differentiation process, its high concentration results in a decreased in proliferation and differentiation as well as an increase in mortality rate [29], [34], [135], [136]. In addition, Mg^{2+} ions in low concentration has shown to upregulate early osteoblastic differentiation, while it inhibits late differentiation phase [136]. Cell culture experiments have also shown that the application of Mg^{2+} ions alters the protein secretion of MSCs [27], [134]. For instance, proteins of S100A10 and BASP1 are differentially expressed for MSCs treated with low dosage of Mg^{2+} ions [134].

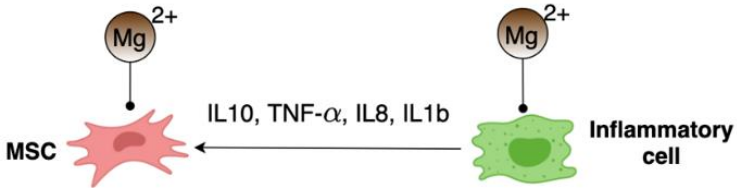

Figure II-5: Mg^{2+} ions regulate MSCs activities in both direct and indirect way. The indirect way includes the stimulation of macrophage productions, e.g. interleukins such as IL10 and IL8, which in return affect MSCs response. The image is taken from [108].

Empirical data have also shown the significance of Mg^{2+} ions in regulating the inflammatory response, e.g. macrophage polarization and cytokine release, and thereby indirectly affecting osteogenesis [20], [137], [138]. Deficiency and surplus of Mg^{2+} ions can both significantly affect the profile of macrophage cytokine release [30]. The pro-inflammatory cytokines of TNF-a, IL6, and IL8 as well as the anti-inflammatory cytokines of IL10 and IL4 have been shown to be regulated by Mg^{2+} ions a dose-dependent way [30]. For instance, Mg^{2+} ions deficiency and surplus upregulate and downregulate the TNF-a level, respectively [30], [139]. The regulatory effects of Mg^{2+} ions on macrophages is partly due to metabolism change, as Mg^{2+} ions directly influence the role of ATP in cellular metabolism [30]. Mg^{2+} ions is also a signaling protein that involves in multiple intracellular pathways such as non-canonical pathway of NF-kB and MAPK pathway [30], [139]. The mentioned inflammatory cytokines are determinant factors in MSCs osteogenic activities. The indirect effect of Mg^{2+} ions on osteogenesis through macrophage is reported to even overweight the direct impact of Mg^{2+} ions on MSCs [30].

References

[1] D. R. Carter, G. S. Beaupré, N. J. Giori, and J. A. Helms, "Mechanobiology of skeletal regeneration," *Clin. Orthop. Relat. Res.*, no. 355 Suppl, pp. S41-55, 1998, doi: Non-programmatic.

[2] J. S. Yu and N. Bagheri, "Multi-class and multi-scale models of complex biological phenomena," *Curr. Opin. Biotechnol.*, vol. 39, pp. 167–173, 2016, doi: 10.1016/j.copbio.2016.04.002.

[3] B. Zhang, H. Ye, and A. Yang, "Mathematical modelling of interacting mechanisms for hypoxia mediated cell cycle commitment for mesenchymal stromal cells," *BMC Syst. Biol.*, vol. 12, no. 1, p. 35, Dec. 2018, doi: 10.1186/s12918-018-0560-3.

[4] D. Lehotzky and G. K. H. Zupanc, "Cellular Automata Modeling of Stem-Cell-Driven Development of Tissue in the Nervous System," *Dev. Neurobiol.*, p. dneu.22686, May 2019, doi: 10.1002/dneu.22686.

[5] C. Zhao, T. X. Medeiros, R. J. Sové, B. H. Annex, and A. S. Popel, "A data-driven computational model enables integrative and mechanistic characterization of dynamic macrophage polarization," *iScience*, p. 102112, 2021, doi: 10.1016/j.isci.2021.102112.

[6] I. Trejo and H. V Kojouharov, "Understanding the fundamental molecular mechanism of osteogenic differentiation from mesenchymal stem cells," vol. 14, no. 2, pp. 687–698, 2019.

[7] M. Hoffmann, J. P. Kuska, M. Zscharnack, M. Loeffler, and J. Galle, "Spatial organization of mesenchymal stem cells in vitro-results from a new individual cell-based model with podia," *PLoS One*, vol. 6, no. 7, 2011, doi: 10.1371/journal.pone.0021960.

[8] G. Nikolai, Cynthia and Madey, "Tools of the trade: A survey of various agent based modeling platforms," *J. Artif. Soc. Soc. Simul.*, vol. 12, no. 2, 2009.

[9] T. H. Wideman, A. J. Zautra, and R. R. Edwards, "NIH Public Access," vol. 154, no. 11, pp. 2262–2265, 2014, doi: 10.1016/j.pain.2013.06.005.Re-Thinking.

[10] R. J. H. Ross, C. A. Yates, and R. E. Baker, "Inference of cell-cell interactions from population density characteristics and cell trajectories on static and growing domains," *Math. Biosci.*, vol. 264, no. 1, pp. 108–118, 2015, doi: 10.1016/j.mbs.2015.04.002.

[11] E. van der Vaart, M. A. Beaumont, A. S. A. Johnston, and R. M. Sibly, "Calibration and evaluation of individual-based models using Approximate Bayesian Computation," *Ecol. Modell.*, vol. 312, pp. 182–190, Sep. 2015, doi: 10.1016/j.ecolmodel.2015.05.020.

[12] J. Nourisa, B. Zeller-Plumhoff, H. Helmholz, B. Luthringer-Feyerabend, V. Ivannikov, and R. Willumeit-Römer, "Magnesium ions regulate mesenchymal stem cells population and osteogenic differentiation: a fuzzy agent-based modeling approach," *Comput. Struct. Biotechnol. J.*, vol. 19, pp. 4110–4122, 2021, [Online]. Available: https://doi.org/10.1016/j.csbj.2021.07.005

[13] D. C. Betts and R. Müller, "Mechanical regulation of bone regeneration: Theories,

models, and experiments," *Front. Endocrinol. (Lausanne).*, vol. 5, no. DEC, pp. 1–14, 2014, doi: 10.3389/fendo.2014.00211.

[14] L. Geris, J. Vander Sloten, and H. Van Oosterwyck, "Connecting biology and mechanics in fracture healing: An integrated mathematical modeling framework for the study of nonunions," *Biomech. Model. Mechanobiol.*, vol. 9, no. 6, pp. 713–724, 2010, doi: 10.1007/s10237-010-0208-8.

[15] C. J. Wilson, M. A. Schütz, and D. R. Epari, "Computational simulation of bone fracture healing under inverse dynamisation," *Biomech. Model. Mechanobiol.*, vol. 16, no. 1, pp. 5–14, 2017, doi: 10.1007/s10237-016-0798-x.

[16] C. S. Bahney *et al.*, "Cellular biology of fracture healing," *J. Orthop. Res.*, vol. 37, no. 1, pp. 35–50, 2019, doi: 10.1002/jor.24170.

[17] Fu, Liu, Halim, Ju, Luo, and Song, "Mesenchymal Stem Cell Migration and Tissue Repair," *Cells*, vol. 8, no. 8, p. 784, 2019, doi: 10.3390/cells8080784.

[18] R. Gilbert, M. Vickaryous, and A. Viloria-Petit, "Signalling by Transforming Growth Factor Beta Isoforms in Wound Healing and Tissue Regeneration," *J. Dev. Biol.*, vol. 4, no. 2, p. 21, 2016, doi: 10.3390/jdb4020021.

[19] Y. Zhang, T. Böse, R. E. Unger, J. A. Jansen, C. J. Kirkpatrick, and J. J. J. P. van den Beucken, "Macrophage type modulates osteogenic differentiation of adipose tissue MSCs," *Cell Tissue Res.*, vol. 369, no. 2, pp. 273–286, 2017.

[20] X. Zhang, Q. Chen, and X. Mao, "Magnesium Enhances Osteogenesis of BMSCs by Tuning Osteoimmunomodulation," *Biomed Res. Int.*, vol. 2019, 2019, doi: 10.1155/2019/7908205.

[21] F. da Silva Lima *et al.*, "An insight into the role of magnesium in the immunomodulatory properties of mesenchymal stem cells," *J. Nutr. Biochem.*, vol. 55, pp. 200–208, 2018, doi: 10.1016/j.jnutbio.2018.02.006.

[22] M. Croes *et al.*, "Proinflammatory mediators enhance the osteogenesis of Human Mesenchymal stem cells after lineage commitment," *PLoS One*, vol. 10, no. 7, pp. 1–14, 2015, doi: 10.1371/journal.pone.0132781.

[23] G. E. Glass, J. K. Chan, A. Freidin, M. Feldmann, N. J. Horwood, and J. Nanchahal, "TNF-α promotes fracture repair by augmenting the recruitment and differentiation of muscle-derived stromal cells," *Proc. Natl. Acad. Sci.*, vol. 108, no. 4, pp. 1585–1590, 2011, doi: 10.1073/pnas.1018501108.

[24] E. Chen *et al.*, "Concentration-dependent, dual roles of IL-10 in the osteogenesis of human BMSCs via P38/MAPK and NF-kB signaling pathways," *FASEB J.*, vol. 32, no. 9, pp. 4917–4929, 2018, doi: 10.1096/fj.201701256RRR.

[25] L. Gong, Y. Zhao, Y. Zhang, and Z. Ruan, "The macrophage polarization regulates MSC osteoblast differentiation in vitro," *Ann. Clin. Lab. Sci.*, vol. 46, no. 1, pp. 65–71, 2016.

[26] R. Willumeit-Römer, "The Interface Between Degradable Mg and Tissue," *Jom*, vol. 71,

no. 4, pp. 1447–1455, 2019, doi: 10.1007/s11837-019-03368-0.

[27] M. Omidi, "Investigation of the Impact of Magnesium Implants on the Proteomes of Bone Cells and Bone Tissue," 2017.

[28] N. A. Agha, R. Willumeit-Römer, D. Laipple, B. Luthringer, and F. Feyerabend, "The degradation interface of magnesium based alloys in direct contact with human primary osteoblast cells," *PLoS One*, vol. 11, no. 6, pp. 1–20, 2016, doi: 10.1371/journal.pone.0157874.

[29] A. Burmester, R. Willumeit-Römer, and F. Feyerabend, "Behavior of bone cells in contact with magnesium implant material," *J. Biomed. Mater. Res. - Part B Appl. Biomater.*, vol. 105, no. 1, pp. 165–179, 2015, doi: 10.1002/jbm.b.33542.

[30] W. Qiao *et al.*, "TRPM7 kinase-mediated immunomodulation in macrophage plays a central role in magnesium ion- induced bone regeneration," *Nat. Commun.*, vol. 12, no. 2885, 2021, doi: 10.1038/s41467-021-23005-2.

[31] Y. Wang *et al.*, "Unraveling the osteogenesis of magnesium by the activity of osteoblasts in vitro," *J. Mater. Chem. B*, vol. 6, no. 41, pp. 6615–6621, 2018.

[32] L. Xu, R. Willumeit-römer, and B. J. C. Luthringer-feyerabend, "Effect of magnesium-degradation products and hypoxia on the angiogenesis of human umbilical vein endothelial cells," vol. 98, pp. 269–283, 2019, doi: 10.1016/j.actbio.2019.02.018.

[33] Z. Shan, X. Xie, X. Wu, S. Zhuang, and C. Zhang, "Development of degradable magnesium-based metal implants and their function in promoting bone metabolism (A review).," *J. Orthop. Transl.*, vol. 36, pp. 184–193, Sep. 2022, doi: 10.1016/j.jot.2022.09.013.

[34] A. Burmester, B. Luthringer, R. Willumeit, and F. Feyerabend, "Comparison of the reaction of bone-derived cells to enhanced MgCl2-salt concentrations," *Biomatter*, vol. 4, p. e967616, 2014, doi: 10.4161/21592527.2014.967616.

[35] P. K. J. Han, "Conceptual, methodological, and ethical problems in communicating uncertainty in clinical evidence.," *Med. Care Res. Rev.*, vol. 70, no. 1 Suppl, pp. 14S-36S, Feb. 2013, doi: 10.1177/1077558712459361.

[36] N. Eling, M. D. Morgan, and J. C. Marioni, "Challenges in measuring and understanding biological noise.," *Nat. Rev. Genet.*, vol. 20, no. 9, pp. 536–548, Sep. 2019, doi: 10.1038/s41576-019-0130-6.

[37] W. Wan *et al.*, "Synergistic Effect of Matrix Stiffness and Inflammatory Factors on Osteogenic Differentiation of MSC," *Biophys. J.*, vol. 117, no. 1, pp. 129–142, 2019, doi: 10.1016/j.bpj.2019.05.019.

[38] A. Krinner, M. Zscharnack, A. Bader, D. Drasdo, and J. Galle, "Impact of oxygen environment on mesenchymal stem cell expansion and chondrogenic differentiation," *Cell Prolif.*, vol. 42, no. 4, pp. 471–484, 2009, doi: 10.1111/j.1365-2184.2009.00621.x.

[39] M. A. Tabatabai, Z. Bursac, W. M. Eby, and K. P. Singh, "Mathematical modeling of

stem cell proliferation," *Med. Biol. Eng. Comput.*, vol. 49, no. 3, pp. 253–262, 2011, doi: 10.1007/s11517-010-0686-y.

[40] L. E. Wadkin, S. Orozco-Fuentes, I. Neganova, M. Lako, A. Shukurov, and N. G. Parker, "The recent advances in the mathematical modelling of human pluripotent stem cells," *SN Appl. Sci.*, vol. 2, no. 276, pp. 1–14, 2020, doi: 10.1007/s42452-020-2070-3.

[41] E. S. Bayrak, H. Mehdizadeh, B. Akar, S. I. Somo, E. M. Brey, and A. Cinar, "Agent-based modeling of osteogenic differentiation of mesenchymal stem cells in porous biomaterials," *2014 36th Annu. Int. Conf. IEEE Eng. Med. Biol. Soc. EMBC 2014*, pp. 2924–2927, 2014, doi: 10.1109/EMBC.2014.6944235.

[42] R. György, M. E. Klontzas, M. Kostoglou, N. Panoskaltsis, A. Mantalaris, and M. C. Georgiadis, "Capturing mesenchymal stem cell heterogeneity during osteogenic differentiation: an experimental-modeling approach," *Ind. Eng. Chem. Res.*, vol. 58, no. 31, pp. 13900–13909, 2019, doi: 10.1021/acs.iecr.9b01988.

[43] C. Ament and E. P. Hofer, "A fuzzy logic model of fracture healing," *J. Biomech.*, vol. 33, no. 8, pp. 961–968, 2000, doi: 10.1016/S0021-9290(00)00049-X.

[44] B. B. Aldridge, J. Saez-Rodriguez, J. L. Muhlich, P. K. Sorger, and D. A. Lauffenburger, "Fuzzy Logic Analysis of Kinase Pathway Crosstalk in TNF/EGF/Insulin-Induced Signaling," *PLoS Comput. Biol.*, vol. 5, no. 4, 2009, doi: 10.1371/journal.pcbi.1000340.

[45] M. S. Nobile *et al.*, "Fuzzy modeling and global optimization to predict novel therapeutic targets in cancer cells," *Bioinformatics*, vol. 36, no. 7, pp. 2181–2188, 2019, doi: 10.1093/bioinformatics/btz868.

[46] T. Szikszai *et al.*, "Agent-Based Modeling of Cancer Stem Cell Driven Solid Tumor Growth," *Infect. Immun.*, vol. 13, no. 11, pp. 96–103, 2015, doi: 10.1007/7651.

[47] C. Kuhn and S. Checa, "Computational modeling to quantify the contributions of VEGFR1, VEGFR2, and lateral inhibition in sprouting angiogenesis," *Front. Physiol.*, vol. 10, no. MAR, pp. 1–14, 2019, doi: 10.3389/fphys.2019.00288.

[48] B. Lambert, A. L. MacLean, A. G. Fletcher, A. N. Combes, M. H. Little, and H. M. Byrne, "Bayesian inference of agent-based models: a tool for studying kidney branching morphogenesis," *J. Math. Biol.*, vol. 76, no. 7, pp. 1673–1697, 2018, doi: 10.1007/s00285-018-1208-z.

[49] M. Wang and N. Yang, "Computational simulation of the influence of mechanical stability on growth factors activities during bone fracture healing," *IEEE Access*, vol. 7, pp. 9827–9835, 2019, doi: 10.1109/ACCESS.2019.2892125.

[50] F. Niemeyer, L. Claes, A. Ignatius, N. Meyers, and U. Simon, "Simulating lateral distraction osteogenesis," *PLoS One*, vol. 13, no. 3, p. e0194500, 2018.

[51] D. L. DeAngelis and S. G. Diaz, "Decision-making in agent-based modeling: A current review and future prospectus," *Front. Ecol. Evol.*, vol. 6, p. 237, 2019.

[52] S. F. Railsback and V. Grimm, *Agent-based and individual-based modeling: a practical*

introduction. Princeton university press, 2019.

[53] M. Cardinot, C. O'Riordan, J. Griffith, and M. Perc, "Evoplex: A platform for agent-based modeling on networks," *SoftwareX*, vol. 9, pp. 199–204, Jan. 2019, doi: 10.1016/j.softx.2019.02.009.

[54] L. Zhang, Z. Wang, J. A. Sagotsky, and T. S. Deisboeck, "Multiscale agent-based cancer modeling," *J. Math. Biol.*, vol. 58, no. 4–5, pp. 545–559, 2009.

[55] S. Abar, G. K. Theodoropoulos, P. Lemarinier, and G. M. P. O'Hare, "Agent Based Modelling and Simulation tools: A review of the state-of-art software," *Computer Science Review*, vol. 24. Elsevier Ireland Ltd, pp. 13–33, May 01, 2017. doi: 10.1016/j.cosrev.2017.03.001.

[56] C. M. Macal, "Everything you need to know about agent-based modelling and simulation," *J. Simul.*, vol. 10, no. 2, pp. 144–156, 2016.

[57] G. Morvan, "Multi-level agent-based modeling - A literature survey," 2012, [Online]. Available: http://arxiv.org/abs/1205.0561

[58] M. A. Beaumont, "Annual Review of Statistics and Its Application Approximate Bayesian Computation," 2018, doi: 10.1146/annurev-statistics-030718.

[59] A. Lutz and U. Nackenhorst, "A computational approach on the osseointegration of bone implants based on a bio-active interface theory," *GAMM Mitteilungen*, vol. 32, no. 2, pp. 178–192, 2009, doi: 10.1002/gamm.200910015.

[60] S. Irandoust and S. Müftü, "The interplay between bone healing and remodeling around dental implants," *Sci. Rep.*, vol. 10, no. 1, pp. 1–10, 2020, doi: 10.1038/s41598-020-60735-7.

[61] C. J. Boyle, A. B. Lennon, M. Early, D. J. Kelly, C. Lally, and P. J. Prendergast, "Computational simulation methodologies for mechanobiological modelling: a cell-centred approach to neointima development in stents," *Philos. Trans. R. Soc. A Math. Phys. Eng. Sci.*, vol. 368, no. 1921, pp. 2919–2935, 2010, doi: 10.1098/rsta.2010.0071.

[62] W. Jin, E. T. Shah, C. J. Penington, S. W. McCue, P. K. Maini, and M. J. Simpson, "Logistic Proliferation of Cells in Scratch Assays is Delayed," *Bull. Math. Biol.*, vol. 79, no. 5, pp. 1028–1050, 2017, doi: 10.1007/s11538-017-0267-4.

[63] A. M. Uhrmacher and D. Weyns, *Multi-Agent systems: Simulation and applications*. CRC press, 2009.

[64] W. der Hoek and M. Wooldridge, "Multi-agent systems," *Found. Artif. Intell.*, vol. 3, pp. 887–928, 2008.

[65] M. Niazi and A. Hussain, "Agent-based computing from multi-agent systems to agent-based models: A visual survey," *Scientometrics*, vol. 89, no. 2, pp. 479–499, 2011, doi: 10.1007/s11192-011-0468-9.

[66] R. J. Allan, *Survey of agent based modelling and simulation tools*. Science & Technology

Facilities Council London, 2010.

[67] J. Metzcar, Y. Wang, R. Heiland, and P. Macklin, “A Review of Cell-Based Computational Modeling in Cancer Biology,” *JCO Clin. Cancer Informatics*, no. 3, pp. 1–13, Feb. 2019, doi: 10.1200/cci.18.00069.

[68] M. S. Nobile *et al.*, “Modeling cell proliferation in human acute myeloid leukemia xenografts,” *Bioinformatics*, vol. 35, no. 18, pp. 3378–3386, Sep. 2019, doi: 10.1093/bioinformatics/btz063.

[69] T. Gan, Y. Yang, J. Hao, Z. Liao, and X. Zhu, “Speeding up Collective Cell Migration Using Deep Reinforcement Learning,” in *Proceedings - 2018 IEEE International Conference on Bioinformatics and Biomedicine, BIBM 2018*, Jan. 2019, pp. 1277–1280. doi: 10.1109/BIBM.2018.8621416.

[70] T. C. Schelling, “Models of segregation,” *Am. Econ. Rev.*, vol. 59, no. 2, pp. 488–493, 1969.

[71] M. Shamil, F. Farheen, N. Ibtehaz, I. M. Khan, M. S. Rahman, and others, “An agent-based modeling of COVID-19: validation, analysis, and recommendations,” *Cognit. Comput.*, pp. 1–12, 2021.

[72] C. C. Kerr *et al.*, “Covasim: an agent-based model of COVID-19 dynamics and interventions,” *PLOS Comput. Biol.*, vol. 17, no. 7, p. e1009149, 2021.

[73] P. P. Rezaeiye *et al.*, “Agent programming with object oriented (C++),” in *2017 Second International Conference on Electrical, Computer and Communication Technologies (ICECCT)*, 2017, pp. 1–10.

[74] T. Rentsch, “Object oriented programming,” *ACM Sigplan Not.*, vol. 17, no. 9, pp. 51–57, 1982.

[75] B. P. Zeigler, *Object-oriented simulation with hierarchical, modular models: intelligent agents and endomorphic systems*. Academic press, 2014.

[76] M. Soheilypour and M. R. K. Mofrad, “Agent-Based Modeling in Molecular Systems Biology,” *BioEssays*, vol. 40, no. 7, pp. 1–8, 2018, doi: 10.1002/bies.201800020.

[77] S. Gao, C. Xiang, K. Qin, and C. Sun, “Mathematical modeling reveals the role of hypoxia in the promotion of human mesenchymal stem cell long-term expansion,” *Stem Cells Int.*, vol. 2018, 2018, doi: 10.1155/2018/9283432.

[78] A. P. Browning, S. W. McCue, R. N. Binny, M. J. Plank, E. T. Shah, and M. J. Simpson, “Inferring parameters for a lattice-free model of cell migration and proliferation using experimental data,” *J. Theor. Biol.*, vol. 437, pp. 251–260, 2018, doi: 10.1016/j.jtbi.2017.10.032.

[79] E. Borgiani, G. N. Duda, and S. Checa, “Multiscale modeling of bone healing: Toward a systems biology approach,” *Frontiers in Physiology*, vol. 8, no. MAY. 2017. doi: 10.3389/fphys.2017.00287.

[80] C. A. Yates, “Discrete and continuous models for tissue growth and shrinkage,” *J. Theor. Biol.*, vol. 350, pp. 37–48, Jun. 2014, doi: 10.1016/j.jtbi.2014.01.041.

[81] C. Irons, M. J. Plank, and M. J. Simpson, “Lattice-free models of directed cell motility,” *Phys. A Stat. Mech. its Appl.*, vol. 442, no. July 2015, pp. 110–121, 2016, doi: 10.1016/j.physa.2015.08.049.

[82] C. M. Glen, M. L. Kemp, and E. O. Voit, “Agent-based modeling of morphogenetic systems: Advantages and challenges,” *PLoS Comput. Biol.*, vol. 15, no. 3, p. e1006577, 2019.

[83] Gerlee, “A Hybrid Cellular Automaton Model of Clonal Evolution in Cancer: The Emergence of the Glycolytic Phenotype,” vol. 27, no. 4, pp. 1–19, 2008, doi: 10.1037/a0032811.Child.

[84] P. Van Liedekerke, A. Buttenschön, and D. Drasdo, “Off-lattice agent-based models for cell and tumor growth: numerical methods, implementation, and applications,” in *Numerical methods and advanced simulation in biomechanics and biological processes*, Elsevier, 2018, pp. 245–267.

[85] K. A. Rejniak and A. R. A. Anderson, “Hybrid models of tumor growth.,” *Wiley Interdiscip. Rev. Syst. Biol. Med.*, vol. 3, no. 1, pp. 115–125, 2011, doi: 10.1002/wsbm.102.

[86] D. Drasdo, A. Buttenschön, and P. Van Liedekerke, “Agent-based lattice models of multicellular systems: numerical methods, implementation, and applications,” in *Numerical Methods and Advanced Simulation in Biomechanics and Biological Processes*, Elsevier, 2018, pp. 223–238.

[87] J. Nourisa, B. Zeller-Plumhoff, H. Helmholz, B. Luthringer-Feyerabend, V. Ivannikov, and R. Willumeit-Römer, “Magnesium ions regulate mesenchymal stem cells population and osteogenic differentiation: A fuzzy agent-based modeling approach,” *Comput. Struct. Biotechnol. J.*, vol. 19, pp. 4110–4122, 2021, doi: 10.1016/j.csbj.2021.07.005.

[88] J. Poleszczuk, P. Macklin, and H. Enderling, “Agent-Based Modeling of Cancer Stem Cell Driven Solid Tumor Growth.,” *Methods Mol. Biol.*, vol. 1516, pp. 335–346, 2016, doi: 10.1007/7651_2016_346.

[89] J. Xiao, P. Andelfinger, D. Eckhoff, W. Cai, and A. Knoll, “A survey on agent-based simulation using hardware accelerators,” *ACM Computing Surveys*, vol. 51, no. 6. Association for Computing Machinery, Jan. 01, 2019. doi: 10.1145/3291048.

[90] S. Tisue and U. Wilensky, “Netlogo: A simple environment for modeling complexity,” in *International conference on complex systems*, 2004, vol. 21, pp. 16–21.

[91] N. Collier, “Repast: An extensible framework for agent simulation,” *Univ. Chicago’s Soc. Sci. Res.*, vol. 36, p. 2003, 2003.

[92] R. Nourisa, Jalil and Zeller-Plumhoff, Berit and Willumeit-Romer, “CppyABM: An open-source agent-based modeling library to integrate C++ and Python,” *Softw. Pract. Exp.*, vol. 52, no. 6, pp. 1337--1351, 2022.

[93] J. W. Reinhardt, D. A. Krakauer, and K. J. Gooch, “Complex matrix remodeling and durotaxis can emerge from simple rules for cell-matrix interaction in agent-based models.,” *J. Biochem. Eng.*, vol. 135, no. 7, p. 071003, 2013, doi: 10.1115/1.4024463.

[94] S. Luke, C. Cioffi-Revilla, L. Panait, K. Sullivan, and G. Balan, “Mason: A multiagent simulation environment,” *Simulation*, vol. 81, no. 7, pp. 517–527, 2005.

[95] A. Borshchev, S. Brailsford, L. Churilov, and B. Dangerfield, “Multi-method modelling: AnyLogic,” *Discret. Simul. Syst. Dyn. Manag. Decis. Mak.*, pp. 248–279, 2014.

[96] N. Mohamed and J. Al-Jaroodi, “MidCloud: an agent-based middleware for effective utilization of replicated Cloud services,” *Softw. Pract. Exp.*, vol. 45, no. 3, pp. 343–363, 2015.

[97] D. Nichol, M. Robertson-Tessi, A. R. A. Anderson, and P. Jeavons, “Model genotype-phenotype mappings and the algorithmic structure of evolution,” *J. R. Soc. Interface*, vol. 16, no. 160, p. 20190332, Nov. 2019, doi: 10.1098/rsif.2019.0332.

[98] G. Jäger, “Replacing Rules by Neural Networks A Framework for Agent-Based Modelling,” 2019, doi: 10.3390/bdcc3040051.

[99] W. Deveaux, K. Hayashi, and K. Selvarajoo, “Defining rules for cancer cell proliferation in TRAIL stimulation,” *npj Syst. Biol. Appl.*, vol. 5, no. 1, Dec. 2019, doi: 10.1038/s41540-019-0084-5.

[100] F. Liu, M. Heiner, and M. Yang, “Fuzzy stochastic petri nets for modeling biological systems with uncertain kinetic parameters,” *PLoS One*, vol. 11, no. 2, pp. 1–19, 2016, doi: 10.1371/journal.pone.0149674.

[101] J. Bordon, M. Moskon, N. Zimic, and M. Mraz, “Fuzzy Logic as a Computational Tool for Quantitative Modelling of Biological Systems with Uncertain Kinetic Data.,” *IEEE/ACM Trans. Comput. Biol. Bioinforma.*, vol. 12, no. 5, pp. 1199–1205, 2015, doi: 10.1109/TCBB.2015.2424424.

[102] I. Iancu, “A Mamdani type fuzzy logic controller,” *Fuzzy Log. Control. Concepts, Theor. Appl.*, pp. 325–350, 2012.

[103] D. G. Checa S, Prendergast PJ, “Inter-species investigation of the mechano-regulation of bone healing: comparison of secondary bone healing in sheep and rat,” *J Biomech*, vol. 44, no. 7, pp. 1237–45, 2011.

[104] S. Checa and P. J. Prendergast, “A mechanobiological model for tissue differentiation that includes angiogenesis: A lattice-based modeling approach,” *Ann. Biomed. Eng.*, vol. 37, no. 1, pp. 129–145, 2009, doi: 10.1007/s10439-008-9594-9.

[105] D. M. Camacho, K. M. Collins, R. K. Powers, J. C. Costello, and J. J. Collins, “Next-Generation Machine Learning for Biological Networks,” *Cell*, vol. 173, no. 7. Cell Press, pp. 1581–1592, Jun. 14, 2018. doi: 10.1016/j.cell.2018.05.015.

[106] A. Sadollah, “Introductory Chapter: Which Membership Function is Appropriate in Fuzzy System?,” in *Fuzzy Logic Based in Optimization Methods and Control Systems*

and Its Applications, A. Sadollah, Ed. Rijeka: IntechOpen, 2018. doi: 10.5772/intechopen.79552.

[107] I. A. Hameed, "Using Gaussian membership functions for improving the reliability and robustness of students' evaluation systems," *Expert Syst. Appl.*, vol. 38, no. 6, pp. 7135–7142, 2011, doi: 10.1016/j.eswa.2010.12.048.

[108] J. Nourisa, B. Zeller-plumhoff, and R. Willumeit-ro, "The osteogenetic activities of mesenchymal stem cells in response to Mg 2 + ions and inflammatory cytokines : A numerical approach using fuzzy logic controllers," *PLoS Comput. Biol.*, pp. 1–24, 2022, doi: 10.1371/journal.pcbi.1010482.

[109] J. Steens and D. Klein, "Current Strategies to Generate Human Mesenchymal Stem Cells In Vitro.," *Stem Cells Int.*, vol. 2018, p. 6726185, 2018, doi: 10.1155/2018/6726185.

[110] F. Loi, L. A. Córdova, J. Pajarinen, T. Lin, Z. Yao, and S. B. Goodman, "Inflammation, fracture and bone repair," *Bone*, vol. 86, pp. 119–130, 2016.

[111] A. Musiał-Wysocka, M. Kot, and M. Majka, "The Pros and Cons of Mesenchymal Stem Cell-Based Therapies.," *Cell Transplant.*, vol. 28, no. 7, pp. 801–812, Jul. 2019, doi: 10.1177/0963689719837897.

[112] Z. Wang, "Regulation of Cell Cycle Progression by Growth Factor-Induced Cell Signaling.," *Cells*, vol. 10, no. 12, Nov. 2021, doi: 10.3390/cells10123327.

[113] J. E. Aubin, "Mesenchymal Stem Cells and Osteoblast Differentiation," *In Vivo (Brooklyn).*, pp. 85–107, 2008.

[114] D. E. Discher, D. J. Mooney, and P. W. Zandstra, "Growth factors, matrices, and forces combine and control stem cells," *Science (80-.).*, vol. 324, no. 5935, pp. 1673–1677, 2009.

[115] M. Romero-López *et al.*, "Macrophage effects on mesenchymal stem cell osteogenesis in a three-dimensional in vitro bone model," *Tissue Eng. - Part A*, vol. 26, no. 19–20, pp. 1099–1111, 2020, doi: 10.1089/ten.tea.2020.0041.

[116] J. S. Park, N. F. Huang, K. T. Kurpinski, S. Patel, S. Hsu, and S. Li, "Mechanobiology of mesenchymal stem cells and their use in cardiovascular repair.," *Front. Biosci.*, vol. 12, pp. 5098–5116, 2007, doi: 10.2741/2551.

[117] D. E. Ingber, "Mechanobiology and diseases of mechanotransduction," *Ann. Med.*, vol. 35, no. 8, pp. 564–577, 2003, doi: 10.1080/07853890310016333.

[118] J. H. W. B. P. Thampatty, "An introductory review of cell mechanobiology," pp. 1–16, 2006, doi: 10.1007/s10237-005-0012-z.

[119] F. Carty, B. P. Mahon, and K. English, "The influence of macrophages on mesenchymal stromal cell therapy: Passive or aggressive agents," *Clin. Exp. Immunol.*, vol. 188, no. 1, pp. 1–11, 2017, doi: 10.1111/cei.12929.

[120] G. Valles, F. Bensiamar, L. Maestro-Paramio, E. García-Rey, N. Vilaboa, and L.

Saldaña, “Influence of inflammatory conditions provided by macrophages on osteogenic ability of mesenchymal stem cells,” *Stem Cell Res. Ther.*, vol. 11, no. 1, pp. 1–15, 2020, doi: 10.1186/s13287-020-1578-1.

[121] J. Lee, H. Byun, S. K. Madhurakkat Perikamana, S. Lee, and H. Shin, “Current advances in immunomodulatory biomaterials for bone regeneration,” *Adv. Healthc. Mater.*, vol. 8, no. 4, p. 1801106, 2019.

[122] P. R. Kuzyk and E. H. Schemitsch, “The basic science of peri-implant bone healing.,” *Indian J. Orthop.*, vol. 45, no. 2, pp. 108–115, Mar. 2011, doi: 10.4103/0019-5413.77129.

[123] Y. Hériveaux, S. Le Cann, M. Fraulob, E. Vennat, V.-H. Nguyen, and G. Haïat, “Mechanical micromodeling of stress-shielding at the bone-implant interphase under shear loading.,” *Med. Biol. Eng. Comput.*, vol. 60, no. 11, pp. 3281–3293, Nov. 2022, doi: 10.1007/s11517-022-02657-2.

[124] D. Prodanov and J. Delbeke, “Mechanical and Biological Interactions of Implants with the Brain and Their Impact on Implant Design.,” *Front. Neurosci.*, vol. 10, p. 11, 2016, doi: 10.3389/fnins.2016.00011.

[125] N. Eliaz, “Corrosion of Metallic Biomaterials: A Review.,” *Mater. (Basel, Switzerland)*, vol. 12, no. 3, Jan. 2019, doi: 10.3390/ma12030407.

[126] M. Rahman, N. K. Dutta, and N. Roy Choudhury, “Magnesium Alloys With Tunable Interfaces as Bone Implant Materials.,” *Front. Bioeng. Biotechnol.*, vol. 8, p. 564, 2020, doi: 10.3389/fbioe.2020.00564.

[127] C. Chang, S. Yue, W. Li, L. Lu, and X. Yan, “Study on microstructure and tribological behavior of the selective laser melted MgZnCa alloy,” *Mater. Lett.*, vol. 309, p. 131439, 2022.

[128] K. Miura, N. Yamada, S. Hanada, T.-K. Jung, and E. Itoi, “The bone tissue compatibility of a new Ti--Nb--Sn alloy with a low Young’s modulus,” *Acta Biomater.*, vol. 7, no. 5, pp. 2320–2326, 2011.

[129] Z. Zhao *et al.*, “Capturing magnesium ions via microfluidic hydrogel microspheres for promoting cancellous bone regeneration,” *ACS Nano*, vol. 15, no. 8, pp. 13041–13054, 2021.

[130] P. Chakraborty Banerjee, S. Al-Saadi, L. Choudhary, S. E. Harandi, and R. Singh, “Magnesium Implants: Prospects and Challenges.,” *Mater. (Basel, Switzerland)*, vol. 12, no. 1, Jan. 2019, doi: 10.3390/ma12010136.

[131] W. Jahnen-Dechent and M. Ketteler, “Magnesium basics.,” *Clin. Kidney J.*, vol. 5, no. Suppl 1, pp. i3–i14, Feb. 2012, doi: 10.1093/ndtplus/sfr163.

[132] D. Fiorentini, C. Cappadone, G. Farruggia, and C. Prata, “Magnesium: Biochemistry, Nutrition, Detection, and Social Impact of Diseases Linked to Its Deficiency.,” *Nutrients*, vol. 13, no. 4, Mar. 2021, doi: 10.3390/nu13041136.

[133] S. Ni, X.-B. Xiong, and X.-Y. Ni, “MgCl2 promotes mouse mesenchymal stem cell osteogenic differentiation by activating the p38/Osx/Runx2 signaling pathway,” *Mol. Med. Rep.*, vol. 22, no. 5, pp. 3904–3910, 2020.

[134] L. A. Moreno *et al.*, “Understanding Protein Networks Using Vester’s Sensitivity Model,” *IEEE/ACM Trans. Comput. Biol. Bioinforma.*, vol. 17, no. 4, pp. 1440–1450, 2018, doi: 10.1109/TCBB.2018.2885757.

[135] S. Yoshizawa, A. Brown, A. Barchowsky, and C. Sfeir, “Magnesium ion stimulation of bone marrow stromal cells enhances osteogenic activity, simulating the effect of magnesium alloy degradation,” *Acta Biomater.*, vol. 10, no. 6, pp. 2834–2842, 2014, doi: 10.1016/j.actbio.2014.02.002.

[136] D.-H. Leem, Yea-Hyun and Lee, Kang-Sik and Kim, Jung-Hwa and Seok, Hyun-Kwang and Chang, Jae-Suk and Lee, “Magnesium ions facilitate integrin alpha 2-and alpha 3-mediated proliferation and enhance alkaline phosphatase expression and activity in hBMSCs,” *J. Tissue Eng. Regen. Med.*, vol. 10, pp. 527–536, 2016, doi: 10.1002/term.

[137] R. W. Li *et al.*, “The influence of biodegradable magnesium alloys on the osteogenic differentiation of human mesenchymal stem cells,” *J. Biomed. Mater. Res. Part A*, vol. 102, no. 12, pp. 4346–4357, 2014.

[138] L. Díez-Tercero, L. M. Delgado, E. Bosch-Rué, and R. A. Perez, “Evaluation of the immunomodulatory effects of cobalt, copper and magnesium ions in a pro inflammatory environment,” *Sci. Rep.*, vol. 11, no. 1, pp. 1–13, 2021, doi: 10.1038/s41598-021-91070-0.

[139] F. da S. Lima and R. A. Fock, “A review of the action of magnesium on several processes involved in the modulation of hematopoiesis,” *Int. J. Mol. Sci.*, vol. 21, no. 19, pp. 1–22, 2020, doi: 10.3390/ijms21197084.

Part III. Publications

III.1. CppyABM: an open-source agent-based modeling library to integrate C++ and Python

Agent-based modeling (ABM) is a popular method for examining the complex behavior that arises from the interactions between multiple autonomous agents. Both Python and C++ are widely used for ABM due to their unique characteristics. C++ offers exceptional performance, while Python provides ease-of-use and extensive libraries for data science, visualization, and machine learning. To bring together these benefits, we present CppyABM, a framework that offers uniform ABM semantics and development styles in both C++ and Python, as well as the tools to bind functions and types from C++ to Python. With CppyABM, users can choose either language depending on their expertise and the nature of the model, or combine them to take advantage of both. We demonstrate the capabilities of CppyABM through examples in computational biology, ecology, and virology, implemented using different combinations of C++ and Python, and compare the performance of these implementations. Our results indicate that models entirely or partially implemented in C++ outperform those that are purely implemented in Python.

Nourisa J, Zeller-Plumhoff B, Willumeit-Römer R. CppyABM: An open-source agent-based modeling library to integrate C++ and Python. Software: Practice and Experience. 2022. 52(6). 1337-51. DOI: 10.1002/spe.3067.

Contribution of Jalil Nourisa:

Literature search	Problem definition	Software development	Data analysis	Manuscript drafting
Primary role	Primary role	Primary role	Primary role	Primary role

Received: 16 February 2021 | Revised: 21 July 2021 | Accepted: 24 December 2021

DOI: 10.1002/spe.3067

RESEARCH ARTICLE

WILEY

CppyABM: An open-source agent-based modeling library to integrate C++ and Python

Jalil Nourisa | **Berit Zeller-Plumhoff** | **Regine Willumeit-Römer**

Institute of Metallic Biomaterials, Helmholtz Zentrum Hereon, Geesthacht, Germany

Correspondence
Jalil Nourisa, Institute of Metallic Biomaterials, Helmholtz Zentrum Hereon, Max-Planck-Straße 1, 21502 Geesthacht, Germany.
Email: jalil.nourisa@hereon.de

Funding information
Helmholtz Zentrum Hereon

Abstract

Agent-based modeling (ABM) has been extensively used to study the collective behavior of systems emerging from the interaction of numerous independent individuals called agents. Python and C++ are commonly used for ABM thanks to their unique features; the latter offers superior performance while the former provides ease-of-use and rich libraries in data science, visualization, and machine learning. We present the framework CppyABM that unifies these features by providing identical ABM semantic and development styles in both C++ and Python as well as the essential binding tools to expose a certain functionality from C++ to Python. The binding feature allows users to tailor and further extend a type or function within Python while it is originally defined in C++. Using CppyABM, users can choose either C++ or Python depending on their expertise and the specialty of the model or combine them to benefit from the advantages of both languages simultaneously. We provide showcases of CppyABM capabilities using several examples in computational biology, ecology, and virology. These examples are implemented in different formats using either C++ or Python or a combination of both to provide a comparison between the performance of implementation scenarios. The results of the example show a clear performance advantage of the models entirely or partly implemented in C++ compared to purely Python-based implementations.

KEYWORDS

agent-based modeling, C++, Python

1 | INTRODUCTION

Agent-based models are used to simulate complex phenomena which are composed of discrete entities called agents that interact with one another and with the environment.[1–3] The motivation behind agent-based modeling (throughout this article, both "agent-based modeling" and "agent-based model" are designated as "ABM") is to investigate the population-level macroscopic properties emerging from agents acting on the microscopic scale.[1,4] ABM is widely used

Abbreviations: ABM, agent-based modeling; DSLs, domain-specific languages; NNs, neural networks.

in many disciplines such as ecology, climate science, economics, biology, agriculture, sociology, and social sciences.[5,6] Significant attention has been given to the development of ABM toolkits in the past two decades, and numerous software and libraries have been developed with different features and capabilities.[7–14] However, despite a large number of ABM tools, there is still a substantial tendency among engineers and scientists to develop in-house models from scratch. This can be time-consuming, error-prone, and potentially pose transparency and reusability issues.[7,15] Although such decisions can stem from many reasons, the shortcomings of the current ABM toolkits can play a significant role in this matter.[7,16,17]

A large number of general-purpose ABM software including the famous platform of Netlogo[8] provide modeling tools through domain-specific languages (DSLs).[5,12] DSLs serve to ease the model development process by offering a clear, high-level, easy-to-read syntax.[18,19] However, they pose several disadvantages such as the cost of learning a new language, the constraints in the contribution of non-domain experts in the development process, the difficulties in integration with other libraries and frameworks, and the lack of a large support community.[18,19] By contrast, open-source ABM libraries such as Mason[11] and Repast[9] that use public programming languages as the user interface can potentially mitigate the aforementioned problems.[5,12] These libraries provide template classes and built-in functions that are designed to be further tailored and extended according to the specialties of novel ABMs.[12,20] However, the majority of such platforms suffer from excessive complexity in design, lack of sufficient documentation, and intrinsic limitations associated with the programming languages underlying the software.[12]

Based on several surveys, ABM libraries are dominantly available in two programming languages of Java and C++.[12,20–22] Since these languages offer modularity in the code design by leveraging object-oriented programming, they particularly favor the nature of ABM.[23] Java is a compiled language that executes on all operating platforms with no further measure, which makes it an appealing choice for software developers. C++ owes its popularity to performance and efficiency in memory management and is therefore suitable for large-scale simulations. However, despite numerous merits, coding in C++ and, to a relatively lesser extent, Java can be fairly cumbersome, rendering it unsuitable in particular for rapid prototyping and testing purposes.[24] In addition, Java and C++ lack rich data analysis and machine learning libraries which are commonly used in ABM.[3,25,26] The latter is of particular importance due to the increasing trend of incorporating neural networks (NNs) into ABMs to address the complexities in governing the agents' decision-making processes.[27,28] Such simulations are heavily based on the continuous communication between NNs and ABMs and therefore require a native interface between the two model types to reduce the computational overhead. Although there have been several attempts to introduce machine learning libraries into Java and C++,[29–31] the versatility, ease of use, and the available community in these domains are deficient especially compared to languages such as Python and R. Therefore, the choice of Java and C++ for fast prototyping, model training, data analysis, and visualization can be significantly difficult and time-consuming.

By comparison, Python as a cross-platform, general-purpose programming language, characterized as an easy-to-use interactive program, is a strong choice for rapid prototyping.[32] Python offers a broad range of versatile libraries for data analysis, visualization, optimization, and machine learning as well as a large community for support.[32,33] Python has also been used in several ABM toolkits to primarily serve as a plugin language to extend certain functionalities[12] and also as the prime language of Mesa.[34] Mesa, as a Python-based ABM library, has gained popularity in the last few years mainly for small-scale simulations. However, Mesa suffers from several problems in its design that prevent it from becoming a suitable choice for broader use cases. First, Mesa only enables simulations in two dimensions, while there is a substantial demand in the ABM community toward three-dimensional modeling.[12,35] Second, the architecture of Mesa lacks the so-called "Patch" class which is commonly implemented in other ABM platforms to model non-movable domain variables.[8,11,12,36] Moreover, the choice of Mesa for medium scale and large scale ABMs faces serious challenges due to the inherent performance issues associated with Python as a high-level programming language.[37]

In order to make use of the advantages of both C++ in terms of computational efficiency and Python in terms of prototyping and available data science and machine learning libraries, we propose a free, open-source ABM library named CppyABM to combine the power of both languages in a single platform. In the following, we will first present the design, features, and capabilities of the proposed library and then provide three examples as showcases of its application.

2 | CPPYABM

CppyABM is a C++ 17 based, header-only ABM library available under the Apache 2.0 License.[38] The library uses smart pointers for efficient memory management, standard containers for simplicity and robustness, and Cmake for

platform-free compilation. CppyABM employs pybind11 to expose types and functions from C++ to Python. The documentation of the library is available on GitHub.*

2.1 | Design

ABM is possible via object-oriented programming in CppyABM as depicted in Figure 1. The three classes of *Env*, *Agent*, and *Patch* are available to serve as the base components of ABM. The *Agent* class abstracts movable objects, whereas *Patch* is designed to simulate the properties of non-movable elements. A *Patch* object can accommodate agents as well as heterogeneous variables across the domain. The *Env* class is designed to provide essential tools to coordinate model components. In the design of CppyABM, there is a three-way connection between the base classes of *Env*, *Agent*, and *Patch* which enables full information retrieval among the model components; (1) within the *Env* class, pointers to all *Agent* and *Patch* objects are accessible through STL† containers; (2) *Agent* and *Patch* objects store an internal pointer to the *Env* object which allows them to access universal variables and functions; and (3) an *Agent* and its host *Patch* hold a pointer to one another's objects (see Figure 2A). These connections are updated once the *Agent* relocates to a new *Patch*. In order to keep these mutual connections valid for the models inheriting the base classes, we use a template pattern in the design of CppyABM which updates the pointers by receiving the declaration of the derived classes (see Figure 1).

In the design of CppyABM, the *Env* object stores *Agent* and *Patch* classes as shared pointers. However, the mutual connections between *Agent* and *Patch* and their connections to the *Env* object are all created using weak pointers. This design allows single ownership of the objects within the *Env* class and therefore prevents memory leakage once an object is removed from the model. For example, if an agent is deleted from the container, its connection to the host patch will be eliminated automatically.

2.2 | Multi-agent and multi-patch simulation

CppyABM enables the simulation of multi-agent systems in two different ways; through the specialization of the *Agent* class uniquely for each class of agents, or using the class attribute of `agent-class` to define distinguished behavior for each subset of agents. The former requires setting up a new class for each agent type, while the latter allows encapsulation of all properties of agents in one class. The class attribute of `agent-class` is defined during the creation of Agent objects

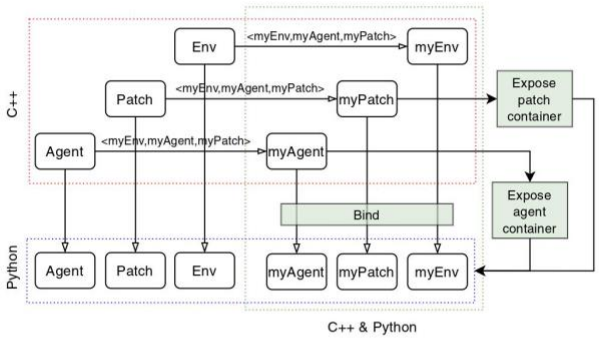

FIGURE 1 The scheme of agent-based model development in CppyABM. The base classes of *Env*, *Patch*, and *Agent* are originally written in C++ but are out-of-the-box identically available in Python. These classes can be inherited in both languages to construct agent-based models. In C++, the base classes are inherited by providing the declaration of the derived classes, for example, *myEnv*, *myAgent*, and *myPatch*, as template arguments to update the internal connections between the components. The ABM written in C++ can be fully or partly exposed to Python for further development using the built-in class of `Bind`. This class executes a series of functions to expose default members and functions as part of the derived classes. *Agent* and *Patch* containers are exposed using `EXPOSE_AGENT_CONTAINER` and `EXPOSE_PATCH_CONTAINER`, respectively, to reflect the changes made in Python to the original copies of the objects. The full arrows indicate inputs while the empty arrows indicate inheritance

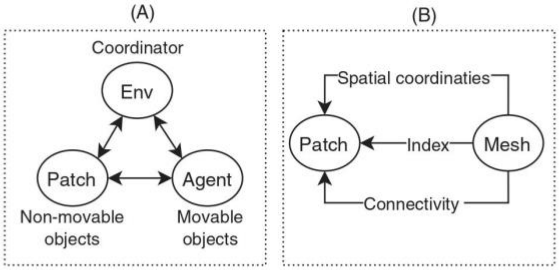

FIGURE 2 (A) Three-way connectivity of CppyABM base classes which enables full accessibility within a model. (B) The geometry discretization is done by using Mesh objects that contain spatial information of elements such as coordinates and connectivity to adjacent elements. By having this information, any complex geometry can be simulated using the *Patch* class

by assigning a unique name, that is, the label of the agent class. This label can then be used to define functions unique to each agent type.

In CppyABM, the *Patch* class is designed to simulate non-movable objects. The Patch object can also accommodate agents. A single-patch object is defined to allow only one resident agent at a time, while a multi-patch can incorporate more than one agent at a time. The Patch class in CppyABM is by default multi-patch, that is, permitting more than one agent to be stored in a single patch. However, all built-in functions, which are involved in the management of the residing agents, can be instructed to allow only one agent. For example, the *Env* function of `place_agent`, which locates a given agent object, for example, `agent_obj`, at the given patch object, for example, `destination_patch`, requires a flag argument of `True` or `False`, indicating whether to allow multiple agents in a patch or not, respectively.

2.3 | Object storage and management

Agent and *Patch* objects are stored in separate STL containers within the *Env* class; a map container is used to store *Patch* objects where each object is identified by a unique ID called *index* (see Figure 2B); *Agent* objects are stored in a vector container. The template functions of `generate_agent` and `generate_patch` are available to instruct *Agent* and *Patch* objects generation, respectively. These functions require minimum adjustment from users to correctly create and store these objects. Using these functions is especially recommended within Python models in order to handle issues that arise due to differences in object management between Python and C++. Python by nature requires object ownership. Therefore, the real objects need to be stored in Python while C++ holds pointers to the objects. To this end, these functions are designed to store the real objects within Python and add a copy of them to the standard containers in C++ as shared pointers. This approach only requires duplicate memory for the storage of the pointers but not the real objects and is therefore negligible. The agent and patch repositories within Python need to be constantly updated to remove inactivated agents and eliminate the risk of memory loss. This task is done by the `update_repo` function.

2.4 | Modeling space

CppyABM enables ABM on arbitrary two- or three-dimensional geometries. In the library's design, a discrete representation of the geometry containing spatial coordinates and connectivity is encapsulated in a *Mesh* object. For regular 2D and 3D geometries, the library provides the essential tools to generate *Mesh* objects. For complex geometries, the user can manually construct a set of *Mesh* objects and then create patches according to the specifications of the mesh (see Figure 2B). *Patch* objects are identified by *index* variables similar to *Mesh* elements. This design allows the constructed ABM to directly communicate with another model created using the same mesh and thereby powers the notion of multiscale modeling.[39]

Env	Agent	Patch	Meshing tools	Binding tools
setup_domain setup_agents place_agent remove_agent process_move process_hatch random_activation serial_activation	move order_move order_hatch order_switch disappear	index coords neighbor_patches set_agents get_agents remove_agent empty_neighbor neighbor_agents	space::grid2 space::grid3	EXPOSE_AGENT_CONTAINER EXPOSE_PATCH_CONTAINER Bind expose_defaults expose_env expose_agent expose_patch

FIGURE 3 A shortlist of the built-in functions and class members provided by CppyABM to assist in agent-based model development

2.5 | Built-in functions

A series of built-in functions are provided to assist in model development as shown in Figure 3. For example, within the *Env* class, `setup_domain` and `setup_agents` assist in the initialization of the model by automatic creation of *Patch* and *Agent* objects, respectively. The functions of `activate_serial` and `activate_random` set the execution order of the agents into serial and random, respectively. Within the *Agent* class, functions such as `order_move` and `order_hatch` automatically take care of *Agent* movement and replication, respectively, by receiving a few instructions as arguments. Within the *Patch* class, several built-in functions exist to manage the setting and removal of residing agents and local variables. To create a mesh, so far two built-in functions of `grid2` and `grid3` are available that create a rectangular domain in two- and three-dimensional space. These functions provide the option of defining periodic boundary conditions in which the facing edges/surfaces share a neighborhood. Additionally, CppyABM provides several functions for Python binding of an agent-based model written in C++.

2.6 | Python binding

In principle, two types of bindings are provisioned in CppyABM, namely embedding and extending. The former exposes types, classes, and functions written in C++ to Python. The latter allows a functionality originally declared or defined in C++ to be implemented or further extended in Python. A typical binding process can consist of a mix of both types and generally follows three main steps; (1) the exposure of agent and patch containers. pybind11 automatically converts variables that are constructed from the STL container. This internal conversion does not allow pass-by-reference semantics by default and thereby any modifications made in Python are not valid within C++. To overcome this, the agent and patch containers that are STL-based are defined as *opaque* which disables this automatic conversion. CppyABM offers two functions of `EXPOSE_AGENT_CONTAINER` and `EXPOSE_PATCH_CONTAINER` to serve this purpose. These functions are called on the derived agent and patch classes before the binding process begins (see Figure 1); (2) the exposure of default attributes. Several essential functions and classes such as exceptions, mesh generators, and default members of the base classes are automatically exposed using the built-in class of `Bind`. The class executes several built-in functions such as `expose_defaults`, `expose_env`, `expose_agent`, and `expose_patch`; (3) the exposure of additional attributes of derived classes. Pybind11 semantics of `def` and `def_readwrite` are used to bind class members and functions, respectively. These functions are called on the class objects returned by `Bind` defined in step (2).

In order to expose a model from C++ to Python for extension purposes, an additional step is required to inform the module that the given function needs to be (further) implemented in a later stage. To this end, a trampoline class is required to be defined and passed to the expose functions introduced in step (3). The three classes of `tramEnv`, `tramAgent`, and `tramPatch` are provided by CppyABM to automatically define trampolines for the default members. To expose a new function defined in the derived class, the built-in trampolines must be inherited and extended to incorporate the new additions. For this purpose, the pybind11 function of `PYBIND11_OVERLOAD` is used to expose new class functions. A detailed explanation including examples for both embedding and extension is available in the online documentation.

2.7 | Visualization

We use a free open-source Python library named RTvisualize[40] for real-time visualization of agent-based models. The package is developed in-house and licensed under MIT for public use. Several built-in functions are provided for the automatic generation of plots such as scatter and line plots. For further flexibility, the package can also receive plot functions from the user to fully customize the graphs. For ABM, the built-in scatter plots can be used for the realization of agents in the spatial domain, the map plots can serve to visualize heterogeneous variables across the domain, and the line plots can monitor the progression of a variable in the course of the simulation. Both scatter and map plots visualize the snapshot of the system in a given visualization step, in contrast to line plots that incorporates the element of time. In order to use RTvisualize in its current version, users are instructed to output their real-time data in the form of CSV files in a specific format depending on the desired graph type. To visualize agents in the spatial domain using the scatter plot, the user should provide the coordinates, that is, x, y, and z, of each agent together with the name, size, and the desired color of agents. The coordinates of each agent can be obtained by retrieving the `coord` variable of the host Patch. This enables a multi-agent display of the agents' positions in the space as they can be distinguished based on their type, size, and color. Further information can be also visualized on the agents by setting up customized graphs. Similarly, the map plots receive the coordinates of patches together with the specific quantities intended for visualization. The line plots receive a vector of data for each variable tagged by the variable's name. Such plots can visualize as many variables as intended on a single graph. RTvisualize reads and visualizes the content of the CSV files and actively updates the graphs according to instant changes made to the files.

2.8 | Batch runner

Due to the stochastic nature of ABMs, multiple repetitions of a simulation are required to correctly observe a pattern in the outcomes. CppyABM provides a tool named "batch runner" to enable the execution of multiple replicas of a model. The batch runner receives the model object and executes the simulation for the given number of times, either in serial or parallel. This tool is available in both Cpp and Python. The parallelization is performed using Message Parallel Interface (MPI) which can significantly reduce the computational time.

2.9 | Integration of third-party packages

CppyABM is intended to be a lightweight library and does not provide statistical, data analysis, or machine learning libraries out-of-the-box. However, the third-party libraries such as SciPy and NumPy for python or GSL and Boost for C++ can be installed separately, and integrated into CppyABM during simulation. The example section displays the showcases of such integrations.

3 | SHOWCASES OF CPPYABM

In this section, three examples in different domains of simulation with unique requirements are provided. The first example is a use case of a single patch model where each patch can only accommodate one agent at a time, while examples 2 and 3 allow multiple agents in a patch. Complex behavioral properties of agents such as relocation, proliferation, inheritance from mother agents, dying, and switching between different agent types are presented in these examples.

3.1 | Agent-based simulation of cellular interactions

In recent years, an increasing number of studies have been using ABM to simulate cell and molecule interactions for the investigation of the patterns of various tissue growth.[41–43] We use an idealized model of tissue regeneration following damage to demonstrate the application of CppyABM (see Figure 4). In this model, a square simulation domain consisting of a 1000×1000 grid is created, where each patch has a length of $15\,\mu m$ which corresponds to the average cell size and only accommodates one agent at a time. 2000 cells are initially distributed randomly in the domain except in

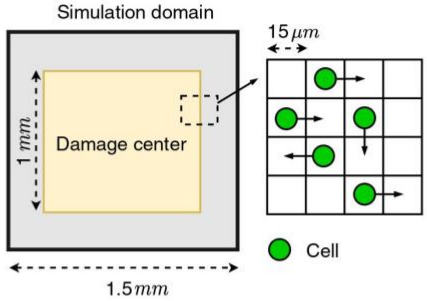

FIGURE 4 The simplified model of tissue regeneration following injury. Damage is created in the center of the simulation domain where the residing cells and tissue are wiped out. During the simulation, cells interact with one another and with the environment and as a result, produce tissue

the damage center where cells are eliminated due to the damage. The model allows cells to migrate and proliferate to infiltrate the damaged site and synthesize new tissue to heal the damage. Cells can also die if there is a high concentration of cells due to nutrition deficiency. Each step of the model corresponds to 1 h of healing time. The simulation runs for 14 days.

Two general approaches are taken for the implementation of the described example. First, the example is implemented in two formats using purely Python (Py) or purely C++ (Cpp), which is described in Section 3.1.1. Second, the models developed in the previous approach are extended to include new functionalities as described in Section 3.1.2. Both models of Py and Cpp were extended similarly within Python. The purpose of this section is to demonstrate the implementation and binding tools available in CppyABM as well as to compare the performance of Python versus C++ using the mixed models of both. The documented examples are available online.[‡]

3.1.1 | Primary models

The *Cell* class is defined based on *Agent* to simulate cellular reactions. The *Patch* class is extended as *Tissue* to encapsulate the properties of tissue such as the local density of extracellular tissue matrix (ECM). The *Domain* is designed as an extension of *Env* to initialize the model and run the simulation. The schematic of the simulation is depicted in Figure 5. The model was initialized by (1) creating a mesh using the built-in function of `grid2`, (2) setting up patches according to the mesh using `setup_domain`, and (3) generating agents and randomly distributing them among the patches. Once the model is initialized, an iterative process is implemented in which first an individual call is sent to the `step` function of cell objects to perform cellular reactions, and second, the domain is updated to reflect the cells' outcomes to the simulation world. The built-in functions of `order_move` and `order_hatch` are used for cell migration and proliferation, respectively. Once a cell is programmed to die, the internal flag of `disappear` is set to `true`. The library takes care of the agent's removal from the repository as well as freeing the host patch. The model is visualized in real-time by outputting the cell distribution in the domain, the density map of ECM, and the trajectory of cell count in the course of healing.

3.1.2 | Extended models

In the extended model, the attribute `cycle_t` of *Cell*, which determines cell proliferation cycle and was a constant in the previous models, is set differently for each *Cell* object using a NN model. To this end, a new attribute termed `age` is added to the *Cell* class and is set to an arbitrary value between 0 and 100. Also, a single-layer NN model with an arbitrary number of 128 nodes is created by randomly initializing its weights. The NN model is added as a new variable of *Cell* termed `policy` which receives `age` as the input and estimates `cycle_t`. These modifications account for the fact that cells become less proliferative due to aging. The NN model is implemented as a Python class using the third-party library of PyTorch and is imported to the main program. The implementation of the NN model can be found online.[§]

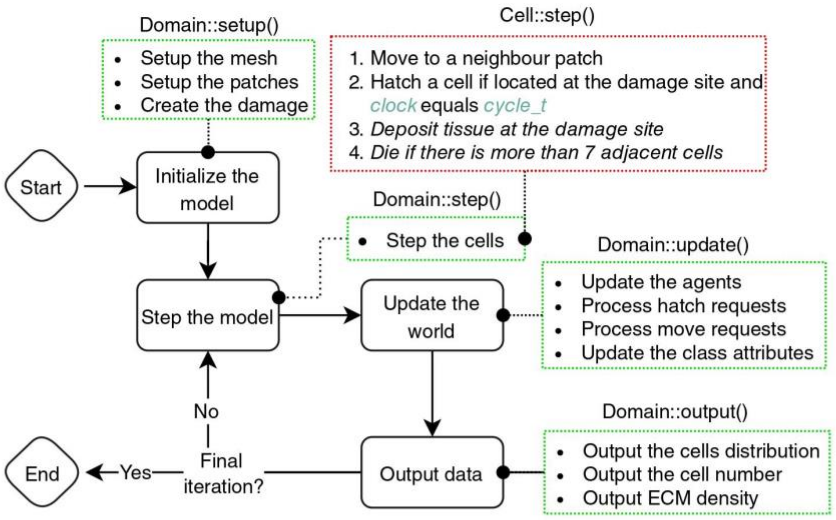

FIGURE 5 The schematic of the simulation of tissue regeneration after injury. The processes contained in green boxes are carried out within the *Domain* class while those in red are executed in the *Cell* class. Once the model is initialized using the `setup` function of the *Domain* class, an iteration process starts. At each iteration, the `step` function of *Cell* is executed to perform cellular reactions. Then, the `update` function of *Domain* is called to execute the hatch and move requests received from the agents. After, the domain updates the variables, outputs the data for visualization, and starts a new iteration. This process continues until the iteration step (t) reaches the final step (t_f)

The described changes are accommodated in two models of Pyy and Cppy which are built on top of Py and Cpp, respectively. Pyy is the extended version of Py, entirely written in Python. To implement this addition in Cppy, the model written in C++, that is, Cpp, is exposed and extended within Python as depicted in Figure A1. The extended models initialize cells with a unique `cycle_t` value for each cell using the NN model. The rest of the model execution is identical to the previous models. For different implementation scenarios, the class members and methods of *Domain*, *Cell*, and *Tissue* were given in Figure A2. It can be seen that the described models are mostly similar. However, since the models in Python need to store the objects locally (see Section 2.1), two functions of `generate_agent` and `generate_patch` have an extra step of storing the agent and patch objects within Python. The local variables of `agents_repo` and `patches_repo` are assigned as the storage for agents and patches, respectively. Also, the function `update_repo` is defined within Python to frequently update `agents_repo` by removing inactive agents.

In order to account for the inherent stochasticity in the agent-based model, we ran all models 10 times.

3.1.3 | Results

The results of the simulation of the tissue regeneration in response to damage are given in Figure 6. Initially, cells populate the border of the damage site (day 2) and then infiltrate into the center via the migration process (Figure 6A). In the meantime, cells deposit ECM to heal the damage which starts to appear on day 2 and completely covers the damage center on day 14 (Figure 6A). The evolution of cell numbers in the course of simulation is given in Figure 6B. The primary models, that is, Cpp and Py, produced similar trends for the cell count over the course of the simulation. Similarly, the results obtained for the extended models, that is, Cppy and Pyy, were similar but slightly different from the previous two models (Figure 6B). The observed differences among these models can be explained by the value assigned for the cell proliferation cycle, that is, `cycle_n`. In the primary models, it is assumed that cells proliferate every 12 h, that is, `cycle_n = 12`. In the extended models, `cycle_n` is determined based on the age of the cell using the neural network model. The variable of age is set to a random variable between 0 and 100. Since the neural network model is initialized arbitrarily, the results indicate that the input–output of the model creates an average `cycle_n` of lower than 12. Therefore, cells proliferate faster, and also reach the plateau faster (see Figure 6B). From the computational angle, Cpp, Py, Cppy, and Pyy required on average of 11, 67, 121, and 181 MB of memory, respectively, and took 39, 104, 75, and 154 s CPU time, respectively

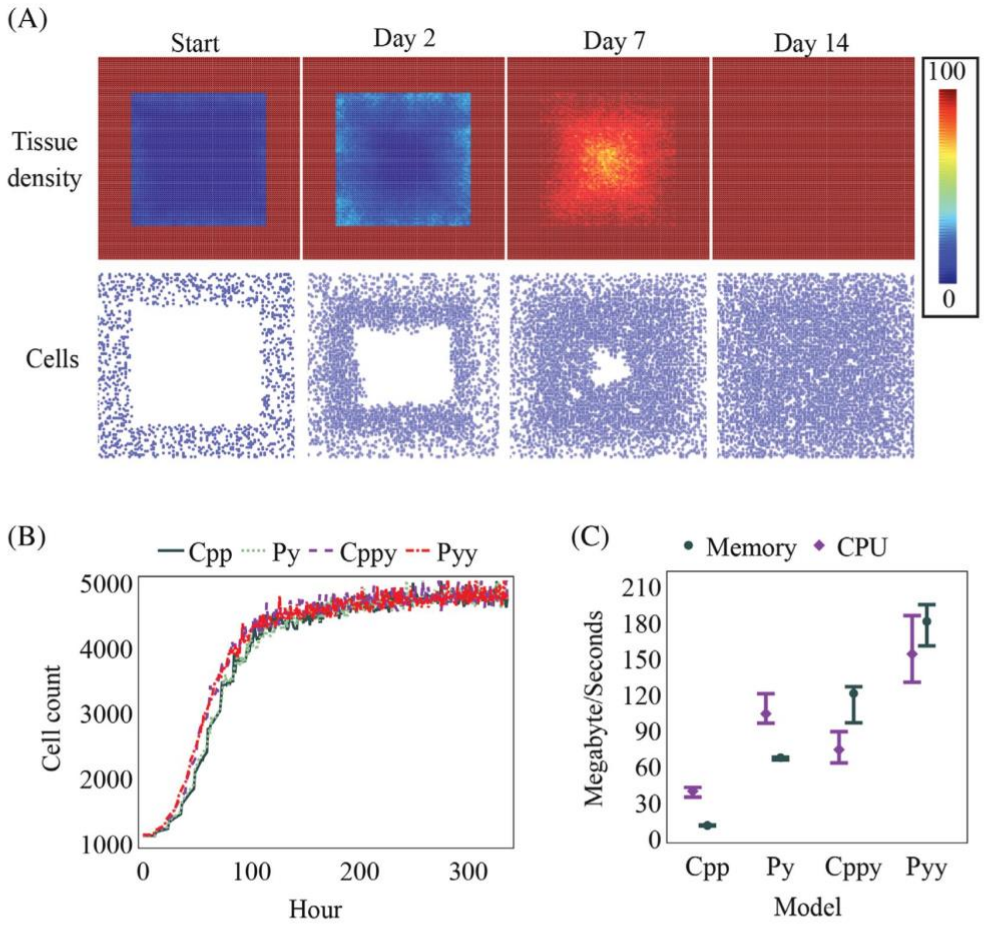

FIGURE 6 The simulation results of the tissue regeneration following an injury. (A) The evolution of cell distribution and tissue density within the simulation domain. (B) The trajectory of cell number in the course of healing. (C) A comparison of memory usage (MB) and CPU time (s) consumed for different models. The data represent medians and variations of the results obtained from 10 times run. Cpp and Py simulate the primary cellular model (see Section 3.1.1), while Pyy and Cppy simulate the extended cellular model (see Section 3.1.2)

(Figure 6C), by running on a personal MacBook (3.1 GHz Dual-Core Intel Core i5) with the Clang version of 11.0.3 and Python version of 3.7.9.

3.2 | Agent-based simulation of wolf sheep predation

In this section, the famous example of the wolf sheep predation is reimplemented using CppyABM.[¶] This example shows the importance of stability in predator–prey ecosystems where the system maintains itself despite the fluctuations in the population sizes. This simple ecological model consists of three main entities of wolves, sheep, and grass. The wolves and sheep move randomly in the field. Wolves eat sheep, and sheep feed on grass. Both wolves and sheep spend energy per move and die if they run out of energy, which is refilled by feeding. They both asexually breed by giving birth to a new wolf or sheep. The grass replenishes at a constant rate.

The described problem is simulated in three formats of purely Cpp, purely Python, and mixed Cpp and Python. They are denoted as Cpp, Py, and Cppy, respectively, in the rest of the section. The *Agent* class is specialized to simulate the behavioral properties of wolves and sheep which represents a multi-agent problem. In the Py model, two separate classes of *Wolf* and *Sheep* are defined to specialize the behavioral properties of wolves and sheep,

respectively. However, in the Cpp model, the single class of *Animal* is created to simulate both sheep and wolves. In this approach, the class attribute of `agent_class` is used to define different properties according to the agent type. These different approaches demonstrate the different possibilities of multi-agent simulation in CppyABM, as discussed in Section 2.2. The rest of the implementation is identical between Cpp and Py. The *GrassPatch* is defined as the specialized form of *Patch* class to simulate the growth of grass. The patch object allows the co-existence of multiple agents at once, that is, multi-patch properties. The *WolfSheep* class is defined based on the *Env* class to store the agent and patch objects and to run the simulation. In the Cppy implementation, the *Patch* and *Agent* classes are written in Cpp, and the *Env* class is implemented in Python. The documented examples are available online.**

The model is initialized by randomly distributing the agents among the patches. Then, the model is iteratively executed for the given number of steps. At each time step, the agents commit four actions; randomly moving one patch at a time; feeding (either grass or sheep depending on the agent type), breeding (if the condition is met), and dying (if the condition is met). A square domain consisting of 100×100 units are created as the simulation environment. 2000 sheep and 500 wolfs are initially introduced to the model. The fate of the modeled ecosystem is controlled by five parameters; the reproduction rates of sheep and wolves; the quantity of the energy received by eating ($\times 2$ for sheep and wolves); and the regrowth rate of the grass. The simulation runs 1000 steps and is repeated 20 times to account for the stochasticity in the system. We studied the effect of the regrowth rate of sheep on the population dynamics by running the in-silico experiments for two different values of this parameter.

3.2.1 | Results

The fluctuation in the population of the wolves and sheep obtained from the simulation is given in Figure 6A,B. It can be seen that the system reaches a stable population for both species for different reproduction rates assigned for sheep. Similar observations can be found by alternating other parameters as long as the remaining proportion of sheep to wolf is sufficient enough for the wolves to sustain life. From the computational angle, Cpp, Py, and Cppy required on average of 26, 72, and 47 MB of memory, respectively, and took 35, 154, and 66 s CPU time, respectively (in Figure 6C), by running on a personal MacBook (3.1 GHz Dual-Core Intel Core i5) with the Clang version of 11.0.3 and Python version of 3.7.9.

3.3 | Agent-based simulation of the spread of infectious diseases such as COVID-19

To demonstrate the application of CppyABM for a real-world problem, we reimplement the model published by Núñez-Corrales and Jakobsson 2020,[44] which is available on the GitHub repository.†† This study simulates the spread of infectious diseases such as COVID-19. The model is composed of a 2D lattice model with 225×190 units and 1000 agents distributed randomly within the domain. Each single grid, that is, patch, is allowed to accommodate more than one agent at a time, that is, multi-patch. Each step in the model accounts for 15 min, which is the minimum amount of time needed for a susceptible person to acquire the virus once located in the same grid as an infected person, that is, Dwell time. Agents can move randomly one patch at a time in their Moore neighborhood after spending the Dwell time in the current location.

The model is calibrated based on the demographic data obtained for the Champaign-Urbana Public Health District. Among these data are the important parameters of the initial proportion of agents that are exposed to the disease, the proportion of individuals who remain asymptomatic, the proportion of severe cases, and the probability of contagion per agent per interaction. The mortality rates are associated with gender (male/female) and age groups (every 10-year intervals), that is, male has a higher mortality chance compared to female, and the mortality rate increases by age. The simulation runs for 153 days (14,688 iterations of 15 min), similar to the original model, with the replica number of 30 to account for the stochasticity of the model. The number of active cases, that is, symptomatic positive, is studying for the different scenarios of (1) 25% of the population is tested, (2) 50% of the population is tested, (3) 75% of the population is tested, and (4) no testing is conducted. These scenarios are combined with the process of lifting the shelter at home order, that is, individuals are not constrained to their position, on day 125. Further information about this example is given in Appendix A.

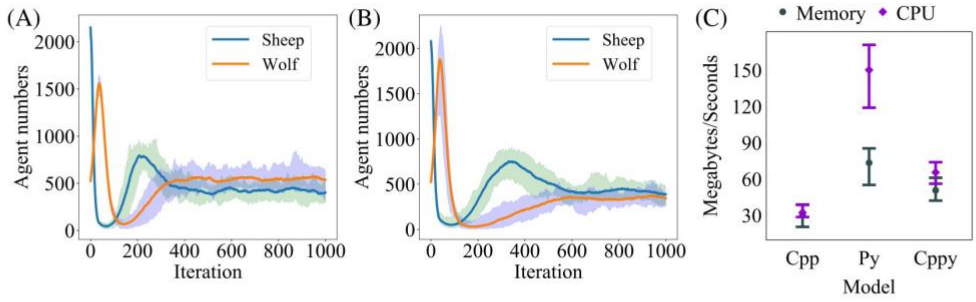

FIGURE 7 The simulation results of the wolf sheep predation. The trajectory of the wolfs and sheep numbers in the course of the simulation for the scenarios of (A) the sheep reproduction chance of 0.04 per iteration and (B) the sheep reproduction chance of 0.08 per iteration. The solid line and the shadowed area show the mean and the heterogeneity of the results obtained from 20 replicas of the same model. (C) A comparison of memory usage (MB) and CPU time (s) consumed for the models of Py (purely Python), Cpp (purely Cpp), and Cppy (a mix of Python and Cpp). The data represent medians and the standard deviation of the results obtained from 20 replicas of the same model

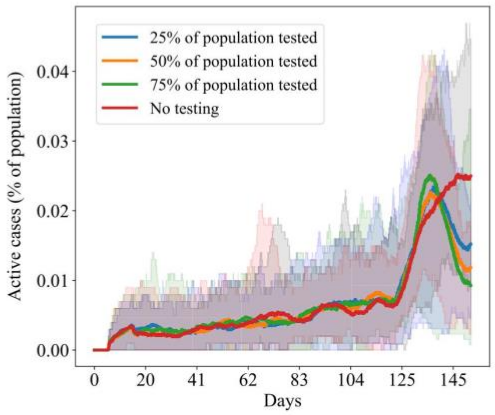

FIGURE 8 The simulation results of the spread of COVID-19. The trajectory of the active cases (symptomatic positive) is given in the course of the simulation for the different scenarios of no testing, 25%, 50%, and 75% testing of the whole population. The solid line and the shadowed area show the mean and the heterogeneity of the results of 30 replicas of the same model. The number of the infected cases increase in the course of simulation. The sharp jump on day 125 is caused due to lifting the order of the shelter at home

3.3.1 | Results

The development of the number of active cases in the course of simulation is given in Figure 8. The sharp jump on day 125 is due to lifting the restriction of the shelter at home. It can be seen that testing can significantly control the number of active cases as the more fraction of the population is tested, the lower the active cases. For further discussion, refer to the original article.[44] It can be also seen that the stochasticity in the system causes large variations in the results (notice the shaded area in Figure 7). Therefore, the high number of replicas is essential to draw a valid trend in the results. Similar trends are presented in the original paper.[44]

4 | DISCUSSION

In order to demonstrate the application of CppyABM, we simulated several problems from different disciplines in different formats of Cpp, Py, and Cppy (see Section 3). While simulating the same problem, Cpp required a significantly lower amount of memory and CPU time compared to Py (see Figures 6C and 7C). That is, the memory usage and CPU time were, respectively, 6 and 2.67 times smaller in example 1 and 2.7 and 4.4 times smaller in example 2. The memory usage

and CPU time required by Cppy were 1.5 and 2 times less than Pyy in example 1. Similarly, the memory usage and CPU time required by Cppy were 1.6 and 2.3 times less than Py in example 2. This directly stems from higher memory usage and inferior performance of Python compared to C++. In example 1, the considerable increase in the memory usage of Cppy and Pyy compared to the Cpp and Py is due to the inclusion of the NN model. For the mixed model of Cppy, even though it simulates a larger process than Py, the required CPU time was still significantly lower (75–104 s). This shows the power of CppyABM in employing the performance of C++ within Python.

Additionally, CppyABM offers several improvements over the available Python-based library of Mesa. CppyABM provides 3D modeling on any arbitrary shape which is not available in Mesa. Also, Mesa provides only two generic classes of *Agent* and *Env* to serve as the basis of agent and environment development, respectively.[34] CppyABM distinguishes movable objects from non-movable ones by the addition of the *Patch* class, similar to Netlogo,[8] which offers more efficient management of different entities. In addition, the visualization in CppyABM is unbounded to the agent-based model's run. This allows independent model execution while any update to the model's results is visualized in real-time.

In CppyABM, agents are stored using an STL vector while patches are managed using an STL map. Allocating different storage containers for *Agent* and *Patch* objects permit separate management of each class's objects which can improve the execution efficiency. Map as a container offers efficient look-up time, that is, O(log[n]), and is therefore ideal for the management of *Patch* objects where they are stored and retrieved through *index* variables. However, agents are not identified via keys and therefore are stored in a vector container. The insertion of agent objects to the container always occurs from the end of the vector which is optimal. During the deletion process, the inactive agents are first relocated to the end of the vector and then deleted to avoid the overhead of memory reallocation. Within *Env* class, objects are retrieval is generally requested through iteration over the entire collections rather than look-up. Map and vectors offer similar performance for this purpose.

CppyABM in its current version has several limitations that require improvement in the future. First, the library runs in serial. Recent agent-based models tend to grow in size by simulating a large number of agents and thereby requiring high computational performance. We will employ parallel computing in the next steps to improve the applicability of the library for large-scale simulations. Third, the current visualization approach in CppyABM is based on RTvisualize which is a general-purpose visualization package. We intend to specialize this package for ABM to further automate visualization tasks. Fourth, CppyABM in its current version only provides tools for the creation of regular geometries. We will improve this by creating an interface to receive irregular geometries via standard formatting such as The Visualization Toolkit (VTK). Fifth, the entity of Edge, also known as Connector, is not implemented yet in CppyABM. This entity is an essential element of ABM on networks/graphs and will be accommodated in the next versions of CppyABM. Finally, the model binding from C++ to Python is currently based on Pybind11 which creates an overhead every time to probe the Python interpreter within C++. This is especially problematic when there is a frequent C++ call to a function defined within Python. We will improve the performance of such cases in the future.

5 | CONCLUSION

In this article, we proposed CppyABM as an open-source library for general-purpose ABM based on two public languages of C++ and Python. CppyABM provides ABM tools in both languages in identical syntax and development styles enabling users to choose the right language based on their expertise and the specifics of their simulations. Also, in order to fully benefit from the merits of both languages at the same time, CppyABM provides essential tools to exclusively expose certain parts of the model written within C++ to Python for further extension. Besides, the library provides several built-in functions that are widely demanded in ABM. These functions intend to ease the model development as well as reduce the risk of faulty implementation or memory mismanagement. Since these functions run within C++, they can also improve the performance compared to the equivalent code written in Python and are therefore recommended. CppyABM is an open-source project and is intended to be ever-evolving. Active development by the authors as well as the contribution of its future users will improve the library primarily in terms of scalability, visualization, and versatility.

ACKNOWLEDGMENT

This study was financially supported by Helmholtz Zentrum Hereon.

ENDNOTES

*https://github.com/janursa/CppyABM
†Standard Template Library.
‡https://github.com/janursa/CppyABM/tree/master/examples
§https://github.com/janursa/CppyABM/blob/master/examples/cellular_interactions/Pyy/policy.py
¶https://github.com/projectmesa/mesa-examples/tree/master/examples/WolfSheep
**https://github.com/janursa/CppyABM/tree/master/examples/wolf_sheep
††https://github.com/snunezcr/COVID19-mesa

DATA AVAILABILITY STATEMENT

The data that support the findings of this study are openly available in janursa/CppyABM v1.0.20 at https://doi.org/10.5281/zenodo.5120939.

ORCID

Jalil Nourisa https://orcid.org/0000-0002-7539-4396

REFERENCES

1. Railsback SF, Grimm V. *Agent-Based and Individual-Based Modeling: A Practical Introduction*. Princeton University Press; 2019.
2. Zou J, Huss M, Abid A, Mohammadi P, Torkamani A, Telenti A. A primer on deep learning in genomics. *Nat Genet*. 2019;51(1):12-18. doi:10.1038/s41588-018-0295-5
3. Beu TA. *Introduction to Numerical Programming: A Practical Guide for Scientists and Engineers Using Python and C/C++*. CRC Press; 2014.
4. Macal CM, North MJ. Agent-based modeling and simulation. Proceedings of the 2009 Winter Simulation Conference (WSC); 2009:86-98.
5. Allan RJ. *Survey of Agent Based Modelling and Simulation Tools*. Science & Technology Facilities Council; 2010.
6. Macal CM. Everything you need to know about agent-based modelling and simulation. *J Simul*. 2016;10(2):144-156.
7. Xiao J, Andelfinger P, Eckhoff D, Cai W, Knoll A. A survey on agent-based simulation using hardware accelerators. *ACM Comput Surv*. 2019;51(6):1-35. doi:10.1145/3291048
8. Tisue S, Wilensky U. Netlogo: a simple environment for modeling complexity. Proceedings of the International Conference on Complex Systems; Vol. 21, 2004:16-21.
9. Collier N. Repast: an extensible framework for agent simulation. *Univ Chicago's Soc Sci Res*. 2003;36:2003.
10. Luna F, Stefansson B. *Economic Simulations in Swarm: Agent-Based Modelling and Object Oriented Programming*. Vol 14. Springer Science & Business Media; 2012.
11. Luke S, Cioffi-Revilla C, Panait L, Sullivan K, Balan G. Mason: a multiagent simulation environment. *Simulation*. 2005;81(7):517-527.
12. Abar S, Theodoropoulos GK, Lemarinier P, O'Hare GMP. Agent based modelling and simulation tools: a review of the state-of-art software. *Comput Sci Rev*. 2017;24:13-33. doi:10.1016/j.cosrev.2017.03.001
13. Ghaffarizadeh A, Heiland R, Friedman SH, Mumenthaler SM, Macklin P. PhysiCell: an open source physics-based cell simulator for 3-D multicellular systems. *PLoS Comput Biol*. 2018;14(2):e1005991. doi:10.1371/journal.pcbi.1005991
14. Borshchev A, Brailsford S, Churilov L, Dangerfield B. Multi-method modelling: AnyLogic. *Discret Simul Syst Dyn Manag Decis Mak*. 2014;248-279.
15. Perkel JM. A toolkit for data transparency takes shape. *Nature*. 2018;560(7718):513-516.
16. Melo LS, Sampaio RF, Leão RPS, Barroso GC, Bezerra JR. Python-based multi-agent platform for application on power grids. *Int Trans Electr Energy Syst*. 2019;29(6):e12012. doi:10.1002/2050-7038.12012
17. Cardinot M, O'Riordan C, Griffith J, Perc M. Evoplex: a platform for agent-based modeling on networks. *SoftwareX*. 2019;9:199-204. doi:10.1016/j.softx.2019.02.009
18. Mernik M, Heering J, Sloane AM. When and how to develop domain-specific languages. *ACM Comput Surv*. 2005;37(4):316-344.
19. Fowler M. *Domain-Specific Languages*. Pearson Education; 2010.
20. Nikolai C, Madey G. Tools of the trade: a survey of various agent based modeling platforms. *J Artif Soc Soc Simul*. 2009;12(2).
21. Kardas G, Challenger M, Yildirim S, Yamuc A. Design and implementation of a multiagent stock trading system. *Softw Pract Exp*. 2012;42(10):1247-1273.
22. Briola D, Micucci D, Mariani L. A platform for P2P agent-based collaborative applications. *Softw Pract Exp*. 2019;49(3):549-558. doi:10.1002/spe.2657
23. Rezaeiye PP, Rezaeiye PP, Beig EFGM, et al. Agent programming with object oriented (C++). Proceedings of the 2017 2nd International Conference on Electrical, Computer and Communication Technologies (ICECCT); 2017:1-10.
24. Hadjerrouit S. Java as first programming language: a critical evaluation. *ACM SIGCSE Bull*. 1998;30(2):43-47.
25. Rand W. Machine learning meets agent-based modeling: when not to go to a bar. Proceedings of the Conference on Social Agents: Results and Prospects; 2006.
26. Kavak H, Padilla JJ, Lynch CJ, Diallo SY. Big data, agents, and machine learning: towards a data-driven agent-based modeling approach. Proceedings of the Annual Simulation Symposium; 2018:1-12.
27. van der Hoog S. Deep learning in (and of) agent-based models: a prospectus; 2017. arXiv Prepr arXiv170606302.

28. DeAngelis DL, Diaz SG. Decision-making in agent-based modeling: a current review and future prospectus. *Front Ecol Evol*. 2019;6:237.
29. Abeel T, de Peer Y, Saeys Y. Java-ml: a machine learning library. *J Mach Learn Res*. 2009;10:931-934.
30. Kohavi R, John G, Long R, Manley D, Pfleger K. MLC++: a machine learning library in C++. Proceedings of the 6th International Conference on Tools with Artificial Intelligence. TAI 94; 1994:740-743.
31. Curtin RR, Cline JR, Slagle NP, et al. MLPACK: a scalable C++ machine learning library. *J Mach Learn Res*. 2013;14:801-805.
32. Van Rossum G. Python programming language. Proceedings of the USENIX Annual Technical Conference; Vol 41, 2007:36.
33. Srinath KR. Python—the fastest growing programming language. *Int Res J Eng Technol*. 2017;4(12):354-357.
34. Masad D, Kazil J. MESA: an agent-based modeling framework. Proceedings of the 14th PYTHON in Science Conference; 2015:53-60.
35. Zhang L, Wang Z, Sagotsky JA, Deisboeck TS. Multiscale agent-based cancer modeling. *J Math Biol*. 2009;58(4–5):545-559.
36. Uhrmacher AM, Weyns D. *Multi-Agent Systems: Simulation and Applications*. CRC Press; 2009.
37. Prechelt L. An empirical comparison of C, C++, Java, Perl, Python, Rexx and Tcl. *IEEE Comput*. 2000;33(10):23-29.
38. Nourisa J. janursa/CppyABM v1.0.20; February 2021. doi:10.5281/zenodo.5120939
39. Borgiani E, Duda GN, Checa S. Multiscale modeling of bone healing: toward a systems biology approach. *Front Physiol*. 2017;8:287. doi:10.3389/fphys.2017.00287
40. Nourisa J. janursa/RTvisualize: first publish on Zenodo; February 16, 2021. doi:10.5281/ZENODO.4542741
41. Tartarini D, Mele E. Adult stem cell therapies for wound healing: biomaterials and computational models. *Front Bioeng Biotechnol*. 2016;3:206. doi:10.3389/fbioe.2015.00206
42. Gan T, Yang Y, Hao J, Liao Z, Zhu X. Speeding up collective cell migration using deep reinforcement learning. Proceedings of the 2018 IEEE International Conference on Bioinformatics and Biomedicine, BIBM 2018; 2019:1277-1280; Institute of Electrical and Electronics Engineers Inc. doi:10.1109/BIBM.2018.8621416
43. Nourisa J, Zeller-Plumhoff B, Helmholz H, Luthringer-Feyerabend B, Ivannikov V, Willumeit-Römer R. Magnesium ions regulate mesenchymal stem cells population and osteogenic differentiation: a fuzzy agent-based modeling approach. *Comput Struct Biotechnol J*. 2021;19:4110-4122.
44. Núñez-Corrales S, Jakobsson E. The epidemiology workbench: a tool for communities to strategize in response to COVID-19 and other infectious diseases. medRxiv; 2020:20159798. doi:10.1101/2020.07.22.20159798

How to cite this article: Nourisa J, Zeller-Plumhoff B, Willumeit-Römer R. CppyABM: An open-source agent-based modeling library to integrate C++ and Python. *Softw: Pract Exper*. 2022;1-15. doi: 10.1002/spe.3067

APPENDIX A. FURTHER ELABORATION OF THE AGENT-BASED SIMULATION OF THE SPREAD OF INFECTIOUS DISEASES SUCH AS COVID-19

In this example, agents can obtain one of the eight epidemiological states of Susceptible (default), Exposed (when a susceptible agent comes in contact with potentially infected agents), Asymptomatic (an undetected infectious agent who is not showing symptoms), Symptomatic (an infectious agent who is showing symptoms), Asymptomatic Detected (a detected infectious agent who is not showing symptoms), Severe (symptomatic agents that need some form of hospitalization), Recovered (recovered patient), Decease (dead agent). The complete definition of these terms can be found in the original paper.[44] The behavioral properties of agents are dependent on the epidemiological state as well as the given policies (introduced later in the text). For example, when an agent is in the state of Symptomatic, it is quarantined and is not allowed to move from its location until the recovery time is exhausted. Several probabilistic concepts are embedded in the behavior of agents. For instance, each agent is initialized with individual incubation and recovery times determined by Poisson distributions.

Four types of public policies are simulated to combat the spread of the virus namely self-isolation, social distancing, contact tracing, and testing. Self-isolation is modeled by constraining a portion of the population in their position for a certain period of time. The factor of social distancing is simulated by decreasing the contagion probability per contact as a linear function of the distance between two agents residing in a single patch. The process of testing is modeled by randomly choosing agents from the population (those with the states of Susceptible and Asymptomatic) within a certain period of time and quarantining asymptomatic agents immediately. The factor of contact tracing is implemented by following up on those who have been in contact with an infected patient within a period of 2 days. All agents found in contact are assigned to the groups of susceptible, symptomatic, or asymptomatic detected.

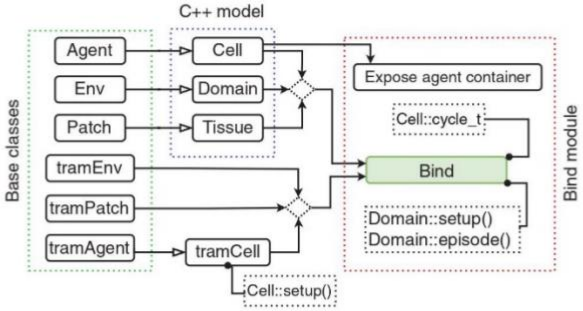

FIGURE A1 The scheme of the exposure process from C++ to Python. The `Bind` receives the model developed in C++ (blue box) together with the trampoline classes. The base *tramAgent* was extended as *tramCell* by declaring the `setup` function of *Cell* to be overwritten in Python. This function initializes the value of `cycle_t` for each agent using the neural-network model; `tramEnv` declares the extensibility of the base functions such as `generate_agent` and `generate_patch`. The module also binds the *Cell* variable of `cycle_t` as well as *Domain* methods of `setup` and `episode`. These functions are directly called within Python for model setup and execution. The agent container is exposed using `EXPOSE_AGENT_CONTAINER`. The full arrows indicate inputs while the empty arrows indicate inheritance

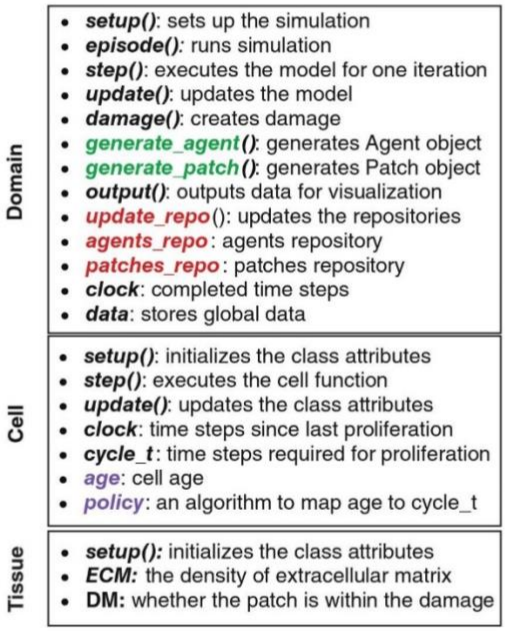

FIGURE A2 The list of the attributes of *Domain*, *Cell*, and *Tissue* classes. The presence or absence of "()" at the end of an attribute indicates whether it is a variable or method, respectively. The members in black are identical for all models, that is, Cpp, Py, Pyy, and Cppy; those in green are slightly different in Cpp compared to Py, Pyy, and Cppy (see Section 3.1); the members in red are only defined in Py, Pyy, and Cppy. The members in purple are the extended attributes that are only defined in Pyy and Cppy

III.2. Magnesium ions regulate mesenchymal stem cells population and osteogenic differentiation: A fuzzy agent-based modeling approach

Several empirical studies have investigated the role of mesenchymal stem cells (MSCs) in bone regeneration and the impact of magnesium (Mg) ions on MSC growth and osteogenesis. In this research, we utilize an agent-based model to understand the spatial and temporal dynamics of the MSC population and osteogenic differentiation in response to Mg2+ ions. A fuzzy-logic controller is designed to control the actions of the cells by predicting cellular behaviors including proliferation, differentiation, migration, and mortality in response to bioregulatory factors such as Mg2+, pH, BMP2, and TGF-β1. The model is validated using empirical data obtained from three sets of cell culture experiments. The model accurately reflects the observed data, including cell count, viability, DNA content, and markers of differentiation such as alkaline phosphate (ALP) and osteocalcin (OC). The results show that the optimal concentration of Mg2+ ions for MSC growth is between 3-6 mM, and that the concentration affects the differentiation markers, with ALP increasing and OC decreasing in response to the ions. The model also highlights the differences in cell behavior based on the culture conditions, such as the sensitivity to Mg2+ ions. The proposed model offers valuable insights for the study of bone regeneration around Mg-based implants, where the release of ions from the degradation of the implant interacts with local cells and impacts the regeneration process.

Nourisa J, Zeller-Plumhoff B, Helmholz H, Luthringer-Feyerabend B, Ivannikov V, Willumeit-Römer R. Magnesium ions regulate mesenchymal stem cells population and osteogenic differentiation: A fuzzy agent-based modeling approach. Computational and structural biotechnology journal. 2021. 19. 4110-22. DOI: 10.1016/j.csbj.2021.07.005.

Contribution of Jalil Nourisa:

Literature search	Problem definition	Data acquisition	Software development	Data analysis	Manuscript drafting
Primary role	Primary role	Primary role	Primary role	Primary role	Primary role

Computational and Structural Biotechnology Journal 19 (2021) 4110–4122

COMPUTATIONAL ANDSTRUCTURAL BIOTECHNOLOGY JOURNAL

journal homepage: www.elsevier.com/locate/csbj

Magnesium ions regulate mesenchymal stem cells population and osteogenic differentiation: A fuzzy agent-based modeling approach

Jalil Nourisa *, Berit Zeller-Plumhoff, Heike Helmholz, Bérengère Luthringer-Feyerabend, Vladimir Ivannikov, Regine Willumeit-Römer

Helmholtz Zentrum Hereon, Institute of Metallic Biomaterials, Max-Planck-Straße 1, 21502 Geesthacht, Germany

ARTICLE INFO

Article history:
Received 9 April 2021
Received in revised form 5 July 2021
Accepted 7 July 2021
Available online 09 July 2021

Keywords:
Magnesium ions
Agent-based simulation
Fuzzy logic-based approach
Mesenchymal stem cells
Cell population
Osteogenic differentiation
Approximate Bayesian calculation

ABSTRACT

Mesenchymal stem cells (MSCs) are proliferative and multipotent cells that play a key role in the bone regeneration process. Empirical data have repeatedly shown the bioregulatory importance of magnesium (Mg) ions in MSC growth and osteogenesis. In this study, we propose an agent-based model to predict the spatiotemporal dynamics of the MSC population and osteogenic differentiation in response to Mg^{2+} ions. A fuzzy-logic controller was designed to govern the decision-making process of cells by predicting four cellular processes of proliferation, differentiation, migration, and mortality in response to several important bioregulatory factors such as Mg^{2+} ions, pH, BMP2, and TGF-β1. The model was calibrated using the empirical data obtained from three sets of cell culture experiments. The model successfully reproduced the empirical observations regarding live cell count, viability, DNA content, and the differentiation-related markers of alkaline phosphate (ALP) and osteocalcin (OC). The simulation results, in agreement with the empirical data, showed that Mg^{2+} ions within 3–6 mM concentration have the highest stimulation effect on cell population growth. The model also correctly reproduced the stimulatory effect of Mg^{2+} ions on ALP and its inhibitory effect on OC as the early and late differentiation markers, respectively. Besides, the numerical simulation shed light on the innate cellular differences of the cells cultured in different experiments in terms of the proliferative capacity as well as sensitivity to Mg^{2+} ions. The proposed model can be adopted in the study of the osteogenesis around Mg-based implants where ions released due to degradation interact with local cells and regulate bone regeneration.

1. Introduction

Mesenchymal stem cells (MSCs) are the key players in bone fracture healing [1]. MSCs increase cell population through a fast proliferation process and differentiate into multiple cell types involved in bone tissue regeneration, in particular osteoblasts [2]. The proliferation process occurs through a cascade of cell cycle events including the two major processes of DNA synthesis and actual division of the parent cell into two daughter cells [2]. The specialization of MSCs toward osteoblasts involves a complex intracellular interaction and is shown to occur continuously with recognizable intermediate cells such as osteoprogenitors and pre-osteoblasts [3]. During osteogenic differentiation, MSCs experience a decline in proliferative capacity and gain osteoblastic properties [4]. The onset of MSC differentiation to osteoblasts and the progression along this lineage are controlled by various signals such as growth factors, mechanical signals, and biomaterials [5,6].

Magnesium (Mg)-based biomaterials are biodegradable which makes them an attractive choice in the orthopedic application and medical-technical industry [6,7]. Mg implants degrade at the implantation site resulting in an alteration in the microenvironment of the local tissue. Mg^{2+} ions released during degradation are demonstrated by several *in vivo* and *in vitro* studies to regulate gene and protein expressions associated with cell growth and osteogenesis [7–9]. The release of Mg^{2+} ions in high concentrations is also associated with the alteration of the microenvironment pH [9], causing an alkaline condition and consequently interfering with a broad range of physiological processes [10–12]. In order to design an effective Mg-based implant, it is essential to study the bioregulatory mechanisms of Mg^{2+} ions and identify the optimal conditions to promote osteogenic activities [13,14]. So far, the empirical approach has been the only means to study the bioregulatory effect of Mg-based materials. In this study, we aim

* Corresponding author.
E-mail address: jalil.nourisa@gmail.com (J. Nourisa).

https://doi.org/10.1016/j.csbj.2021.07.005

at numerically investigating the physiological interaction of Mg^{2+} ions with MSCs.

We choose agent-based modeling ("agent-based model" and "agent-based modeling" are both abbreviated as ABM) to address the current problem. ABM provides a multiscale investigation of a system as a direct observation can be made on individual cells while the cumulative results are captured at the population level [19–21]. ABM has been widely used in the literature to study cellular responses [15,17,18]. A common challenge in ABM is the abstraction of cellular behavior which requires an algorithm to correctly govern the decision-making process [22,23]. Such an algorithm receives cellular inputs at the microscale and predicts cellular behavior. Several approaches have been proposed in the literature to simulate the decision-making process such as simple rule definition, differential equations, logic-based approach, and artificial neural networks [15,24–26]. Fuzzy logic (FL)-based have shown great potential in resolving technical barriers between experimental and simulation experts thanks to its plain language [27]. In this approach, knowledge about a system can be formulated in the form of IF-THEN statements, in which IF and THEN are conditions and results, respectively. This plain language can potentially ease the involvement of people with domain knowledge in the rapid development of computer models. Since FLB models can define a system without precise mechanistic information, it is possible to leverage qualitative knowledge in numerical modeling which would be otherwise difficult or impossible using other simulation approaches that require real-valued variables [27]. Due to these advantages, the FL-based approach has already been repeatedly employed in the numerical investigation of bone regeneration [28–30].

In this study, we propose a fuzzy agent-based model to simulate the spatiotemporal dynamics of mesenchymal stem cell population and osteogenic differentiation in response to Mg^{2+} ions. To this end, the available information in the literature regarding the bioregulatory effect of Mg^{2+} ions in tandem with several other important factors is curated and tailored as fuzzy logic rules. Differential equations are used to describe the dynamics of growth factors. The data obtained from three sets of published cell-culture experiments are used to estimate the model's parameters by employing approximate Bayesian calculation.

2. Materials and methods

The proposed ABM in this study consists of three components; a cell model, a model to simulate growth factors, and a coordinator. As shown in Fig. 1, the coordinator initializes the simulation, iteratively executes cells and growth factors, and updates the simulation world. In the rest of this section, we first give an introduction to the ABM. Then, the construction of the cell model is elaborated in detail. Lastly, the process of sensitivity analysis and the calibration is introduced.

2.1. The agent-based model

We use a lattice-based approach where the occupancy of each patch is limited to one cell at a time. A three-dimensional (3D) space with 8 layers in the z-direction is created to account for the observation that the osteoblastic differentiation of MSCs generates more than four cell layers *in vitro* [31]. Further information regarding the geometry of the model, the initialization, and the

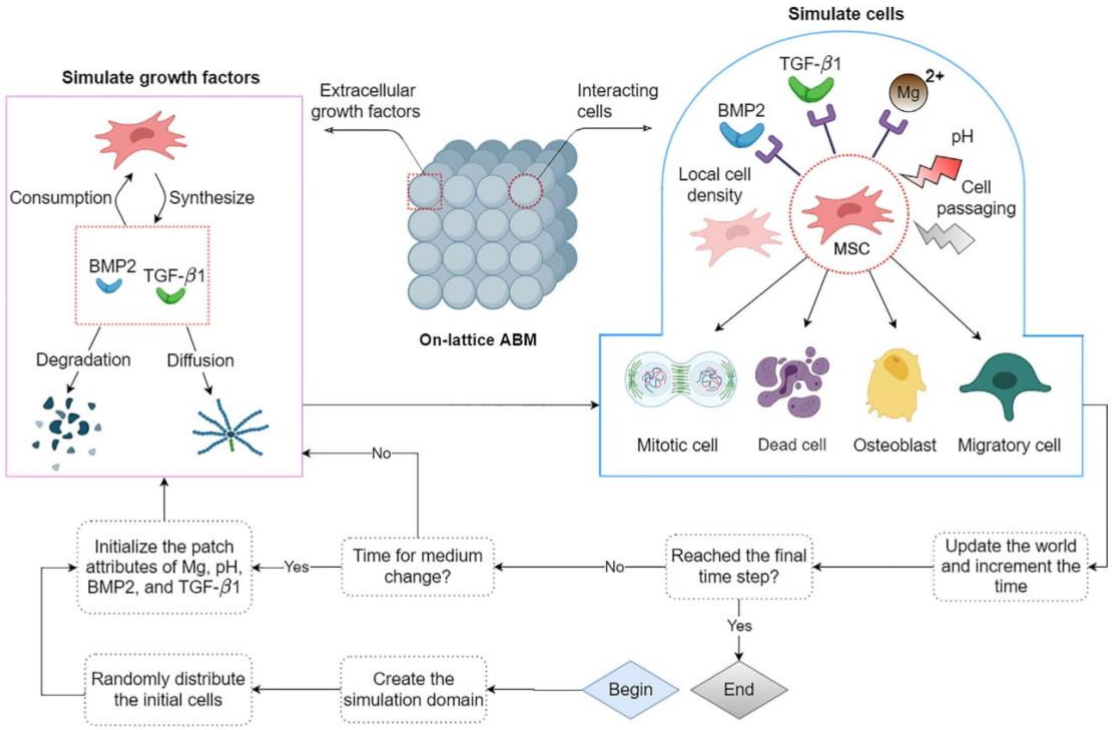

Fig. 1. The workflow of the ABM in this study. Once the model is initialized, cells and growth factors are simulated iteratively, and the simulation world is updated according to their results. For culture experiments longer than 3 days, the content of the growth factors and pH value is reset to the initial values every 2.5 days accounting for the process of medium change [31]. Four cellular events of proliferation, migration, osteoblastic differentiation, and mortality are simulated which are affected by multiple environmental factors. The dynamics of the growth factors are driven by cellular production, cellular consumption, degradation, and diffusion. Each iteration in our simulation represents one hour [34,35]. Some elements of the graph are created with BioRender.com.

boundary conditions can be found in section S1 in the supplements. The dynamics of growth factors are simulated similar to Ribeiro et al [32] and are elaborated in section S2 in the supplement. The software used to develop the model can be found in section S3 in the supplement. The source code of the present model can be found online [33].

2.2. The cell model

We define five inputs of Mg^{2+} ions, alkalinity, TGF-β1, BMP2, and cell density as the bioregulatory cues of the cellular behavior. In addition, two intrinsic factors of maturity and DNA damage are simulated to influence cellular functions. The cell model predicts the four cellular behaviors of proliferation, differentiation, mortality, and migration. A Mamdani-type FL controller is implemented to compute the intensity of the cellular actions as a cumulative result of the stimulatory signal. The FL controller operates in three steps of fuzzification, inference, and defuzzification as shown in Fig. 2 [36].

2.2.1. Cellular inputs and fuzzification

Maturity represents the degree of maturation of MSCs along the line of osteoblast lineage, similar to Krinner et al [17]. The spectrum of maturation is divided into two phases of the early and late differentiation, marked by a parameter termed maturity threshold (M_t). Maturity linearly increases by cell commitment to the differentiation process at each time step of the simulation. During this process, cells lose their characteristics as MSCs and obtain osteoblastic characteristics. Maturity is fuzzified using two linguistic terms as shown in Fig. 2.

DNA damage stands for the irreversible cellular impairment due to harsh environmental conditions. In our simulations, DNA damage can be caused by either cell passaging due to the usage of chemical products and mechanical forces [37] or exposure to a high pH (pH_t) [11]. In the simulation, DNA damage can occur by a base chance (γ_C) at the beginning of the simulation, accounting for cell passaging, or by one hour of exposure (one step of the simulation) to pH_t [11]. The factor of DNA damage is simulated as a crisp quantity that takes the value of either 1 (*high*) or 0 (*low*).

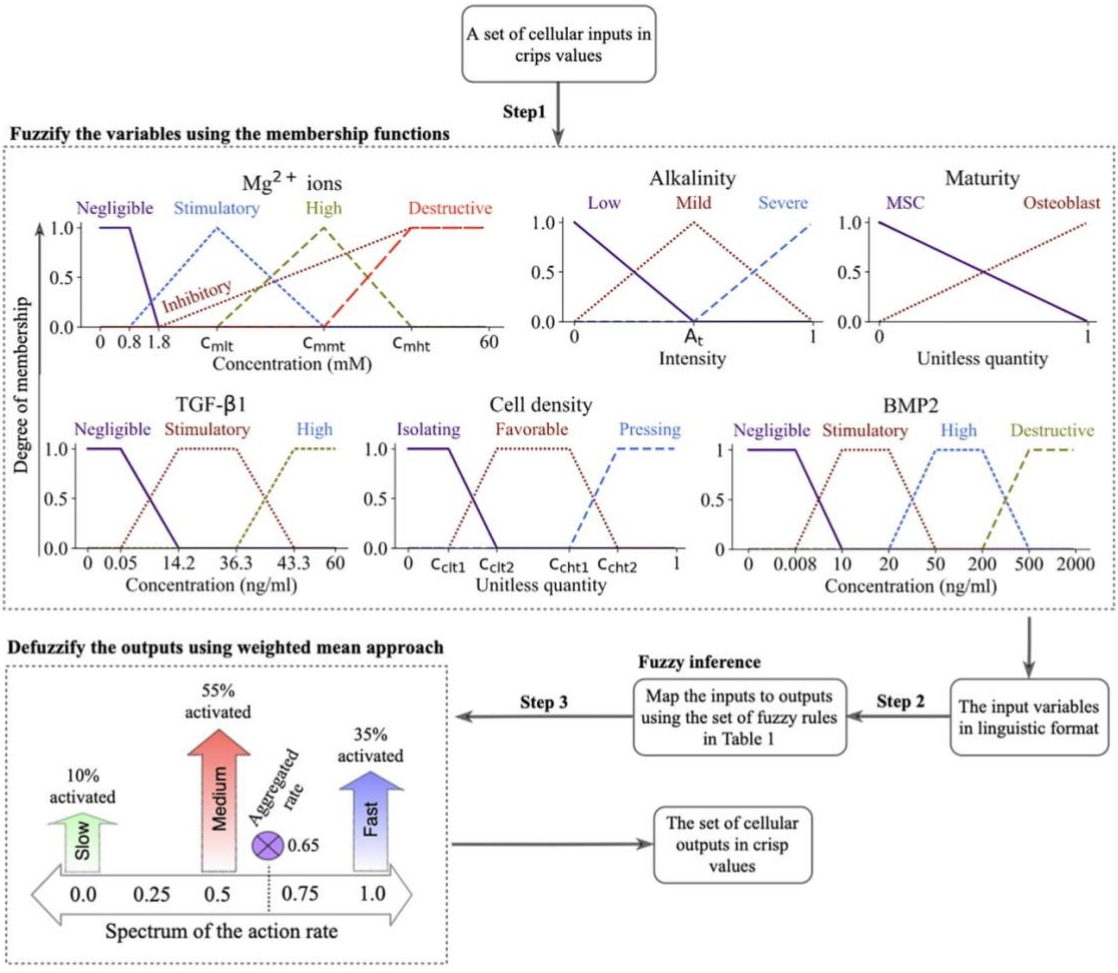

Fig. 2. The complete calculation process of the FL controller in this study. The inputs of the FL controller are converted to linguistic variables using the membership functions (step 1). The decision-making center, which comprises the fuzzy rules, receives the fuzzified inputs and determines which fuzzy outputs are activated (step 2). The final output of the controller is calculated by averaging on the activated outputs using the weighted mean approach (step 3).

Mg^{2+} ions are shown to regulate cellular responses depending on the applied concentration, exposure duration, and the state of cell differentiation [9,38–40]. Mg^{2+} ions within the concentration range of 2–10 mM enhance cell metabolism and upregulate proliferation and early differentiation rate [38,40–43]. However, Mg^{2+} ions above 1.8 mM have shown an inhibitory effect on late differentiation rate and matrix mineralization [40,13]. Also, Mg^{2+} ions at concentrations ranging from 20 to 40 mM is reported toxic and can reduce cell viability [42,44,45]. To account for these observations, we define five linguistic terms to fuzzify the input factor of Mg^{2+} ions (see Fig. 2). The concentration of Mg^{2+} ions below 0.8 mM, which is used in cell culture medium (minimal essential Medium-MEM), are set to *negligible* with no stimulatory effect [9,43]. The *inhibitory* level takes into account the inhibitory effect of Mg^{2+} ions on the late differentiation process. The *stimulatory* level simulates the stimulatory role of Mg^{2+} ions on proliferation and early differentiation process. The toxic effect of Mg^{2+} ions in high concentrations is modeled by *destructive* level. Three parameters of c_{mlt}, c_{mmt}, and c_{mht} mark the peak occurrence of stimulatory, high, and destructive levels.

Alkalinity is defined as the sudden change of the ambient pH with respect to the intracellular pH. Mg^{2+} ions are reported to alter microenvironmental pH [9] (see Fig. S1-A in the supplements), causing an alkaline condition which disrupts cellular reactions. In contrast to permanent DNA damage, we assume that cells can recover from mild alkalinity [9]. This process happens by the adjustment of the cell's internal pH with respect to the ambient pH over time with a constant rate (r_r) [9]. Alkalinity can significantly affect cellular reaction depending on the severity [11]. Several minutes of exposure to severe alkalinity is reported to cause cell contraction and detachment from the culture surface [12]. Severe alkalinity can compromise human MSC renewal capability and growth and thereby downregulate proliferation rate [10]. High alkalinity also reduces cell viability in culture experiments [10]. However, a mild alkaline environment with a pH as high as 8.5 has shown no significant negative effect on osteoblast differentiation [10]. Three linguistic terms are assigned to alkalinity during the fuzzification process as shown in Fig. 2. We assume that both *mild* and *severe* alkalinity can compromise cellular events of proliferation and health, while only *severe* alkalinity affects the differentiation process. The parameter of A_t marks the start of *severe* level.

BMP2 is the most potent BMP heterodimer in the stimulation of osteoblast differentiation [46–48]. BMP2 is shown to affect cell proliferation in a concentration-dependent fashion. BMP2 at the concentration of 10–20 ng/mL promotes cell proliferation [49,50]. However, BMP2 has shown no effect and a negative effect within the concentration ranges of 50–200 ng/mL and 500–2000 ng/mL, respectively [51,52]. BMP2 at the concentration of 10–20 ng/mL has also shown a stimulatory impact on osteogenic differentiation [49,50]. BMP2 at the concentration of 500–2000 ng/mL stimulates cell apoptosis and thereby decreases cell viability [51]. We assign four membership levels to the input of BMP2 as shown in Fig. 2. The *stimulus* level starts from the concentration of 0.008 ng/mL as the lower bound of the physiological concentration reported in *in vitro* experiments [53–55].

TGF-β1 is an important regulatory factor in every stage of bone regeneration [16,56,46]. Within the physiological concentration of 14.2–36.3 ng/mL, TGF-β1 is shown to stimulate the proliferation process, promote early osteoblast differentiation, and inhibit the later phase of differentiation [56,46]. Within the physiological range, TGF-β1 is also shown to block the natural process of apoptosis [57]. The input variable of TGF-β1 is fuzzified according to Fig. 2, where the concentration of 0.05 ng/mL marks the beginning of the *stimulatory* level [58,59].

Cell density is calculated as the normalized number of cells in one patch neighborhood. Cell density is another important factor that is known to affect various cellular reactions such as migration, proliferation, differentiation, and mortality [60]. High cell density results in a phenomenon termed contact inhibition that halts cell growth and initiates the differentiation process [61,62]. Contact inhibition also affects cell migration as cells intend to move toward an area with less crowdedness to receive better nutrition and oxygen [63]. A high degree of crowdedness is also reported to be detrimental for cell nuclei health and can increase cell mortality [64]. Also, cells in solitude show less proliferation capacity and are susceptible to mortality [65,66]. To account for these observations, the input of cell density is fuzzified using three membership functions as depicted in see Fig. 2. The parameters of c_{clt1}, c_{clt2}, c_{cht1}, and c_{cht2} mark the boundaries of different memberships.

2.2.2. Fuzzy inference, defuzzification, and cellular events

Once the cellular inputs are converted into linguistic variables, the rules given in Table 1 are used to determine the intensity of cellular actions. A given set of inputs can simultaneously trigger multiple rules. Thus, we use the weighted fuzzy mean technique to calculate the final output (see Fig. 2) [36]. The outputs of the FL controller are continuous crisp values between 0 and 1. These values are post processed to determine cellular events.

The proliferation, mortality, and migration are simulated as a stochastic process where the chance of occurrence at each time step is calculated,

$$\text{Proliferation chance} = \Omega \cdot (\alpha_P f_P) \cdot \gamma_{P0} \tag{1}$$

$$\text{Mortality chance} = (1 + \alpha_{PM}\delta_P) \cdot (\alpha_M f_M) \cdot \gamma_{M0} \tag{2}$$

$$\text{Migration chance} = f_{Mi} \tag{3}$$

where γ_{P0} and γ_{M0} are the base chances of proliferation and mortality, respectively; f_P, f_M, f_{Mi} are the action rates calculated by the FL controller for proliferation, mortality, and migration, respectively; $\alpha_P$and α_M are the scale factors to scale up the controller's outputs; Ω is a bias function; and δ_P and α_{PM} simulate the mitotic damage and its weight on the mortality chance. It is shown that shortly after proliferation, one of the daughter cells is prone to undergo apoptosis possibly due to asymmetric distribution of pro- and anti-apoptotic proteins during the final stage of cell division [67]. We account for this observation by assigning δ_P ($\delta_P = 1$ if mitosis occurs, and $\delta_P = 0$ otherwise) to one of the daughter cells after the cell cycle. Accounting for the fact that cells need a period of time for growth before the actual process of the division, we use a logistic-based bias function (Ω) to shift the probability distribution toward the end of the cell cycle (see Fig. S1-B in the supplements). The chosen logistic growth rate constrains the proliferation probability around the average time period assigned for proliferation but also leaves a degree of stochasticity in the system. Once a cell commits to proliferation, a daughter cell is created and positioned adjacent to the mother cell. Migration in the present model occurs due to contact inhibition with the chance calculated in Eq. (3). The choice of destination can be arbitrary as long as an adjacent grid is vacant. The motile cell can move one patch at a time step. If all neighboring grids are occupied, no relocation will take place.

Differentiation is simulated as a continuous process with the rate,

$$\text{Differentiation rate} = (\alpha_D f_D) \cdot r_{D0} \tag{4}$$

where r_{D0} is the base rate of differentiation, f_D is the FL controller's output for differentiation, and α_D is the scale factor. Whether the maturity is below or above the maturity threshold

Table 1
Fuzzy logic rules describing the cellular reactions in response to stimulatory signals. To be concise, the combination of different inputs that results in the same cellular output is coded in certain colors; purple (~): any choice of one or more from the given inputs; blue (≈): any choice of two or more from the given inputs. The symbol (−) indicates any of the linguistic levels defined for that variable. If the rule applies for all except a certain level, it is described as 'Not' followed by the linguistic level, e.g. 'Not stimulatory' stands for all levels except stimulatory.

Cellular events	Intensity	Damage	Maturity	Alkalinity	Cell density	Mg^{2+} ions	TGF-β1	BMP2
Proliferation	Very low	~High	~Osteoblast	~Severe	~Pressing or Isolating	-	-	-
	Low	Low	MSC	Mild	Favorable	~Destructive	-	~Destructive
	Medium	Low	MSC	Low	Favorable	~Stimulatory	~Stimulatory	~Stimulatory
	High	Low	MSC	Low	Favorable	≈Stimulatory	≈Stimulatory	≈Stimulatory
	Very high	Low	MSC	Low	Favorable	Stimulatory	Stimulatory	Stimulatory
Early differentiation	Very low	~High	-	~Severe	-	~Destructive	-	-
	Low	Low	-	Low or Mild	Favorable	Not stimulatory	-	-
	Medium	Low	-	Low or Mild	Favorable or Pressing	~Stimulatory	~Stimulatory	~Stimulatory
	High	Low	-	Low or Mild	Pressing	≈Stimulatory	≈Stimulatory	≈Stimulatory
	Very high	Low	-	Low or Mild	Pressing	Stimulatory	Stimulatory	Stimulatory
Late differentiation	Very low	~High	~Osteoblast	~Severe	-	~Destructive	-	-
	Low	Low	MSC	Low or Mild	Favorable	Inhibitory	-	-
	Medium	Low	MSC	Low or Mild	Favorable or Pressing	~Not Inhibitory	~Negligible	~Stimulatory
	High	Low	MSC	Low or Mild	Pressing	≈Not Inhibitory	≈Negligible	≈Stimulatory
	Very high	Low	MSC	Low or Mild	Pressing	Not Inhibitory	Negligible	Stimulatory
Mortality	Very low	Low	-	Low	Favorable	Not Destructive	Stimulatory	Not Destructive
	Low	Low	-	Low	Favorable	Not Destructive	-	Not Destructive
	Medium	Low	-	~Mild	~Isolating or Pressing	~Destructive	-	~Destructive
	High	Low	-	≈Mild	≈Isolating or Pressing	≈Destructive	-	≈Destructive
	Very high	~High	-	~Severe	-	-	-	-
Migration	Low	~High	-	-	~Not Pressing	-	-	-
	High	Low	-	-	Pressing	-	-	-

(M_t), f_D can indicate the early or late differentiation rate, respectively, produced by the controller. In the present model, cell differentiation and proliferation can occur simultaneously [17].

2.3. Sensitivity analysis and the calibration process

The current model contains 20 free parameters (see Table S2 in the supplementary information). The empirical data to determine the values of these parameters are limited as they are either difficult to measure or represent a combination of several processes. Instead, we use a range of possible values based on empirical observations or estimations and then use the calibration process to precise their values. The empirical data for the calibration process is obtained from three sets of cell culture studies (summarized in section S4 in the supplementary information). Study 1 examines the effect of five different Mg^{2+} ions concentrations on cell population by measuring two parameters of live cell count and viability [68]. Study 2 focuses on the osteogenic differentiation process by measuring the expression of the differentiation-related markers of alkaline phosphate (ALP) and osteocalcin (OC) and growth factors at three time points of 7, 14, and 21 days as a response to two different concentrations of Mg^{2+} ions [43]. Study 3 reports live cell count at three time points of 3, 6, and 9 days for four different Mg^{2+} ions concentrations [69,70]. The combined data provided 72 experimental measurements. All experiments were conducted with human umbilical cord perivascular (HUCPV) cells. We conduct the calibration process on the dataset of each study alone, encoded as C1, C2, and C3, as well as on the combined data of all experiments, encoded as C1-3.

The approximate Bayesian calculation (ABC) is employed for parameter inference [71] (see section S7 in the supplement). However, due to the curse of dimensionality, sufficient sampling in a 20-dimensional space requires a very large number of runs, i.e. in the order of several million [71], which is impractical considering the size of the current model. To overcome this, we employ an iterative calibration process depicted in Fig. 3 that follows three main steps of (1) determining the five most important parameters using the sensitivity analysis, (2) estimating the values of the chosen parameters using ABC, and (3) updating the model with the inferred values and repeating step 1 and 2. We use fractional factorial design and analysis of variance for the sensitivity analysis (see section S6 in the supplement). The iterative calibration process ends once no new parameter is inferred at the previous iteration.

3. Results

In this section, we first present the results of the sensitivity analysis and the calibration process. Then, we show the improvements made on the results during iterative calibration process. Lastly, we compare the results of the simulations to the empirical data.

3.1. The results of the sensitivity analysis and the calibration process

The complete results of the iterative calibration process are given in Fig. S2 in the supplements. It took 5, 8, 5, and 8 iterations for C1, C2, C3, and C1-3, respectively, to complete the calibration process. The significance of the parameters with respect to one another was obtained during the sensitivity analysis (see Fig. 4A). The base proliferation chance (γ_{P0}), the scale factor of proliferation (α_P), and the base mortality chance (γ_{M0}) had the highest impact for C1 and C3. For C2, the top three impactful parameters were the cellular weight (w_c), the scale factor of mortality (α_D), and the base

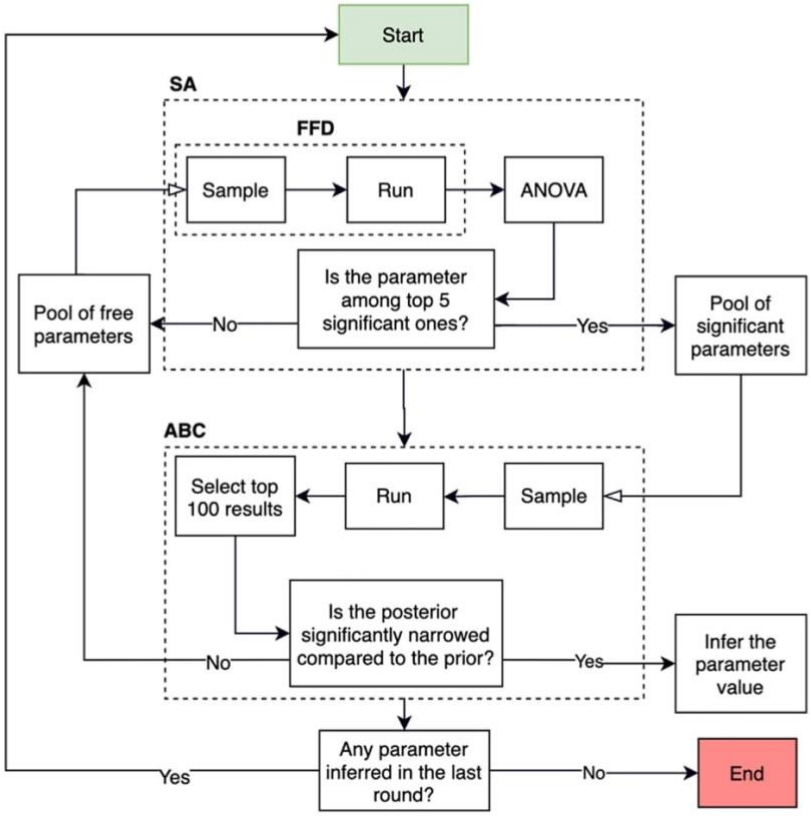

Fig. 3. The iterative calibration process used for the parameter estimation in this study. At each iteration, the top five significant parameters are determined by the sensitivity analysis (SA) that consists of the fractional factorial design (FFD) and the analysis of variance (ANOVA). The significant parameters are sent to ABC for the parameter inference. At each iteration, the model is executed 5000 times with the parameter sets sampled from the pool of significant parameters. The posteriors are generated using the top 100 results. If the posterior is significantly narrower than the prior, the median of the posterior is accepted as the estimated value. If not, the parameter is added to the pool of the free parameters for the next round of calibration.

mortality chance. For C1-3, the top 5 significant parameters were the combination of those in C1, C2, and C3, i.e. γ_{P0}, α_P, γ_{M0}, w_c, and α_D (see Fig. 4A).

The iterative calibration process resulted in the estimation of 8 out of 20 free parameters for C1, 15 for C2, 7 for C3, and 15 for C1-3. The estimated values obtained from different calibration scenarios are given in a normalized format in Fig. 4B. The real values are presented in Table S2 in the supplement. No values were inferred for the parameters of c_{mmt} and c_{mht}, and several parameters were only inferred in certain calibration scenarios. There was a large variation among the estimated values of several parameters during different calibration scenarios. Among them were α_P and γ_{P0}, connected to proliferation process, α_{CM} and γ_{M0}, associated with mortality, and α_D, related to differentiation process (see Fig. 4B).

3.2. The improvements on the goodness of fit (R^2) during the iterative calibration process

During the iterative calibration process, the obtained values of R^2, calculated as the normalized absolute difference between simulation results and the empirical data, were improved as depicted in Fig. 5. The standard deviation indicates the extent of the variations in the mean caused by the uncalibrated parameters. The mean and standard deviation of R^2 respectively increased and decreased 4% and 5% for C1, 6% and 46% for study 2, 7% and 29% for C3, and 9% and 31% for C1-3 during the iteration process. For C2 and C1-3 with higher calibration iterations, the improvements made in the first five iterations accounted for 83% and 93% of the total improvements on the mean and standard deviation, respectively, during C2 and 89% and 96%, respectively, during C1-3.

3.3. Comparison of experimental and simulation results

The agent-based model parametrized with the values accepted by ABC were compared against the empirical data as demonstrated in Figs. 6–10. The fits of the model to the data of each study are given in separate sections in the following.

3.3.1. Study 1

The fits of the model to the data of study 1 are given in Figs. 6 and 7. The model calibrated by C1-3 produced the R^2 of 0.87 and 0.72 for the live cell count and viability, respectively. Overall, Mg^{2+} ions at the concentration of 3 mM resulted in the highest cell population followed by 6 mM, 0.8 mM (control), 12 mM, and 60 mM, which was correctly reproduced by the model (see Fig. 6). For the case of viability, the model closely reproduced the culture data given for Mg^{2+} ions concentration of 60 mM but overestimated the rest (see Fig. 7). Once calibrated against C1, the model's predictions for the viability were considerably improved, i.e. R^2 increased from 0.72 to 0.91 (Fig. 7). The model was able to closely match the culture data for all Mg^{2+} ions. However, the simulation

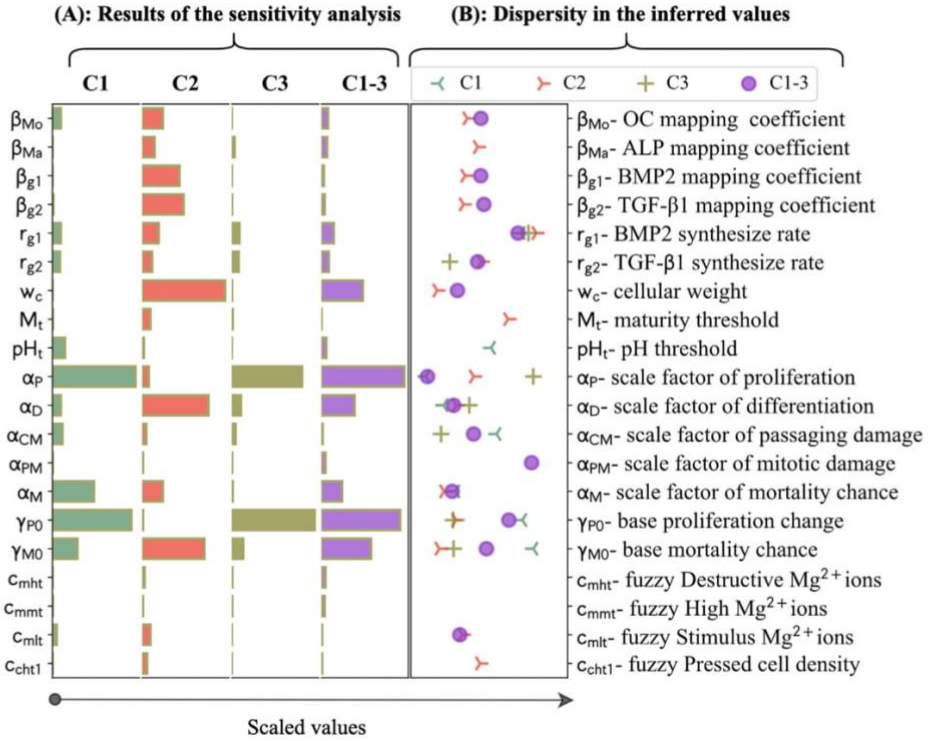

Fig. 4. (A) The results of the sensitivity analysis, obtained during the first iteration of the calibration process for different calibration scenarios of C1, C2, C3, and C1-3. The bars indicate the significance of parameters in comparison with one another. The quantities were scaled with respect to the maximum values. (B) The comparative representation of the values estimated for the free parameters during different calibration scenarios. The values were scaled by dividing by the mean of the priors.

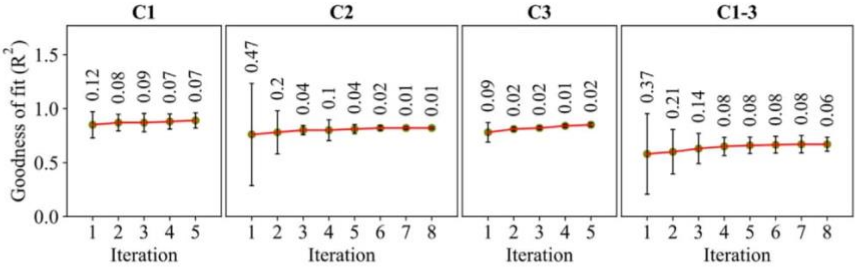

Fig. 5. The evolution of the goodness of fit during the iterative calibration process for different calibration scenarios. The means and standard deviations were obtained from the 100 best results. The numbers above the error bars show the standard deviations.

outcomes showed little change in the case of the live cell count comparing C1 to C1-3 (see Fig. 6).

3.3.2. Study 2

The fits of the model to the data of study 2 are given in Figs. 8 and 9. The model calibrated by C1-3 resulted in an average R^2 of 0.72 for DNA content (see Fig. 8). The model was able to capture the decreasing trend of the DNA content in the course of experiments from day 7 to 21. The model was also in agreement with the culture data in terms of predicting higher DNA contents for the Mg^{2+} ions concentration of 5 mM compared to the control. However, there was an overall overestimation in the predictions made on the day 7 and 14 for both cases. Once calibrated by C2, the R^2 improved from 0.72 to 0.91, and the model's predictions closely matched the culture data in terms of trends and exact values (see Fig. 8).

For the case of ALP and OC, the model calibrated by C1-3 resulted in an average R^2 of 0.91, and 0.77, respectively (see Fig. 8). The culture experiments reported higher ALP for the Mg^{2+} ions concentration of 5 mM on day 7 and lower on day 14 compared to the control, which was correctly captured by the model. The OC content was reported lower for the Mg^{2+} ions concentration of 5 mM compared to the control in all three time points, which was also captured by the model (see Fig. 8). However, the model predicted an increase in OC content from day 7 to 21 which was not in close agreement with the data. Also, the model underestimated the OC content reported for the control in all three measurement points. Once calibrated by C2, the predictions of

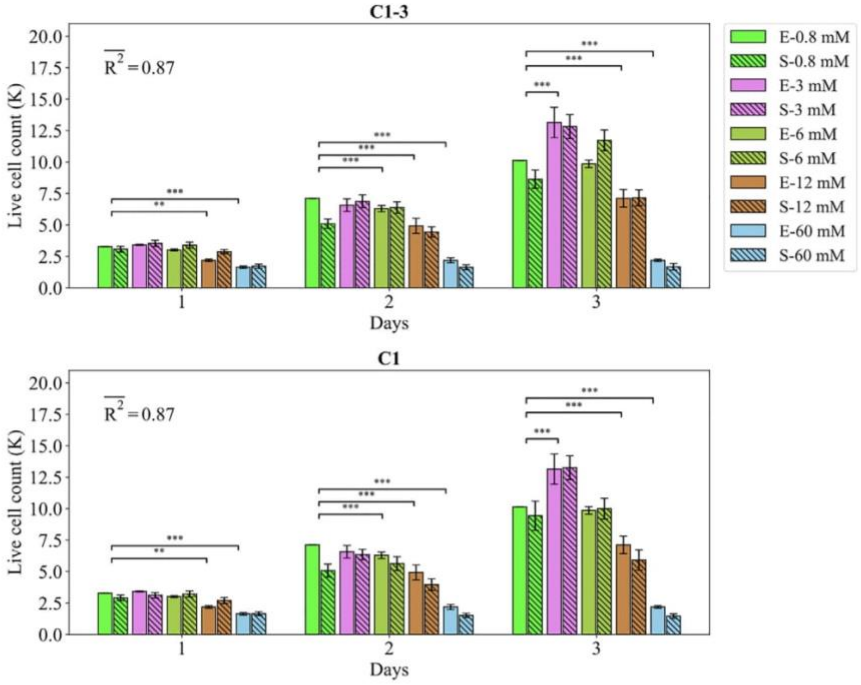

Fig. 6. Fits of the model calibrated by C1-3 and C1 to the empirical data of study 1. Bars indicate the average of the best 100 simulations (S-) and the corresponding empirical data (E-) for increasing Mg^{2+} ion concentrations. The error bars on the empirical data shows the standard deviations. The error bars on the simulation results indicate the standard deviation of the 100 best fits. Stars indicate the statistically significant differences between values given for the empirical data compared to the control (Mg^{2+} concentration of 0.8 mM) ($p < 0.05$ = *; $p < 0.01$ = **; $p < 0.001$ = ***). $\overline{R^2}$ is the average R^2 calculated for each measurement item.

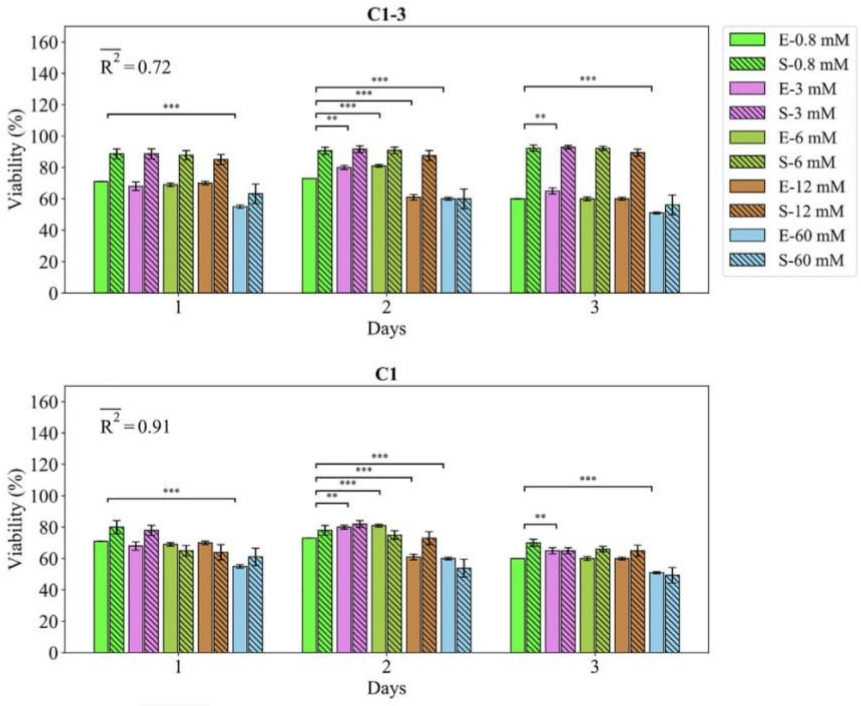

Fig. 7. Fits of the model calibrated by C1-3 and C1 to the empirical data of study 1. Bars indicate the average of the best 100 simulations (S-) and the corresponding empirical data (E-) for increasing Mg^{2+} ion concentrations. The error bars on the empirical data shows the standard deviations. The error bars on the simulation results indicate the standard deviation of the 100 best fits. Stars indicate the statistically significant differences between values given for the empirical data compared to the control (Mg^{2+} concentration of 0.8 mM) ($p < 0.05$ = *; $p < 0.01$ = **; $p < 0.001$ = ***). $\overline{R^2}$ is the average R^2 calculated for each measurement item.

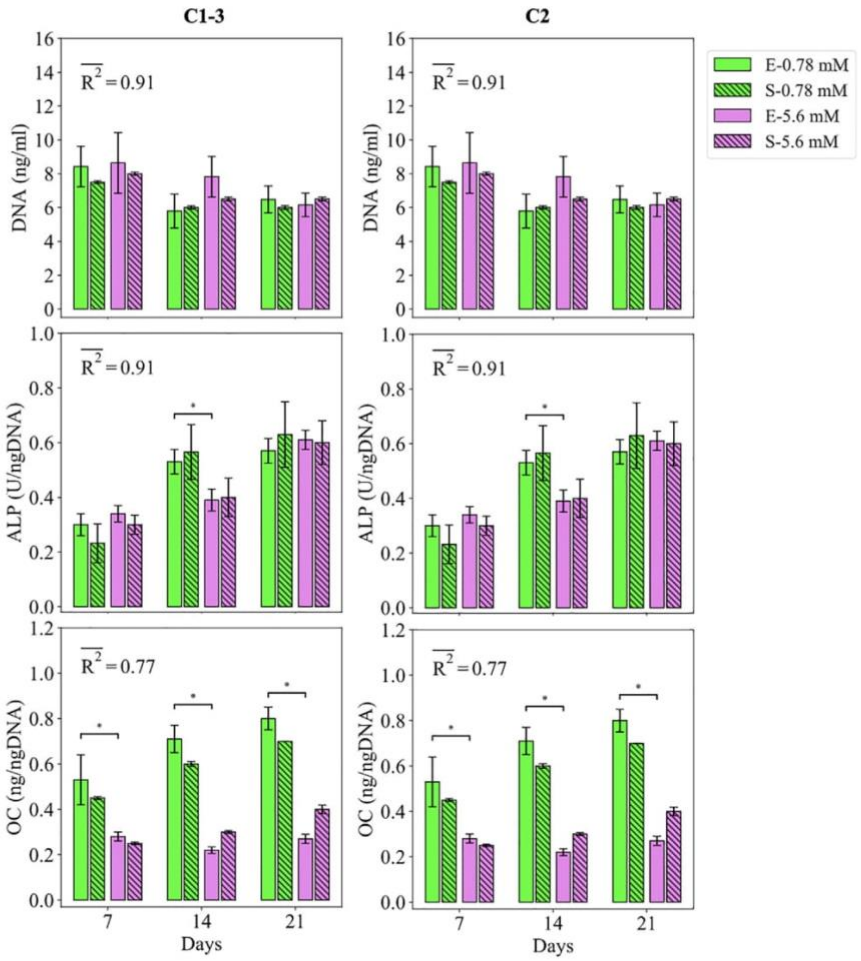

Fig. 8. Fits of the model calibrated by C1-3 and C2 to the empirical data of study 2. Bars indicate the average of the best 100 simulations (S-) and the corresponding empirical data (E-) for different Mg concentrations. The error bars on the empirical data shows the standard deviations. The error bars on the simulation results indicate the standard deviation of the 100 best fits. Stars indicate the statistically significant differences between values given for the empirical data compared to the control (Mg^{2+} concentration of 0.78 mM) ($p < 0.05$ = *; $p < 0.01$ = **; $p < 0.001$ = ***). $\overline{R^2}$ is the average R^2 calculated for each measurement item.

the model for the OC content were closer to the experimental data with 8% improvements in the R^2 (see Fig. 8).

The model calibrated by C1-3 produced the average R^2 of 0.73 and 0.59 for the growth factors of TGF-β1 and BMP2, respectively (see Fig. 9). For both TGF-β1 and BMP2, the cell culture data reported lower values for the condition of 5 mM Mg^{2+} ions compared to the control in all three time points, which was also captured by the model. However, the non-linearity shown in the data, in particular the sharp jump on day 14 of BMP2, was not seen in the model. Once calibrated by C2, the obtained average R^2 increased from 0.73 to 0.76 for TGF-β1 and from 0.59 to 0.68 for BMP2. However, the model was still not in a close match with the culture data.

3.3.3. Study 3

The fits of the model to the data of study 3 are given in Fig. 10. The model calibrated by C1-3 correctly reproduced the trend observed in the cell culture; the live cell count experienced a continuous increase from day 3 to day 9 for all Mg^{2+} ions concentrations; and the highest and lowest live cell count is obtained for 3 mM and 14 mM, respectively. The model disagreed with the data in two aspects; firstly, there was a general overestimation in the predictions of the model especially for the case of the Mg^{2+} ions concentration of 14 mM; and secondly, the culture data reported large variations across different Mg^{2+} ions concentrations, in particular on day 6 and 9, while the model's predictions for different Mg^{2+} ions were close to one another. Once calibrated by C3, there was a substantial increase in the R^2, i.e. from 0.48 to 0.85 (see Fig. 10). The results of the predictions were in close agreement with the culture data both in terms of trend and the exact values.

4. Discussion

The present computer model was initially calibrated using the accumulated data of all three experiments. The model was capable of successfully reproducing several empirical observations, more notably, the live cell count reported in study 1 and the differentiation-related markers of ALP and OC. The results of the simulation, consistent with the experiments, showed that Mg^{2+} ions within the range of 3–6 mM produce the largest hMSC population (see Figs. 6, 7, 10). Also, the model correctly reproduced the culture data in showing that while Mg^{2+} ions stimulate early differentiation, it inhibits the differentiation in the later phase (see

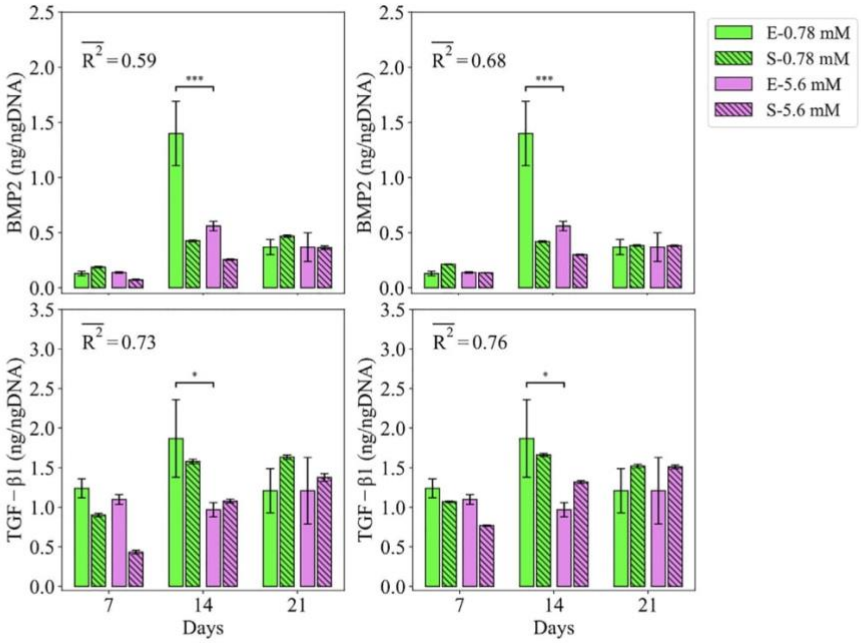

Fig. 9. Fits of the model calibrated by C1-3 and C2 to the empirical data of study 2. Bars indicate the average of the best 100 simulations (S-) and the corresponding empirical data (E-) for different Mg concentrations. The error bars on the empirical data shows the standard deviations. The error bars on the simulation results indicate the standard deviation of the 100 best fits. Stars indicate the statistically significant differences between values given for the empirical data compared to the control (Mg^{2+} concentration of 0.78 mM) ($p < 0.05$ = *; $p < 0.01$ = **; $p < 0.001$ = ***). $\overline{R^2}$ is the average R^2 calculated for each measurement item.

Fig. 8). However, there was an overall discrepancy between the model's predictions and the data for the case of viability, the DNA content, the live cell count reported in study 3, and the growth factors. To investigate whether such disagreement originated from the inherent inability of the model in capturing the complexity of the experiments or from a possible discrepancy among the given empirical data, we conducted the second round of calibration in which the model was tuned against the culture data given for each model separately (C1, C2, and C3).

The results of C1, C2, and C3 showed a significant improvement in the model's accuracy in explaining the population-related data of DNA content, live cell count, and viability data compared to C1-3 (see section 3.3). To better understand the underlying differences between the models calibrated by different sets of data, their estimated parameter values were plotted against one another (see Fig. 4B). The observed variation in the estimated values primarily originates from the exploration of ABC in finding the global minimum based on the summary statistics [72]. However, there were meaningful patterns associated with certain parameters. It was shown that the base proliferation rate (γ_{P0}) was estimated similarly between C1 and C1-3, whereas C2 and C3 produced a notably smaller value. A similar pattern was also verified between the predictions of the models in terms of the live cell count and DNA content; the results of the live cell count predicted for study 1 were similar between C1 and C1-3 (see Fig. 6), while the results of the DNA content predicted for study 2 and live-cell count predicted for study 3 were overall higher for C1-3 compared to C2 and C3 (see Figs. 8 and 10). This suggests that the cells experimented in studies 2 and 3 were less proliferative compared to study 1. Considering that all experiments used a similar cell type (HUCPV) within the passage numbers 3 and 5, such discrepancy might step from the differences in the cell donors [73].

Another proliferation-associated parameter whose value showed a high variation across different calibration schemes was α_P (see Fig. 4B). This parameter simulates the model's sensitivity to the stimuli related to the proliferation process including Mg^{2+} ions as given in Eq. (1). Both C2 and C3 estimated a higher value for α_P compared to C1-3 and C1 (see Fig. 4B). Simultaneously, the model calibrated by C2 and C3 produced a higher contrast across different Mg concentrations in terms of live cell count and DNA contents (see Fig. 10). Hence, it can be understood that the cells cultured in study 1 were fundamentally more sensitive to Mg^{2+} ions compared to study 1 and 2. Such an observation can stem from cell donor dependency or the aging of Mg extract due to long-term storage before cell culture, which subsequently results in less bioactive Mg^{2+} ions.

Studies 2 and 3 lacked the quantitative measurements of cell viability (see Table S1 in the supplements). Instead, a minimum threshold of 50% was used according to similar experiments [39,40,13,74], in order to prevent the calibration process from producing an overall high fitness value at the cost of unrealistic cellular mortality. To satisfy this condition, C1-3 failed to closely reproduce the viability values given in study 1 (see Fig. 7). This implies that no parameter set could simultaneously satisfy the minimum viability assumed for studies 2 and 3 and the measured value in study 1. It can be seen that the cells in study 1 had a higher mortality rate than those in studies 2 and 3 (see Fig. 4B). Considering that the duration of study 1 was shorter than other studies, a higher mortality rate in the early days of culture compared to the later days can justify the observed differences. In our formulations, the factor of the cell passaging damage is assumed to cause permanent DNA damage and thereby contribute to early cellular mortality. However, assigning a large weighting factor for this process (α_{CM}) results in a sudden diminishing of live cells and leaving the remaining cells in solitude. Cells in isolation experience a low proliferation and high mortality rate, according to the assumptions of the FL controller, which further contributes to the shrinkage in the cell population. Therefore, the results of our simulation suggest

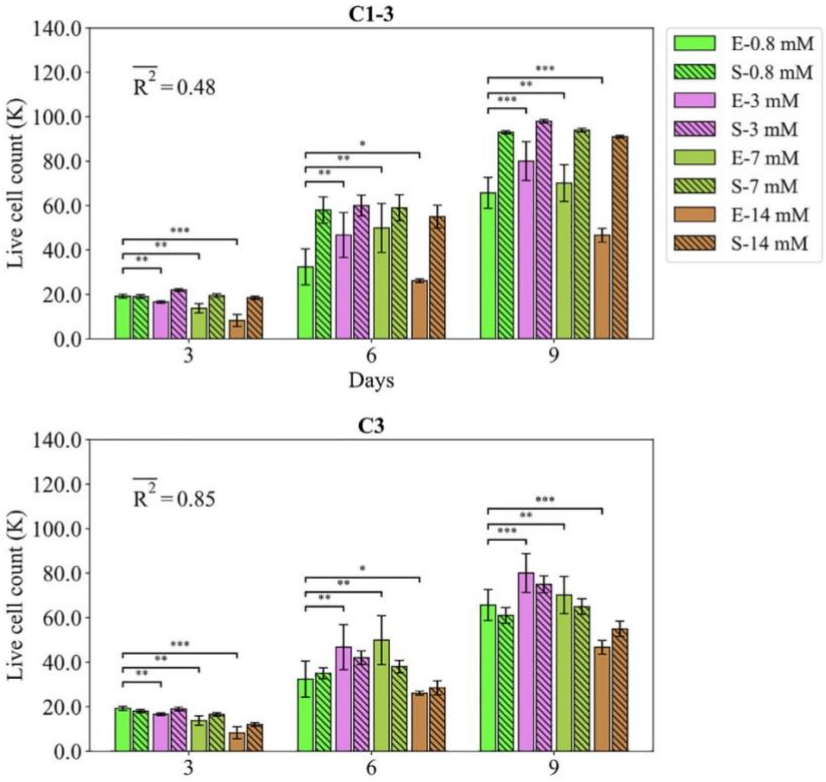

Fig. 10. Fits of the model calibrated by C1-3 and C3 to the empirical data of study 3. Bars indicate the average of the best 100 simulations (S-) and the corresponding empirical data (E-) for different Mg concentrations. The error bars on the empirical data shows the standard deviations. The error bars on the simulation results indicate the standard deviation of the 100 best fits. Stars indicate the statistically significant differences between values given for the empirical data compared to the control (Mg^{2+} concentration of 0.8 mM) ($p < 0.05$ = *; $p < 0.01$ = **; $p < 0.001$ = ***). $\overline{R^2}$ is the average R^2 calculated for each measurement item.

that either the cells cultured in the different studies had fundamental differences in their mortality behavior, or there is another factor that gradually contributes to cellular mortality in the early days of cell culture, which is not included in our formulations.

The experimental cell culture data shows that the content of the growth factors increases from day 7 to 14 and decreases from day 14 to 21. Given the fact that the reported contents for the growth factors were normalized against DNA, the observed jump on day 14 can indicate that cells were more productive within the first period of the experiment compared to the period after day 14. On the other hand, the cells were not fully differentiated before day 21, according to the results of the differentiation markers (see Fig. 8). This implies that the cells produced a higher amount of growth factors within their early differentiation phase compared to the later stage. Such an observation was not seen in the formulation of the present model (see Eq. (9) in the supplementary materials) which was adopted from the literature [75,55]. Further investigations are required to elucidate the relationship between the cellular activity regarding growth factors production and the degree of osteogenic differentiation.

An iterative process was used to calibrate the model's free parameters (see Fig. 3). In the proposed scheme, the iterative calibration process continued until no significant narrowing occurred. Overall, the performance of the model was considerably improved in the course of the iteration (see Fig. 5). In particular, the standard deviation of R^2, which indicates the uncertainty in the predictions of the model, dropped to a negligible value at the end of the iterative process (see Fig. 5). The remaining variation can stem from the stochastic nature of the agent-based modeling. The results also showed that the first few iterations can account for a large portion of the total improvements; for C1 and C2, the first five iterations accounted for over 90 percent of the total improvements (see section 0). This implies that the proposed criteria to stop the calibration process from further iteration, i.e. the significance in narrowing the posterior with respect to the prior, are not optimal. Therefore, the calibration scheme proposed in this study (see Fig. 3) can be further improved in the future by adding the alteration in the mean and standard deviation of R^2 as another factor in controlling the iteration number.

In the present study, we used Markov decision process-based ABM to study the dynamics of cell population and osteoblastic differentiation. The architectural design of our ABM is reminiscent of the modeling paradigm used in reinforcement learning, where decision-maker agents interact with one other and with their micro-environment [76]. The choice of ABM, thus, can facilitate the possible subsequent transformation of our descriptive model into a predictive reinforcement model in the future. The employed FL-based approach as the decision-making center of the agents (cells) offers human-intelligible, discrete components with parsable rules. In contrast to neural networks-based simulations which outsource all the learning burden into one "Blackbox"-like network module [76], the FL-based approach is tractable and conforms to the actual properties of a system. Such an approach is well-suited for investigating and incorporating the experimental datasets which may not be in perfect agreement with each other as was the case in the present study. Once such a model is calibrated, it can serve as the natural basis for neural networks where the problem becomes more tractable for a learning algorithm

Among many limitations of the present computer model, here we discuss a few important ones. Firstly, in the implemented FL controller (see Table 1), the effect of different cellular inputs was combined using the principle of superposition. Due to the lack of information to correctly define the logic of interactions among the stimulatory factors, such an assumption is inevitable and is also made in similar studies [19,75,77]. We speculate that Mg2 + ions combined with TGF-β1 and BMP2 produce synergistic effects which need to be studies in the future. Secondly, we primarily investigated the bioregulatory effects of Mg^{2+} ions by applying the model to the empirical datasets with various concentrations of Mg^{2+} ions. The factor of alkalinity is also inclusively studied as it changes in a linear relationship with the concentration of Mg^{2+}, which is also the case in the culture experiments. The factors of TGF-β1 and BMP2 were individually studied in the previous works [75,55,78] and therefore were not explicitly investigated in this study. Regarding the factor of cell density, we were not able to find any study that quantitatively reported the effect of this factor on the given cellular behaviors. This might step from the fact that a precise monitoring of cellular positioning in a colony for a long period of time, i.e. a few weeks, is not practical. Thirdly, we used discrete grids to create the simulation domain (on-lattice) instead of continuum space, known as the off-lattice approach [79]. The grid-based approach constrains agents' movement to the defined grids while off-lattice simulation provides a continuum reach. However, the former offers superior performance compared to the latter and therefore was favored in our simulations due to the complexity of the model and the computationally demanding method employed for the calibration process. Lastly, substrate stiffness, as an important parameter in guiding osteogenic differentiation [80], was not included in the present study. This important parameter will be incorporated in our future models which will simulate the *in vivo* setup.

5. Conclusion

The fuzzy agent-based computer model presented in this study was generally able to reproduce the empirical observations reported for the MSC population and osteogenic differentiation. The model closely captured the nonlinearities in the regulatory effect of Mg^{2+} ions on multiple cellular processes such as cell proliferation, differentiation, and mortality. The model also showed fundamental differences between the cells cultured in different experiments in terms of proliferation capacity and sensitivity to environmental variables such as Mg^{2+} ions. Moreover, the iterative calibration approach proposed in this study was shown advantageous in improving the performance of the model and is thereby recommended over the single-round calibration method commonly used in the literature. In summary, this study shows the significance of numerical modeling in understanding and objectively explaining the experiments by special attention to the mechanisms underlying cellular processes.

Declaration of Competing Interest

The authors declare that they have no known competing financial interests or personal relationships that could have appeared to influence the work reported in this paper.

Acknowledgements

This work was funded by Helmholtz-Zentrum Geesthacht. The computational work was facilitated by the Maxwell computational resources operated at Deutsches Elektronen-Synchrotron (DESY), Hamburg, Germany. We thank Roland Aydin for his constructive comments on this work.

Appendix A. Supplementary data

Supplementary data to this article can be found online at https://doi.org/10.1016/j.csbj.2021.07.005.

References

[1] I. Trejo and H. V Kojouharov, "Understanding the fundamental molecular mechanism of osteogenic differentiation from mesenchymal stem cells," vol. 14, no. 2, pp. 687–698, 2019.
[2] Holland RE, James F, Pollock,. Holland-Frei cancer medicine 8. PMPH-USA 2010.
[3] Lian JB, Stein GS, Javed A, van Wijnen AJ, Stein JL, Montecino M, et al. Networks and hubs for the transcriptional control of osteoblastogenesis. Rev Endocr Metab Disord 2006;7(1-2):1–16.
[4] J. E. Aubin, "Mesenchymal Stem Cells and Osteoblast Differentiation AND CONTROL OF OSTEOBLAST," In Vivo (Brooklyn)., pp. 85–107, 2008.
[5] Gao C, Peng S, Feng P, Shuai C. Bone biomaterials and interactions with stem cells. Nat Publ Gr 2017;5(October):1–33.
[6] Rahmati M, Silva EA, Reseland JE, Heyward CA, Haugen HJ. Biological responses to physicochemical properties of biomaterial surface. Chem Soc Rev 2020;49 (15):5178–224.
[7] Willumeit-Römer R. The Interface Between Degradable Mg and Tissue. Jom 2019;71(4):1447–55.
[8] L. Hou et al., "In vitro and in vivo studies on biodegradable magnesium alloy," 2014.
[9] L. Wu, F. Feyerabend, A. F. Schilling, R. Willumeit-Romer, and B. J. Luthringer, "Effects of extracellular magnesium extract on the proliferation and differentiation of human osteoblasts and osteoclasts in coculture," Acta Biomater., vol. 27, no. 294–304, 2015.
[10] Fliefel R, Popov C, Tröltzsch M, Kühnisch J, Ehrenfeld M, Otto S. Mesenchymal stem cell proliferation and mineralization but not osteogenic differentiation are strongly affected by extracellular pH. J Craniomaxillofac Surg 2016;44 (6):715–24.
[11] Simão AMS, Bolean M, Hoylaerts MF, Millán JL, Ciancaglini P. Effects of pH on the production of phosphate and pyrophosphate by matrix Vesicles' Biomimetics. Calcif Tissue Int 2013;93(3):222–32.
[12] Taylor AC. Responses of cells to pH changes in the medium. J Cell Biol 1962;15 (2):201–9.
[13] Qi T, Weng J, Yu F, Zhang W, Li G, Qin H, et al. Insights into the role of magnesium ions in affecting osteogenic differentiation of mesenchymal stem cells. Biol Trace Elem Res 2021;199(2):559–67.
[14] H. Zhou, B. Liang, H. Jiang, Z. Deng, and K. Yu, "Magnesium-based biomaterials as emerging agents for bone repair and regeneration: from mechanism to application," J. Magnes. Alloy., no. xxxx, 2021.
[15] Wadkin LE, Orozco-Fuentes S, Neganova I, Lako M, Shukurov A, Parker NG. The recent advances in the mathematical modelling of human pluripotent stem cells. SN Appl Sci 2020;2(276):1–14.
[16] György R, Klontzas ME, Kostoglou M, Panoskaltsis N, Mantalaris A, Georgiadis MC. Capturing mesenchymal stem cell heterogeneity during osteogenic differentiation: an experimental-modeling approach. Ind Eng Chem Res 2019;58(31):13900–9.
[17] Krinner A, Hoffmann M, Loeffler M, Drasdo D, Galle J. Individual fates of mesenchymal stem cells in vitro. BMC Syst Biol 2010;4(1):73. https://doi.org/10.1186/1752-0509-4-73.
[18] E. S. Bayrak, H. Mehdizadeh, B. Akar, S. I. Somo, E. M. Brey, and A. Cinar, "Agent-based modeling of osteogenic differentiation of mesenchymal stem cells in porous biomaterials," 2014 36th Annu. Int. Conf. IEEE Eng. Med. Biol. Soc. EMBC 2014, pp. 2924–2927, 2014.
[19] Kühn C, Checa S. Computational modeling to quantify the contributions of VEGFR1, VEGFR2, and lateral inhibition in sprouting angiogenesis. Front Physiol 2019;10. https://doi.org/10.3389/fphys.2019.00288.
[20] Lambert B, MacLean AL, Fletcher AG, Combes AN, Little MH, Byrne HM. Bayesian inference of agent-based models: a tool for studying kidney branching morphogenesis. J Math Biol 2018;76(7):1673–97.
[21] Nickaeen N, Ghaisari J, Heiner M, Moein S, Gheisari Y. Agent-based modeling and bifurcation analysis reveal mechanisms of macrophage polarization and phenotype pattern distribution. Sci Rep 2019;9(1):1–14.
[22] DeAngelis DL, Diaz SG. Decision-making in agent-based modeling: A current review and future prospectus. Front Ecol Evol 2019;6:237.
[23] Soheilypour M, Mofrad MRK. Agent-Based Modeling in Molecular Systems Biology. BioEssays 2018;40(7):1800020. https://doi.org/10.1002/bies.v40.710.1002/bies.201800020.
[24] Delile J, Herrmann M, Peyriéras N, Doursat R. A cell-based computational model of early embryogenesis coupling mechanical behaviour and gene regulation. Nat Commun 2017;8:1–10.
[25] Wang Z, Wang D, Li C, Xu Y, Li H, Bao Z. Deep reinforcement learning of cell movement in the early stage of C.elegans embryogenesis. Bioinformatics 2018;34(18):3169–77.
[26] Tartarini D, Mele E. Adult stem cell therapies for wound healing: Biomaterials and computational models. Front Bioeng Biotechnol 2016;vol. 3, no. JAN:1–7.

[27] Spolaor S et al. "Towards human cell simulation". Lecture Notes in Computer Science (including subseries Lecture Notes in Artificial Intelligence and Lecture Notes in Bioinformatics) 2019;vol. 11400:221–49.
[28] T. Ren and H. L. Dailey, "Mechanoregulation modeling of bone healing in realistic fracture geometries," Biomech. Model. Mechanobiol., no. 0123456789, 2020.
[29] Liu F, Heiner M, Yang M, Bourdon J. Fuzzy stochastic petri nets for modeling biological systems with uncertain kinetic parameters. PLoS One 2016;11(2): e0149674. https://doi.org/10.1371/journal.pone.0149674.
[30] Wang M, Yang N. Computational simulation of the influence of mechanical stability on growth factors activities during bone fracture healing. IEEE Access 2019;7:9827–35.
[31] Hanna H, Mir LM, Andre FM. In vitro osteoblastic differentiation of mesenchymal stem cells generates cell layers with distinct properties. Stem Cell Res Ther 2018;9(1):203.
[32] F. O. Ribeiro and M. J. Gómez-benito, "In silico Mechano-Chemical Model of Bone Healing for the Regeneration of Critical Defects : The Effect of BMP-2," pp. 1–25, 2015.
[33] Nourisa J. janursa/fuzzyABM: First public release. Zenodo Apr-2021..
[34] Norton KA, Popel AS. Effects of endothelial cell proliferation and migration rates in a computational model of sprouting angiogenesis. Sci Rep 2016;6:Nov.
[35] Browning AP, McCue SW, Binny RN, Plank MJ, Shah ET, Simpson MJ. Inferring parameters for a lattice-free model of cell migration and proliferation using experimental data. J Theor Biol 2018;437:251–60.
[36] Iancu I. A Mamdani type fuzzy logic controller Fuzzy Log Control Concepts. Theor Appl 2012:325–50.
[37] Jin W, Penington CJ, McCue SW, Simpson MJ, Lythe G. A computational modelling framework to quantify the effects of passaging cell lines. PLoS One 2017;12(7):e0181941. https://doi.org/10.1371/journal.pone.0181941.
[38] Yoshizawa S, Brown A, Barchowsky A, Sfeir C. Magnesium ion stimulation of bone marrow stromal cells enhances osteogenic activity, simulating the effect of magnesium alloy degradation. Acta Biomater 2014;10(6):2834–42.
[39] Cecchinato F, Agha NA, Martinez-Sanchez AH, Luthringer BJC, Feyerabend F, Jimbo R, et al. Influence of magnesium alloy degradation on undifferentiated human cells. PLoS One 2015;10(11):e0142117. https://doi.org/10.1371/journal.pone.0142117.
[40] Leem Y-H, Lee K-S, Kim J-H, Seok H-K, Chang J-S, Lee D-H. Yea-Hyun and Lee, Kang-Sik and Kim, Jung-Hwa and Seok, Hyun-Kwang and Chang, Jae-Suk and Lee, "Magnesium ions facilitate integrin alpha 2-and alpha 3-mediated proliferation and enhance alkaline phosphatase expression and activity in hBMSCs". J Tissue Eng Regen Med 2016;10(10):E527–36.
[41] Maradze D, Musson D, Zheng Y, Cornish J, Lewis M, Liu Y. High magnesium corrosion rate has an effect on osteoclast and mesenchymal stem cell role during bone remodelling. Sci Rep 2018;8(1):1–15.
[42] Zhang X, Zu H, Zhao D, Yang K, Tian S, Yu X, et al. Ion channel functional protein kinase TRPM7 regulates Mg ions to promote the osteoinduction of human osteoblast via PI3K pathway: In vitro simulation of the bone-repairing effect of Mg-based alloy implant. Acta Biomater 2017;63:369–82.
[43] Luthringer BJC, Willumeit-Römer R. Effects of magnesium degradation products on mesenchymal stem cell fate and osteoblastogenesis. Gene 2016;575(1):9–20.
[44] Burmester A, Willumeit-Römer R, Feyerabend F. Behavior of bone cells in contact with magnesium implant material. J Biomed Mater Res - Part B Appl Biomater 2017;105(1):165–79.
[45] Wang J, Witte F, Xi T, Zheng Y, Yang K, Yang Y, et al. Recommendation for modifying current cytotoxicity testing standards for biodegradable magnesium-based materials. Acta Biomater 2015;21:237–49.
[46] Ingo Grafe Stefanie Alexander Jonathan R. Peterson Taylor Nicholas Snider Benjamin Levi Brendan Lee et al. 10 5 2018 a022202 10.1101/cshperspect.a022202.
[47] Schmidt-Bleek K, Marcucio R, Duda G. Future treatment strategies for delayed bone healing: an osteoimmunologic approach. J Am Acad Orthop Surg 2016;24 (10):e134–5.
[48] Elsafadi M, Shinwari T, Al-Malki S, Manikandan M, Mahmood A, Aldahmash A, et al. Convergence of TGF$β$ and BMP signaling in regulating human bone marrow stromal cell differentiation. Sci Rep 2019;9(1). https://doi.org/10.1038/s41598-019-41543-0.
[49] Knippenberg M, Helder MN, Zandieh Doulabi B, Wuisman PIJM, Klein-Nulend J. Osteogenesis versus chondrogenesis by BMP-2 and BMP-7 in adipose stem cells. Biochem Biophys Res Commun 2006;342(3):902–8.
[50] Lysdahl H, Baatrup A, Foldager CB, Bünger C. Preconditioning human mesenchymal stem cells with a low concentration of BMP2 stimulates proliferation and osteogenic differentiation in vitro. Biores Open Access 2014;3(6):278–85.
[51] Kim HKW, Oxendine I, Kamiya N. High-concentration of BMP2 reduces cell proliferation and increases apoptosis via DKK1 and SOST in human primary periosteal cells. Bone 2013;54(1):141–50.
[52] A Yamaguchi T Katagiri T Ikeda J M Wozney V Rosen E A Wang et al. Recombinant human bone morphogenetic protein-2 stimulates osteoblastic maturation and inhibits myogenic differentiation in vitro 113 3 1991 681 687.
[53] Wang Y et al. Comparative study of serum levels of BMP-2 and heterotopic ossification in traumatic brain injury and fractures patients. Zhongguo Gu Shang May 2011;24(5):399–403.
[54] Park Y, Kim JW, Kim DS, Kim EB, Park SJ, Park JY, et al. "The bone morphogenesis protein-2 (BMP-2) is associated with progression to metastatic disease in gastric cancer", *Cancer Res.* Treat Off J Korean Cancer Assoc 2008;40(3):127. https://doi.org/10.4143/crt.2008.40.3.127.
[55] F. O. Ribeiro, M. J. Gómez-Benito, J. Folgado, P. R. Fernandes, and J. M. García-Aznar, "In silico mechano-chemical model of bone healing for the regeneration of critical defects: The effect of BMP-2," PLoS One, vol. 10, no. 6, 2015.
[56] Janssens K, ten Dijke P, Janssens S, Van Hul W. Transforming growth factor-beta1 to the bone. Endocr Rev Oct. 2005;26(6):743–74.
[57] Karsdal MA et al. "Matrix Metalloproteinase-dependent Activation of Latent Transforming Growth Factor- $^{N}_{L}$ Controls the Conversion of Osteoblasts into Osteocytes by. Blocking Osteoblast Apoptosis *" 2002;277(46):44061–7.
[58] T. L. Chen and R. L. Bates, "Recombinant Human Transforming Growth Factor Modulates Bone Remodeling in a Mineralizing Bone Organ Culture," vol. 8, no. 4, 1993.
[59] Breen EC, Ignotz RA, McCabe L, Stein JL, Stein GS, Lian JB. TGF$β$ alters growth and differentiation related gene expression in proliferating osteoblasts in vitro, preventing development of the mature bone phenotype. J Cell Physiol 1994;160(2):323–35.
[60] Garg P, Mazur MM, Buck AC, Wandtke ME, Liu J, Ebraheim NA. Prospective review of mesenchymal stem cells differentiation into osteoblasts. Orthop Surg 2017;9(1):13–9.
[61] Pavel M, Renna M, Park SJ, Menzies FM, Ricketts T, Füllgrabe J, et al. Contact inhibition controls cell survival and proliferation via YAP/TAZ-autophagy axis. Nat Commun 2018;9(1). https://doi.org/10.1038/s41467-018-05388-x.
[62] Stoker MGP, Rubin H. Density dependent inhibition of cell growth in culture. Nature 1967;215(5097):171–2.
[63] Liang C-C, Park AY, Guan J-L. In vitro scratch assay: A convenient and inexpensive method for analysis of cell migration in vitro. Nat Protoc 2007;2 (2):329–33.
[64] Qiao L, Farrell GC. The effects of cell density, attachment substratum and dexamethasone on spontaneous apoptosis of rat hepatocytes in primary culture. Vitr Cell Dev Biol - Anim 1999;35(7):417–24.
[65] J. Wu, Y. Fan, and E. S. Tzanakakis, "Increased culture density is linked to decelerated proliferation, prolonged G1 phase, and enhanced propensity for differentiation of self-renewing human pluripotent stem cells," vol. 24, no. 7, pp. 892–903, 2015.
[66] W. Yuan-kun, T. Yuan-kun, Y. Jiashing, and N. Chen, "The Influence of Cell Culture Density on the Cytotoxicity of Adipose-Derived Stem Cells Induced by L-Ascorbic Acid-2- Phosphate," pp. 1–11, 2020.
[67] Bieberich E, MacKinnon S, Silva J, Noggle S, Condie BG. Regulation of cell death in mitotic neural progenitor cells by asymmetric distribution of prostate apoptosis response 4 (PAR-4) and simultaneous elevation of endogenous ceramide. J Cell Biol 2003;162(3):469–79.
[68] Martinez-Sanchez AH. "Cell reactions to the degradation of Mg-based materials. Chondrogenic Differentiation" 2017.
[69] L. Xu, R. Willumeit-römer, and B. J. C. Luthringer-feyerabend, "Effect of magnesium-degradation products and hypoxia on the angiogenesis of human umbilical vein endothelial cells," vol. 98, pp. 269–283, 2019.
[70] L. Xu, R. Willumeit-römer, and B. Luthringer-feyerabend, "Hypoxia influences the effects of magnesium degradation products on the interactions between endothelial and mesenchymal stem cells," vol. 101, pp. 624–636, 2020.
[71] van der Vaart E, Beaumont MA, Johnston ASA, Sibly RM. Calibration and evaluation of individual-based models using Approximate Bayesian Computation. Ecol Modell 2015;312:182–90.
[72] M. A. Beaumont, "Annual Review of Statistics and Its Application Approximate Bayesian Computation," 2018
[73] Sarugaser R, Lickorish D, Baksh D, Hosseini MM, Davies JE. Human umbilical cord perivascular (HUCPV) cells: a source of mesenchymal progenitors. Stem Cells 2005;23(2):220–9.
[74] C. Yang, G. Yuan, J. Zhang, Z. Tang, X. Zhang, and K. Dai, "Effects of magnesium alloys extracts on adult human bone marrow-derived stromal cell viability and osteogenic differentiation," Biomed. Mater., vol. 5, no. 4, 2010.
[75] Geris L, Gerisch A, Sloten JV, Weiner R, Oosterwyck HV. Angiogenesis in bone fracture healing: A bioregulatory model. J Theor Biol 2008;251 (1):137–58.
[76] A. Esteva et al., "A guide to deep learning in healthcare," Nature Medicine, vol. 25, no. 1. Nature Publishing Group, pp. 24–29, 01-Jan-2019.
[77] Zhao C, Mirando AC, Sové RJ, Medeiros TX, Annex BH, Popel AS, et al. A mechanistic integrative computational model of macrophage polarization: Implications in human pathophysiology. PLoS Comput Biol 2019;15(11): e1007468. https://doi.org/10.1371/journal.pcbi.1007468.
[78] Khatibi S, Zhu H-J, Wagner J, Tan CW, Manton JH, Burgess AW. Mathematical model of TGF-βsignalling: feedback coupling is consistent with signal switching. BMC Syst Biol 2017;11(1):48.
[79] F. Merino-Casallo, M. J. Gomez-Benito, Y. Juste-Lanas, R. Martinez-Cantin, and J. M. Garcia-Aznar, "Integration of in vitroand in silicomodels using Bayesian optimization with an application to stochastic modeling of mesenchymal 3D cell migration," Front. Physiol., vol. 9, no. SEP, Sep. 2018.
[80] Bahney CS, Zondervan RL, Allison P, Theologis A, Ashley JW, Ahn J, et al. Cellular biology of fracture healing. J Orthop Res 2019;37(1):35–50.

.

III.3. The osteogenetic activities of mesenchymal stem cells in response to Mg^{2+} ions and inflammatory cytokines: a numerical approach using fuzzy logic controllers

The present study aimed to investigate the effect of Magnesium (Mg2+) ions on the osteoblastic differentiation of mesenchymal stem cells (MSCs) in the presence of inflammation. To achieve this, we proposed a numerical model that utilized a fuzzy logic controller to predict the early and late differentiation rates of MSCs based on the concentrations of Mg2+ ions and various inflammatory cytokines such as TNF-α, IL-10, IL-1β, and IL-8. The model was calibrated using five sets of empirical data obtained from published cell culture experiments. The results showed that the proposed model accurately reflected the concentration- and phase-dependent effect of Mg2+ ions on MSC differentiation, with low concentrations of Mg2+ ions promoting early differentiation and higher concentrations inhibiting late differentiation. The model suggested a concentration of 6–8 mM as being most effective in promoting early differentiation. Additionally, the model highlighted differences in the behavior of cells from different experiments and successfully reproduced the non-linearities in the concentration-dependent role of the inflammatory cytokines. In conclusion, the proposed model provides valuable insights into the study of the osteogenic properties of Mg-based implants in the presence of inflammation.

Nourisa J, Zeller-Plumhoff B, Willumeit-Römer R. The osteogenetic activities of mesenchymal stem cells in response to Mg^{2+} ions and inflammatory cytokines: a numerical approach using fuzzy logic controllers. PLoS computational biology. 2022. 18(9). e1010482. DOI: 10.1371/journal.pcbi.1010482.

Contribution of Jalil Nourisa:

Literature search	Problem definition	Data acquisition	Software development	Data analysis	Manuscript drafting
Primary role	Primary role	Primary role	Primary role	Primary role	Primary role

PLOS COMPUTATIONAL BIOLOGY

RESEARCH ARTICLE

The osteogenetic activities of mesenchymal stem cells in response to Mg^{2+} ions and inflammatory cytokines: a numerical approach using fuzzy logic controllers

Jalil Nourisa*, Berit Zeller-Plumhoff, Regine Willumeit-Römer

Helmholtz Zentrum Hereon, Institute of Metallic Biomaterials, Geesthacht, Germany

* jalil.nourisa@gmail.com

OPEN ACCESS

Citation: Nourisa J, Zeller-Plumhoff B, Willumeit-Römer R (2022) The osteogenetic activities of mesenchymal stem cells in response to Mg^{2+} ions and inflammatory cytokines: a numerical approach using fuzzy logic controllers. PLoS Comput Biol 18(9): e1010482. https://doi.org/10.1371/journal.pcbi.1010482

Editor: Adrianne Jenner, Queensland University of Technology, AUSTRALIA

Received: April 12, 2022

Accepted: August 11, 2022

Published: September 15, 2022

Data Availability Statement: The data required to reproduce these findings are available to download from https://zenodo.org/record/6369939. The processed data required to reproduce these findings are available to download from https://zenodo.org/record/6369939.

Funding: This study is financially supported by Helmholtz Zentrum Hereon. The funders had no role in the study design, data collection and

Abstract

Magnesium (Mg^{2+}) ions are frequently reported to regulate osteogenic activities of mesenchymal stem cells (MSCs). In this study, we propose a numerical model to study the regulatory importance of Mg^{2+} ions on MSCs osteoblastic differentiation in the presence of an inflammatory response. A fuzzy logic controller was formulated to receive the concentrations of Mg^{2+} ions and the inflammatory cytokines of TNF-α, IL-10, IL-1β, and IL-8 as cellular inputs and predict the cells' early and late differentiation rates. Five sets of empirical data obtained from published cell culture experiments were used to calibrate the model. The model successfully reproduced the empirical data regarding the concentration- and phase-dependent effect of Mg^{2+} ions on the differentiation process. In agreement with the experiments, the model showed the stimulatory role of Mg^{2+} ions on the early differentiation phase, once administered at low concentration, and their inhibitory role on the late differentiation phase. The numerical approach used in this study suggested 6–8 mM as the most effective concentration of Mg^{2+} ions in promoting the early differentiation process. Also, the proposed model sheds light on the fundamental differences in the behavioral properties of cells cultured in different experiments, e.g. differentiation rate and the sensitivity of the cultured cells to stimulatory signals such as Mg^{2+} ions. Thus, it can be used to interpret and compare different empirical findings. Moreover, the model successfully reproduced the nonlinearities in the concentration-dependent role of the inflammatory cytokines in early and late differentiation rates. Overall, the proposed model can be employed in studying the osteogenic properties of Mg-based implants in the presence of an inflammatory response.

Author summary

Magnesium (Mg) is an attractive material for bone implants as it fully degrades after implantation, saving pain and cost of the second surgery for implant removal. To advance its application in the orthopedic industry, it is paramount to fully understand the biological impact of the degradation products, in particular Mg^{2+} ions. Here, we propose a

analysis, decision to publish, or preparation of the manuscript.

Competing interests: The authors have declared that no competing interests exist.

computer model to study the effects of Mg^{2+} ions on bone regeneration. The model focuses on stem cells and includes both the direct stimulation effects of Mg^{2+} ions on cells and the indirect stimulus through the inflammatory system. The proposed model successfully reproduced the experimental data of five different studies. The model additionally highlighted differences amongst different experiments in terms of the cellular response to Mg^{2+} ions. The proposed system therefore provides an important addition to the field of Mg implant research.

1 Introduction

Magnesium (Mg)-based biomaterials are an attractive choice in the orthopedic industry due to their biodegradability and superior osteogenic capacity compared to non-degradable metallic implants e.g., titanium alloys [1–3]. Mg^{2+} ions released in the implantation site due to the degradation process modulate a wide range of physiological processes involved in bone fracture healing, in particular osteogenesis [1], [4]. The mediatory effects of Mg^{2+} ions on osteogenic differentiation can be evaluated in two aspects (see Fig 1A). First, Mg^{2+} ions directly modulate multiple signaling pathways associated with the differentiation of mesenchymal stem cells (MSCs) to osteoblasts [5], [6]; Mg^{2+} ions are shown to activate MAPK/ERK and Wnt/ β-catenin signaling pathways which are associated with osteogenic differentiation [7]. Secondly, Mg^{2+} ions mediate the inflammatory response and thereby indirectly guide osteogenesis [8–10].

The inflammatory response is known to play a pivotal role in all stages of bone tissue regeneration [11]–[13]. In particular, macrophages are repeatedly shown to guide osteogenesis [12], [14], [11]. During the healing process, macrophages obtain different functional roles ranging from pro-inflammatory M1 to anti-inflammatory M2 and secrete a multitude of cytokines essential for the osteogenic ability of MSCs [14], [15]. Empirical data have shown the significance of Mg^{2+} ions in modulating macrophage polarization and cytokines production [9], [10], [16], [17]. For instance, Qiao et al. [17] applied Mg^{2+} ions to macrophages in a cell culture environment and observed an upregulation in the production of interleukin (IL)-8, which is

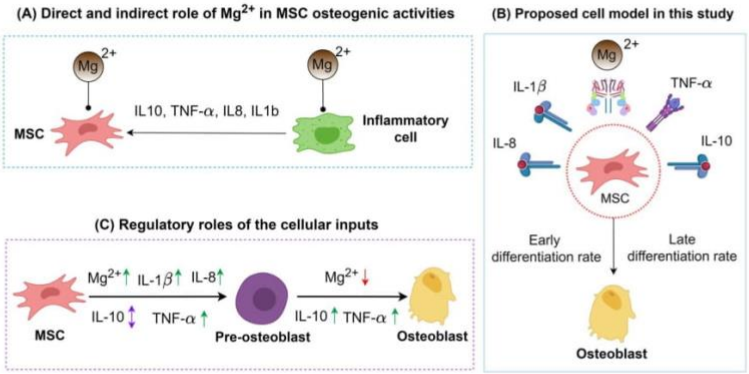

Fig 1. (A) Mg^{2+} ions regulate MSC differentiation in both direct and indirect ways. (B) the cell model proposed in this study receives five cellular signals and predicts early and late differentiation rates. (C) the regulatory role of Mg^{2+} ions and the inflammatory cytokines on the early and late osteogenic differentiation. Upwards arrays in green indicate stimulatory roles; downwards arrays in red indicate inhibitory roles; up-down arrows in purple indicate dose-dependent effect. BioRender.com is used to create some elements of the graph.

https://doi.org/10.1371/journal.pcbi.1010482.g001

an important factor in the osteogenic differentiation of MSCs. Such an indirect influence of Mg^{2+} ions on osteogenesis is reported to even overweight the direct regulatory effect of Mg^{2+} ions on MSCs [17].

Although Mg^{2+} ions are generally shown to promote osteogenesis, multiple studies have reported their detrimental effects on tissue regeneration [8], [18]. Such a conflicting finding implies an incomplete understanding of the role of Mg^{2+} ions in the complex process of fracture healing. In order to effectively design a Mg-based implant, it is paramount to fully understand the bioregulatory role of Mg^{2+} ions on tissue regeneration in the presence of other signaling factors, in particular inflammatory reactions [4], [19][20]. So far, the experimental approach has been the primary method in investigating the physiological roles of Mg^{2+} ions. In recent years, numerous studies have shown the importance of numerical investigation in the study of biological systems and bone-implant design [21–25]. Fuzzy logic (FL) has been given a special attention in quantitative modelling of biological systems with uncertain kinetic data [26][27]. Aldridge et al [28] used FL in describing the dynamics of intracellular pathways of human colon carcinoma cells associated with different growth factors and insulin receptors. Their FL-based simulations successfully produced several predictions of pathways crosstalk and regulation [28]. They also proposed a relationship between MK2 and ERK pathways which was unknown previously [28]. Wang et al [29] and Niemeyer et al [30] employed FL to simulate the transitional formation of different tissues during bone regeneration. They have successfully shown the patterns of bone tissue regeneration under various mechanical environment [29], [30].

Recently, we proposed a fuzzy agent-based model to numerically study the proliferation and osteogenic differentiation of MSCs in response to Mg^{2+} ions [31]. We showed that Mg^{2+} ions within 3-6mM concentration have the highest stimulation effect on cell population growth. The model also captured the stimulatory role of Mg^{2+} ions on early differentiation and its inhibitory effect on the late differentiation process. In this study, as an extension of our previous model, we propose a FL-based model to investigate the osteogenic response of MSCs to Mg^{2+} ions in tandem with the inflammatory cytokines of tumor necrosis factor alpha (TNF-α), interleukin 10 (IL-10), interleukin 1 beta (IL-1β), and IL-8. In the present model, the previously proposed controller for the Mg^{2+} ions is further extended to include the inhibitory role of Mg^{2+} ions on the early osteogenic response once the concentrations is below the physiological level. In addition, five more controllers are presented to account for the regulatory roles of the given inflammatory cytokines.

2 Results

2.1 The overview of the model formulation

In this study, the proposed cell model receives five cellular inputs and predicts the osteogenic differentiation rates (see Fig 1B). The choice of cytokines is based on their importance in osteogenesis and their involvement in the interplay of Mg^{2+} ions with the inflammatory cells, as elaborated in section 4.1. Since the cellular inputs can regulate the early and late differentiation process differently (Fig 1C), two distinguished processes of early- and late differentiation rates are calculated by the model. A FL controller is designed to act as the core calculator of the cell model. In order to define fuzzy rules, we gathered the available information in the literature regarding the regulatory role of the cellular inputs (see section 4.1). A complete introduction to the development of the FL controller is given in section 5. The formulation of the model generated 30 unknown parameters given in S3 Table. We estimated the values of these parameters using a calibration process by employing differential evolution (DE) [32]. The published data of five cell-culture experiments were used for this purpose (see

section 5.5). These experiments reported the bioregulatory effect of Mg2+ ions and different inflammatory cytokines on the osteoblastic differentiation of MSC. In these reports, alkaline phosphate (ALP) was used as the early differentiation marker, while osteocalcin (OC) and alkaline red staining (ARS) were the late differentiation markers. The parameter estimation process was carried out to maximize the fitness value, which is defined as the normalized absolute difference between the simulation results (S) and the empirical observations (E) as $R^2 = |E\text{-}S|/E$. The calibration process was conducted on the dataset of each experiment individually, encoded as C1 to C5, as well as on the combined data of all experiments, encoded as C1-5. Once the model was calibrated, we investigated the sensitivity of the model to the parameters using large-scale simultaneous perturbations (LSSP) and small-scale individual perturbations (SSIP). The details of the calibration process and the sensitivity analysis are given in section 5.6.

2.2 Simulation results versus empirical observations

2.2.1 Study 1. Study 1 reports the regulatory effect of Mg^{2+} ions on the early differentiation rate, measured by ALP [17]. The fits of the simulation results to the data of study 1 are presented in Fig 2. The empirical data suggest that the application of Mg^{2+} ions at the concentration of 8 mM increases the early differentiation rate at both measurement days of 3 and 7 compared to the physiological concentration of 0.8 mM (see Fig 2). Contrarily, the application of Mg^{2+} ions at the concentration of 0.08 mM decreases the early differentiation rate (see Fig 2). These observations were correctly captured by the model calibrated by C1-5 with a fitness value of 0.84. Once calibrated by C1, the model was able to closely reproduce the reported measurements with the average fitness value of 0.92. The variations in the simulation results of study 1 due to SSIP are given in Fig 2 for each measurement item.

2.2.2 Study 2. Study 2 reports the regulatory effects of Mg^{2+} ions on the early and late differentiation rates, measured by ALP and OC, respectively [6]. The fits of the model to the data of study 2 are given in Fig 3. The data suggests that by increasing Mg^{2+} ions from 0.8 to 5 mM, the early differentiation rate increases while the late differentiation rate decreases. The model calibrated by C1-5 was able to capture the former but not the latter. The mean fitness values obtained during Effects of magnesium degradation products on mesenchymal stem cell fate and osteoblastogenesis C1-5 were 0.94 for ALP and 0.49 for OC (see Fig 3). Once calibrated by C2, the model was capable of correctly reproducing both trends and exact values with the

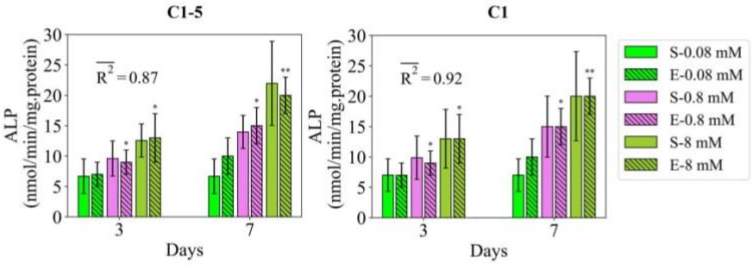

Fig 2. Fits of the model calibrated by C1-5 and C1 to the empirical data of study 1. Bars indicate the simulations (S-) and the corresponding empirical data (E-) for increasing Mg^{2+} ion concentrations. The error bars on the empirical data show the standard deviations. The error bars on the simulation results show the standard deviations obtained during SSIP, i.e. 15% alteration in the estimated parameter values. Stars indicate the statistically significant differences between values given for the empirical data compared to the control, i.e. Mg^{2+} ion concentration of 0.08 mM ($p < 0.05 = {}^{*}$; $p < 0.01 = {}^{**}$). $\overline{R^2}$ is the average fitness value of the simulations for the given measurement item.

https://doi.org/10.1371/journal.pcbi.1010482.g002

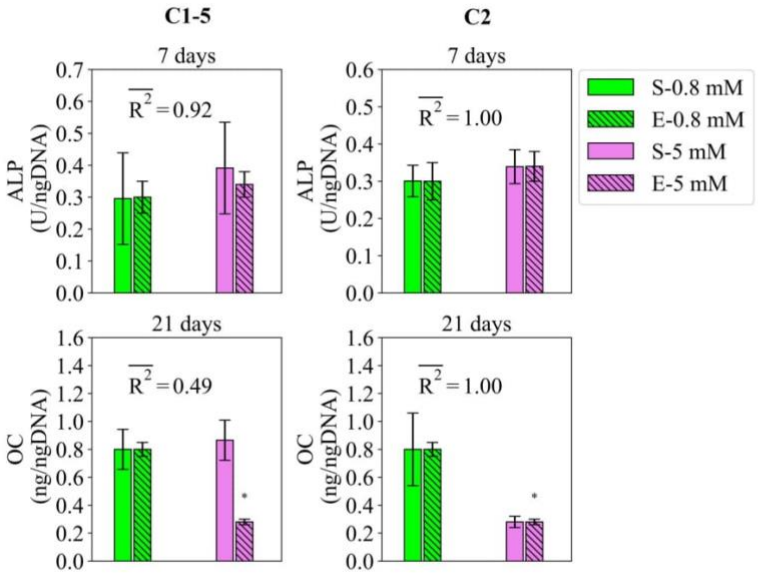

Fig 3. Fits of the model calibrated by C1-5 and C2 to the empirical data of study 2. Bars indicate the simulations (S-) and the corresponding empirical data (E-) for increasing Mg^{2+} ion concentrations. The quantities of ALP and OC are reported at day 7 and 21, repectively. The error bars on the empirical data shows the standard deviations. The error bars on the simulation results show the standard deviations obtained during SSIP, i.e. 15% alteration in the estimated parameter values. Stars indicate the statistically significant differences between values given for the empirical data compared to the control, i.e. Mg^{2+} ion concentration of 0.8 mM ($p < 0.05 = {}^*$). $\overline{R^2}$ is the average fitness value of the simulations for the given measurement item.

https://doi.org/10.1371/journal.pcbi.1010482.g003

fitness values of 1 for both markers (see Fig 3). The variations in the simulation results of study 2 due to SSIP are given in Fig 3 for different measurement items.

2.2.3 Study 3. Study 3 reports the regulatory influence of IL-10 and TNF-α on the early and late differentiation rates, measured by ALP and ARS at day 14 and 21, respectively, for the application period of 48 hours [13]. The fits of the model to the data of study 3 are given in Fig 4 for IL-10 and in Fig 5 for TNF-α. In consistent with the empirical data, the model calibrated by C1-5 showed the stimulatory effect of IL-10 on both early and late differentiation rates within the concentration range of 0 to 10 ng/ml (see Fig 4). The obtained fitness values were 0.88 and 0.97 for ALP and ARS, respectively (see Fig 4). Once calibrated by C3, the fits of the model to the data experienced only a slight improvement (see Fig 4). The variations in the simulation results of study 3 due to SSIP are given in Fig 4 for the case of IL-10.

In agreement with the experiments, the model calibrated by C1-5 successfully captured the stimulatory effect of TNF-α on the differentiation rates at the applied concentration of 1ng/ml (see Fig 5). C1-5 produced the fitness values of 0.91 and 0.93 for ALP and ARS, respectively, for the case of TNF-α (see Fig 5). Once calibrated by C3, the fits of the model improved to 0.95 and 0.96 for ALP and ARS, respectively (see Fig 5). The variations in the simulation results of study 3 due to SSIP are given in Fig 5 for the case of TNF-α.

2.2.4 Study 4. Study 4 reports the effect of IL-10, administrated over 48 hours, on the early and late differentiation rates, measured by ALP and ARS, respectively [33]. The fits of the model to the data of study 4 are given in Fig 6. The data shows the stimulatory effect of IL-10 on the early and later differentiation rates once applied in the concentration range of 0 to 10 ng/ml with a maximum effect at the concentration of 0.1 ng/ml (see Fig 6). However, IL-10

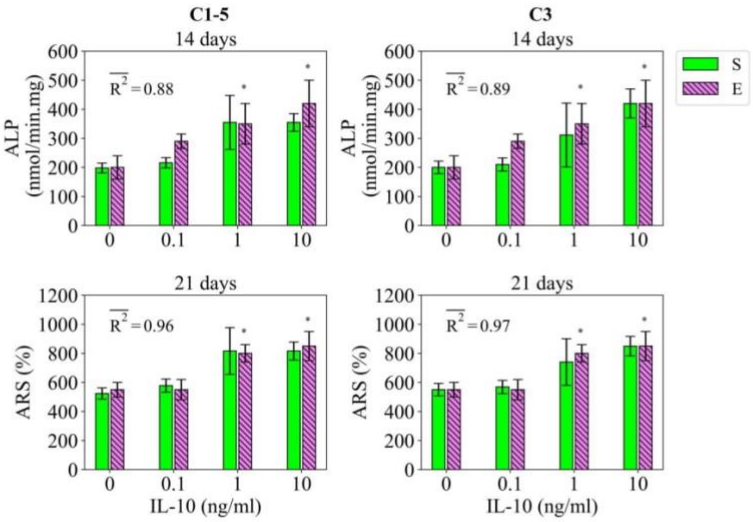

Fig 4. Fits of the model calibrated by C1-5 and C3 to the empirical data of study 3 for the case of IL-10. Bars indicate the simulations (S) and the corresponding empirical data (E). The quantities of ALP and ARS are reported at day 14 and 21, respectively. The error bars on the empirical data shows the standard deviations. The error bars on the simulation results show the standard deviations obtained during SSIP, i.e. 15% alteration in the estimated parameter values. Stars indicate the statistically significant differences between values given for the empirical data compared to the control, i.e. the applied concentration of 0 ng/ml ($p < 0.05 = {}^*$). $\overline{R^2}$ is the average fitness value of the simulations for the given measurement item.

https://doi.org/10.1371/journal.pcbi.1010482.g004

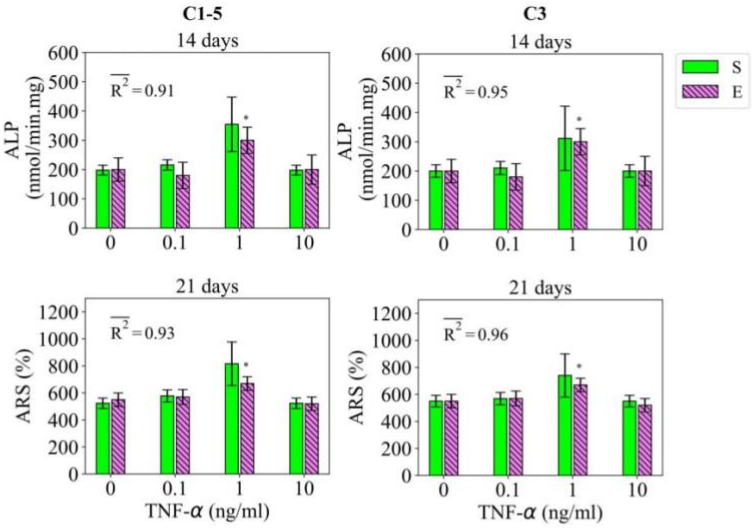

Fig 5. Fits of the model calibrated by C1-5 and C3 to the empirical data of study 3 for the case of TNF-α. Bars indicate the simulations (S) and the corresponding empirical data (E). The quantities of ALP and ARS are reported at day 14 and 21, respectively. The error bars on the empirical data shows the standard deviations. The error bars on the simulation results show the standard deviations obtained during SSIP, i.e. 15% alteration in the estimated parameter values. Stars indicate the statistically significant differences between values given for the empirical data compared to the control, i.e. the applied concentration of 0 ng/ml ($p < 0.05 = {}^*$). $\overline{R^2}$ is the average fitness value of the simulations for the given measurement item.

https://doi.org/10.1371/journal.pcbi.1010482.g005

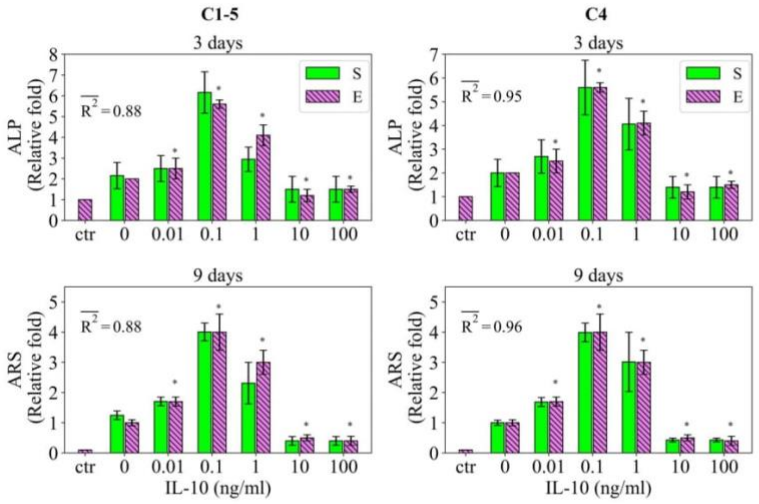

Fig 6. Fits of the model calibrated by C1-5 and C4 to the empirical data of study 4. Bars indicate the simulations (S) and the corresponding empirical data (E). The quantities of ALP and ARS are reported at day 3 and 9, respectively. The data is presented in a relative fold compared to the control, i.e. the undifferentiated case encoded as ctr. The error bars on the empirical data shows the standard deviations. The error bars on the simulation results show the standard deviations obtained during SSIP, i.e. 15% alteration in the estimated parameter values. Stars indicate the statistically significant differences between values given for the empirical data compared to the control ($p < 0.05 = {}^*$). $\overline{R^2}$ is the average fitness value of the simulations for the given measurement item.

https://doi.org/10.1371/journal.pcbi.1010482.g006

shows an inhibitory effect on the differentiation process once applied at 10 ng/ml or more (see Fig 6). The model calibrated by C1-3 successfully captured these observations with the fitness values of 0.85 and 0.82 for ALP and ARS, respectively (see Fig 6). However, the simulation results notably deviate from the empirical data for the applied concentration of 1 ng/ml (see Fig 6). Once calibrated by C4, the simulation results were improved with the fitness values of 0.95 and 0.96 for ALP and ARS, respectively (see Fig 6). The variations in the simulation results of study 4 due to SSIP are given in Fig 6 for different measurement items.

2.2.5 Study 5. Study 5 measures the regulatory effects of IL-8 and IL-1β on the early differentiation rate, measured by ALP [17]. The fits of the model to the data of study 5 are presented in Fig 7. Based on the data, IL-8 stimulates the early differentiation rate in a dose-dependent fashion increasing from 0 to 100 ng/ml (see Fig 7). The model calibrated by C1-5 was not capable of reproducing the increase in ALP from 10 to 100 ng/ml (see Fig 7). Once calibrated by C5, the model reproduced the data throughout all applied concentrations. The fitness value was significantly improved from 0.66 to 0.98 from the case of C1-5 to C5 (see Fig 7). In the case of IL-1β, the empirical data show a significant stimulatory effect at the applied concentration of 10 ng/ml. The simulation results reproduced this observation with a fitness value of 0.87 (see Fig 7). Once calibrated by C5, the match of the simulation results to the data improved resulting in a fitness value of 1 (see Fig 7). By simultaneous application of IL-8 and IL-1β, the data showed a significant upregulation in the measured ALP (see Fig 7). The model calibrated by C1-5 reproduced this observation with a fitness value of 0.80 (see Fig 7). Once calibrated by C5, the simulation results perfectly matched the data with the fitness value of 1 (see Fig 7). The variations in the simulation results of study 5 due to SSIP are given in Fig 7 for different measurement items.

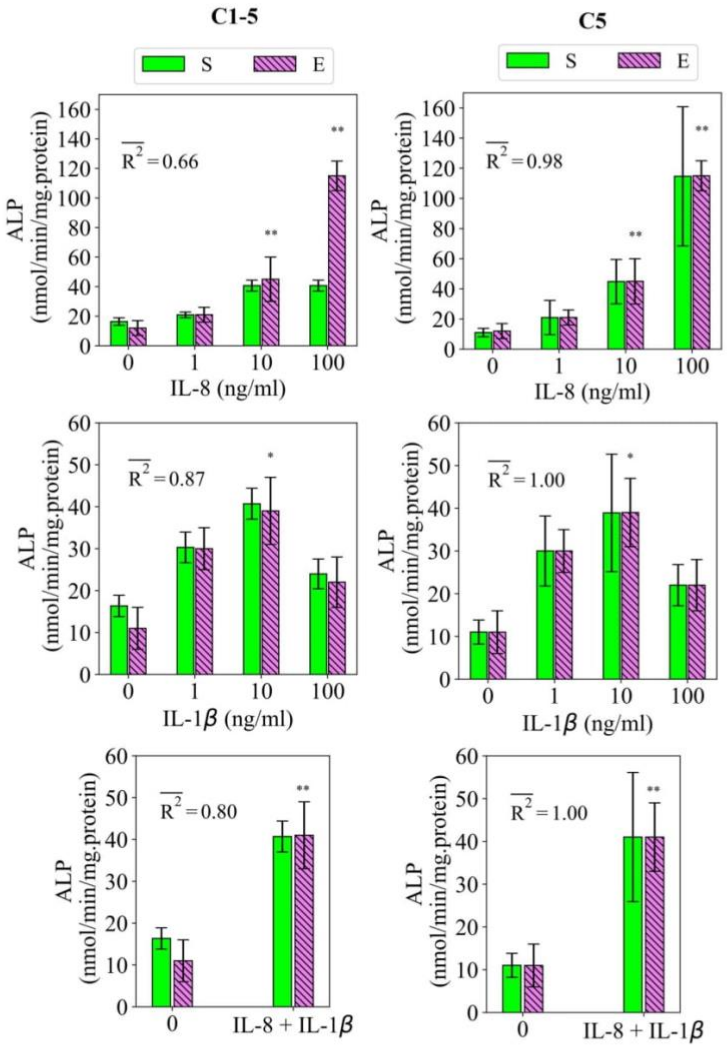

Fig 7. Fits of the model calibrated by C1-5 and C5 to the empirical data of study 5. Bars indicate the simulations (S) and the corresponding empirical data (E). The quantities of ALP are reported at day 9. The error bars on the empirical data shows the standard deviations. The error bars on the simulation results show the standard deviations obtained during SSIP, i.e. 15% alteration in the estimated parameter values. Stars indicate the statistically significant differences between values given for the empirical data compared to the control, i.e. the applied concentration of 0 ng/ml ($p < 0.05$ = *; $p < 0.01$ = **). $\overline{R^2}$ is the average fitness value of the simulations for the given measurement item.

https://doi.org/10.1371/journal.pcbi.1010482.g007

2.3 Results of the calibration process

The inferred parameter values obtained during different runs of C1-5 are given in Fig 8A. The results of the rest of the calibration scenarios, i.e. C1, C2, C3, C4, and C5 can be found in S1 Fig. The exact values of the inferred parameters are given in S3 Table. The results showed that different runs of the estimation process produce different sets of estimated values which can spread over the entire prior ranges (see Fig 8A and S1 Fig). It required 200, 200, 200, 200, 400, and 200 runs for C1, C2, C3, C4, C5, and C1-5, respectively, to reach consistent values for the

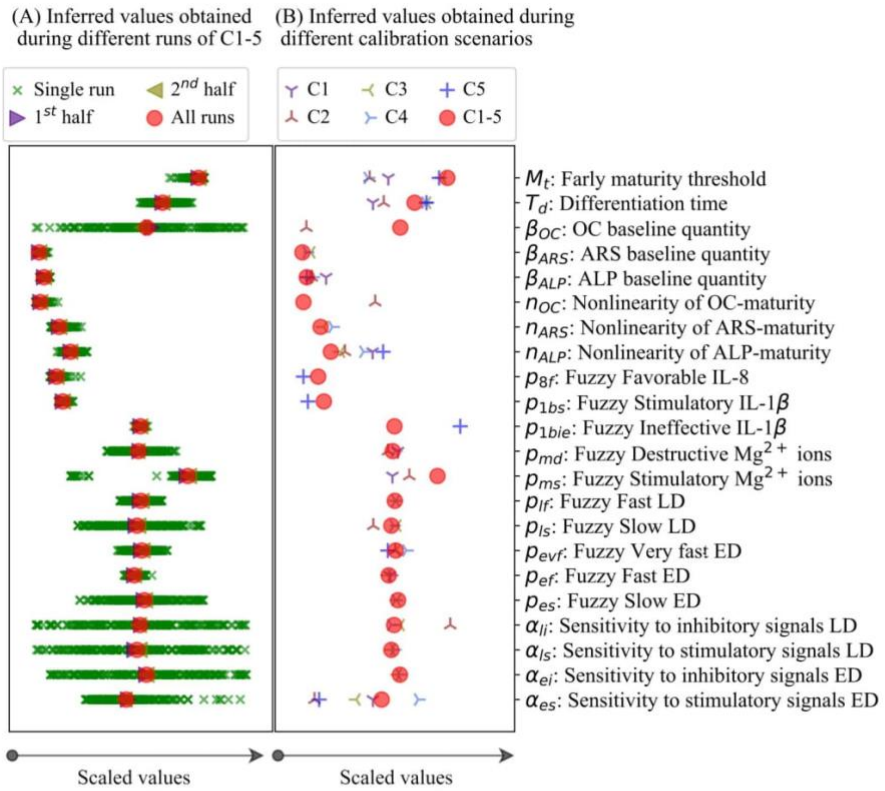

Fig 8. (A) Dispersity of the inferred values obtained during different runs of C1-5. In total, the calibration process is repeated 200 times in order to reach the stable inferred values, which is achieved by overlapping the mean values of all runs with the mean values of the 1st and 2nd halves of all runs. (B) Dispersity of the parameter values obtained during different calibration scenarios of C1, C2, C3, C4, C5, and C1-5. The values were scaled by dividing by the length of the priors. ED and LD stand for early differentiation and late differentiation, respectively.

https://doi.org/10.1371/journal.pcbi.1010482.g008

inferred parameters. The inferred parameter values obtained during different calibration scenarios were plotted in Fig 8B in comparison with each other. The results showed that certain parameters are considerably different among different calibration scenarios. In particular, early maturation threshold (M_t), differentiation time (T_d), and the sensitivity of the early differentiation process to stimulatory signals (α_{es}).

2.4 Results of the sensitivity analysis

The significance of the parameters obtained during different calibration scenarios is provided in Fig 3. It can be seen that LSSP and SSIP suggest different significance orders for the parameters. For instance, in the case of C5, α_{es} (sensitivity of the early differentiation rate to the stimulatory signals) is recognized as the top important parameter using SSIP, while this parameter is not among the top five parameters suggested by LSSP. Overall, the parameters of n_{ALP} and β_{ALP}, which map the simulated maturity to the measured quantity of ALP in experiments, are among the first two significant parameters across different studies. In the second rank are the parameters of M_t (early maturity threshold), T_d (differentiation time), p_{ef} (the *Fast*

membership level of early differentiation), and α_{es}(sensitivity of the early differentiation rate to the stimulatory signals).

3. Discussion

3.1 The overall goodness of the model

In summary, the present model calibrated by the accumulated data of all studies, i.e. C1-5, was able to successfully reproduce most of the important empirical observations reported in studies 1 to 5 (Figs 2–7). In agreement with the experiments, the results of the simulations correctly demonstrated that Mg^{2+} ions in low concentration stimulates the early differentiation process, while at a concentration below the physiological level downregulates the differentiation phase (see Figs 2 and 3). The calibration process suggested 6–8 mM as the optimal concentration of Mg^{2+} ions in promoting the early differentiation rate (see the estimated value of p_{ms} in S3 Table). In addition, the model was capable of reproducing the following observations:

- The stimulatory effect of IL-10, once administrated for 48 hours, on the early and late differentiation processes within the concentration range of 0 to 10 ng/ml (see Fig 4)
- The stimulatory role of TNF-α once applied at the low concentration of 1 ng/ml (see Fig 5)
- The dose-dependent role of IL-10, once administrated over 48 hours, on early and late differentiation processes-an increasing trend in the stimulatory role within the concentration of 0 to 0.1 ng/ml and an inhibitory role at the concentration of above 1 ng/ml (see Fig 9)
- The increasing trend in the stimulatory effect of IL-8 on the early differentiation process within the concentration range of 0 to 10 ng/ml (see Fig 9)

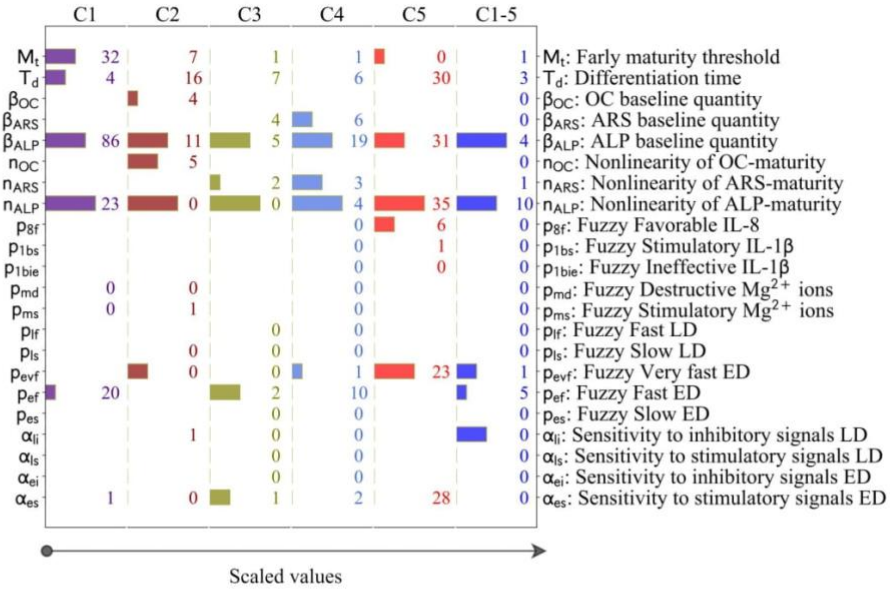

Fig 9. Results of the sensitivity analysis obtained during different calibration scenarios of C1, C2, C3, C4, C5 and C1-5. The bars indicate the five most significant parameters, given on the scale of 1 to 5, obtained from LSSP. The numbers show the results of SSIP in percentage. Those parameters with no values were not involved in that particular study.

https://doi.org/10.1371/journal.pcbi.1010482.g009

- The stimulatory role of IL-1β on the early differentiation rate once applied at the concentration of 10 ng/ml (see Fig 9)
- The cumulative stimulatory effect of IL-8 and IL-1β on the early differentiation process once administrated together (see Fig 9).

However, the simulation results deviated from the experiments in capturing the inhibitory effect of Mg^{2+} ions on the late differentiation process (see Fig 3). In addition, the model was unable to reproduce the increasing trend in the stimulatory effect of IL-8 on the early differentiation rate once the applied concentration increased from 10 to 100 ng/ml (see Fig 7). Moreover, the simulation results were noticeably different from the empirical data for several observations; for instance, the quantity of ALP in study 3 for the applied concentration of 0.1 ng/ml (see Fig 4) and the quantity of ALP in study 4 for the applied concentration of 1 ng/ml (see Fig 6). In the next step, we conducted the calibration process for each study individually, i.e. C1, C2, C3, C4, and C5. The overall fits of the model to the empirical data improved significantly with an average accuracy of over 95 percent (see Figs 2–7).

3.2 Investigating the sources of discrepancy between the data and the simulation

In order to investigate the possible sources of discrepancy among the empirical data of different studies, we examined the estimated parameters obtained during different calibration scenarios (see Fig 8B). The results showed that the values of several parameters were noticeably different between different calibration schemes (see section 2.3). Such discrepancy can stem from either the different exploration of the calibration algorithm in finding the global minimums or the fundamental differences between different studies [31].

As previously noted, the model calibrated by C1-5 could not explain the inhibitory effect of Mg^{2+} ions on the late differentiation process, measured by OC in study 2 (see Fig 3). According to Fig 8B, the parameters of M_t, T_d, β_{OC}, n_{OC}, α_{li}, and α_{es} show divergence between C1-5 and C2 (see Fig 2). β_{OC} and n_{OC}, which map the simulated maturity to OC (see Eq (6)), are not associated with the calculation of the simulated maturity (see Eq (1) in section 4.4). Therefore, we exclude them from further evaluation. To examine the remaining parameters, we first elaborate on the regulatory effect of Mg^{2+} ions on the differentiation process. In the present model, the differentiation process is divided into the early and late phases (see Eq (1)). According to the fuzzy rules, Mg^{2+} ions stimulate the early differentiation rate while inhibiting the late differentiation rate (see Table 1). Therefore, the outcome of the differentiation progress is partly upregulated and partly downregulated by Mg^{2+} ions. M_t and T_d control the degree of contribution of each part in the final outcome of the differentiation process (see Eqs (1) and (2)). The lower quantity of M_t, i.e. maturation threshold, obtained during C2 compared to C1-5 (see Fig 2B) shortens the early maturation phase and consequently constrains the stimulatory role of Mg^{2+} ions on the overall differentiation process. The lower quantity of T_d, i.e. differentiation time, obtained during C2 compared to C1-5 (see Fig 2B) serves a similar purpose; a lower T_d results in an earlier maturation along the differentiation line, consequently limiting the stimulatory influence of Mg^{2+} ions. The evaluation of M_t and T_d suggests that the cells used in the experiments of study 2 possess a lesser differentiation capacity compared to the average of the rest of the studies.

Additionally, α_{es} and α_{li} contribute to the deviation of the model calibrated by C1-5 from the empirical data. α_{es} and α_{li} control the regulatory impact of Mg^{2+} ions on early and late differentiation rates, respectively (see Eq (3)). C2 reports a lower quantity of α_{es} and a higher

Table 1. Fuzzy logic rules define the osteogenic reaction in response to stimulatory inputs. For the qualitative definition of each linguistic term, refer to Fig 10A. The symbol ⊕ indicates that the given conditions must occur simultaneously to produce the given intensity. The symbol ~ indicates that any choice of one or more from the chosen inputs produces the same intensity. The term 'Not', preceded by a linguistic level, indicates that the rule applied for all except the given level. The terms 'ED' and 'LD' stand for early differentiation and late differentiation, respectively. The rules are given in IF/THEN format in S2 Table in.

Cellular events		Cellular inputs				
Event	**Intensity**	**TNF-α**	**IL-10**	**IL-8**	**IL-1β**	**Mg^{2+} ions**
Early differentiation	Slow	~ Inhibitory	~ Inhibitory	-	-	~ Inhibitory ED or Destructive
	Physiological	⊕ Negligible or Ineffective	⊕ Negligible	⊕ Negligible	⊕ Negligible or Ineffective	⊕ Physiological or Ineffective
	Fast	~ Stimulatory	~ Favorable	-	-	~ Stimulatory
	Very fast	-	~ Stimulatory	~ ⊕ Favorable	~ ⊕ Negligible	-
				~ ⊕ Negligible	~ ⊕ Stimulatory	
				~ ⊕ Not Negligible	~ ⊕ Not Negligible	
	Extremely fast	-	-	⊕ Stimulatory	⊕ Negligible	-
Late differentiation	Slow	~ Inhibitory	~ Inhibitory	-	-	~ Inhibitory LD or Destructive
	Physiological	⊕ Negligible or Ineffective	⊕ Negligible	-	-	⊕ Not Inhibitory LD
	Fast	~ Stimulatory	~ Favorable	-	-	-
	Very fast	-	Stimulatory	-	-	-

https://doi.org/10.1371/journal.pcbi.1010482.t001

quantity of α_{li}, respectively, compared to C1-5 (see Fig 2B). These parameters, while possessing lesser significance on the simulation results compared to M_t and T_d (see Fig 9), contribute to reducing the overall effect of Mg^{2+} ions on the late differentiation process. This observation implies that cells used in the experiments of study 2 are more sensitive to stimulatory signals during early differentiation phase and less sensitive during late differentiation phase.

We previously noted that the model calibrated by C1-5 was not capable of capturing the increasing trend in the stimulatory effect of IL-8 on the early differentiation rate moving from 10 to 100 ng/ml, reported in study 5 (see Fig 7). According to Fig 8B, the values of the three parameters of n_{ALP}, p_{1bie}, and α_{es} were notably different between C1-5 and C5. As mentioned earlier, the parameter of n_{ALP} is not relevant in the calculation of the differentiation rate and is, therefore, excluded from further discussion. The parameter of p_{1bie}, which is associated with IL-1β, is also irrelevant in the formulation of IL-8. Thus, we further examine the parameter of α_{es}, i.e. the sensitivity of the differentiation process to the stimulatory factors, which is directly involved in the calculation of the early differentiation rate (see Eq (3)). It can be seen that C1-5 reports a higher quantity of α_{es} compared to C5 (see Fig 2B). According to Eq (3), a higher quantity of α_{es} increases the overall differentiation rate and results in a faster maturation process. Further evaluation of the model calibrated by C1-5 showed that the simulated maturity already reaches 1, i.e. ultimate value, for the applied concentration of 10 ng/ml, leaving no space for further improvement for higher stimulatory signals, e.g. 100 ng/ml (these results were not provided). This observation implies that the cells used in study 5 are less sensitive to stimulatory signals.

3.3 Calibration process

We showed that the employed DE approach results in different sets of parameter values at each run of the calibration process (see Fig 2A). In order to obtain consistent values, we repeated the tuning process at least two hundred times, depending on the study, and used the mean parameter values (see section 3.1). This approach is computationally expensive but results in consistency in the obtained parameter values, which can be used to investigate the differences among different models. Such discrepancy can be due to inherent differences

among different experiments such as donor characteristics, culture medium characteristics, and experimental protocol [11], [17], [34].

3.4 Sensitivity analysis

In order to study the sensitivity of the model to its parameters, we employed two different approaches of LSSP and SSIP. LSSP captures the effect of large and simultaneous variations in the parameter values, while SSIP examines the impact of small and individual perturbations (see section 4.6). Together, these approaches provide a superior understanding of the system compared to the single approach utilized in our previous study [31]. In the formulation of the present model, we assumed non-linear relationships between the simulated maturity and the differentiation markers (see Eq (6)), which was assumed linear in our previous model [31]. The results of the sensitivity analysis showed n_{ALP}, n_{ARS}, and n_{OC}, which control the degree of non-linearity in these relationships, are among the most significant parameters in the model (see Fig 9). The inferred values of these parameters were higher for the case of C1 to C5 compared to C1-5 (see Fig 8 and S3 Table). This is primarily due to the overfitting phenomenon as the calibrated models of C1 to C5 are too closely aligned to the data of individual studies. For the case of C1-5, the values of these parameters are close to 1 (see S3 Table), showing a linear relationship between the simulated maturity and the differentiation markers.

Another significant parameter in the model is β_{ALP}, according to the results of the sensitivity analysis (see Fig 3). This parameter represents the baseline value of ALP secretion when the simulated maturity is zero (see Eq (6)). The estimated values of this parameter lie within 0.4 and 1.4 for different calibration scenarios (see S3 Table). The addition of this parameter to the relationship between the simulated maturity and the differentiation markers is an improvement to the formulation of our previous model, in which the baseline value is assumed zero [31]. The parameters of M_t, T_d, and α_{es} were also shown as the influential parameters according to the sensitivity analysis (see Fig 3). As elaborated earlier, these parameters, which are directly involved in the formulation of the simulated maturity, were the determinant factors in explaining the discrepancy in the simulation results.

3.5 Fuzzy-logic controller as the decision-making center of cell

In the present study, we used FL-based controllers as the deciding center of cells to simulate the process of osteogenic differentiation. FL-based simulations use plain language to describe a system which can potentially help in dissolving technical barriers between simulation and experimental experts easing their involvement in the rapid development of a computer model [26], [35]. Moreover, FL-based models are tractable and interpretable, which makes them a suitable option in investigating and incorporating the experimental datasets which are not in agreement with one another, similar to this study and our previous report [31]. Since the present model receives the signals from the environment and predicts cellular actions, similar to an agent, this descriptive model can serve as a natural basis for the predictive reinforcement model in the future [36].

3.6 Limitations, future developments, and concluding remarks

The proposed computer model in this study has several important limitations. Firstly, we were not able to find sufficient information in the literature to define the quality of interactions between different signaling factors in the FL controller, except for the two factors of IL-8 and IL-1β (see Table 1). A similar limitation was reported in our previous model [31] as well as in other computer models in the literature [37–39]. Further experiments are required to

investigate the potential synergic effects between different cellular inputs, in particular, Mg^{2+} ions with the inflammatory cytokines [17]. Secondly, the proposed model in this study, which simulates the behavior of a single cell, is used to explain the average behavior of the cells cultured in the experiments. We defined several parameters to scale the outputs of the cell model to match the empirical observation (see section 4.5). However, the current model is not able to capture the heterogeneity in the behavior of individual cells. In the next step, the proposed cell model will be incorporated into an agent-based model to address this issue. This can potentially improve the simulation results but will require significantly higher computational costs, i.e. in the order of thousand times. Thirdly, the regulatory effect of substrate stiffness as an important factor in guiding osteogenesis is not incorporated in the present model [40]. This parameter will be included in our future studies. Similarly, transforming growth factor-beta (TGF-β) and bone morphogenic protein (BMP), which are two crucial growth factors in the osteogenic differentiation of MSCs, will be adopted from our previous model [31]. To do so, the quality of interaction between Mg^{2+} ions and these growth factors need to be studied first as Mg^{2+} ions are also reported to influence the activation of transforming growth factor-beta (TGF-β) and bone morphogenic protein (BMP) signaling [8]. Lastly, in this study, we simulated the influence of the inflammatory cytokines, primarily produced by macrophages, on MSC osteogenic differentiation. However, the cross-talk between MSC and macrophage is a double-sided process; macrophage polarization and cytokine production are also regulated by MSC. In the next steps, we will address this problem and complete the circle of MSC-macrophage interaction.

4 Materials and methods

In this section, we first explain the complete process of the development of the FL controller (see Fig 10). The bioregulatory roles of the cellular inputs in the differentiation activities are explained in the following subsection together with the process of converting the qualitative knowledge into the machine-readable algorithm, termed fuzzification. After, the fuzzification process is explained for the cellular outputs. Then, the process of fuzzy inference and defuzzification is elaborated. The outputs of the FL controller require post-processing in order to define the actual rates of early and late differentiation rates. This process is further elaborated in the subsequent section. Finally, we elaborate on the empirical data used for the calibration and sensitivity analysis with the technical details of each process in the following sections. We used several software and packages to develop the current model, which can be found S1 Text. The source code of the present model can be found online [41].

4.1 Cellular inputs and fuzzification process

The first step in the development of the FL controller is to define and fuzzify the cellular inputs (see Fig 10). In this section, we elaborate on the bioregulatory roles of the five signaling factors in the early and late differentiation processes using the information available in the literature. Then, FL membership functions are defined according to this information.

Mg^{2+} ions are shown to affect osteogenic differentiation depending on the concentration and the state of cell differentiation [42–45]. A Mg^{2+} ion concentration of 0.8 mM, which is commonly used as the minimal essential Medium-MEM in cell culture experiments, is considered as the physiological concentration. A concentration below 0.8 mM is shown to delay the early differentiation process of MSCs [17]. Mg^{2+} ions within the concentration range of 2–10 mM is reported to promote early differentiation rate [6], [43], [45–47], while the concentration of Mg^{2+} ions above 1.8 mM is reported inhibitory for late differentiation process [6], [43], [45]–[47]. In addition, a concentration over 20 mM is shown to compromise cell

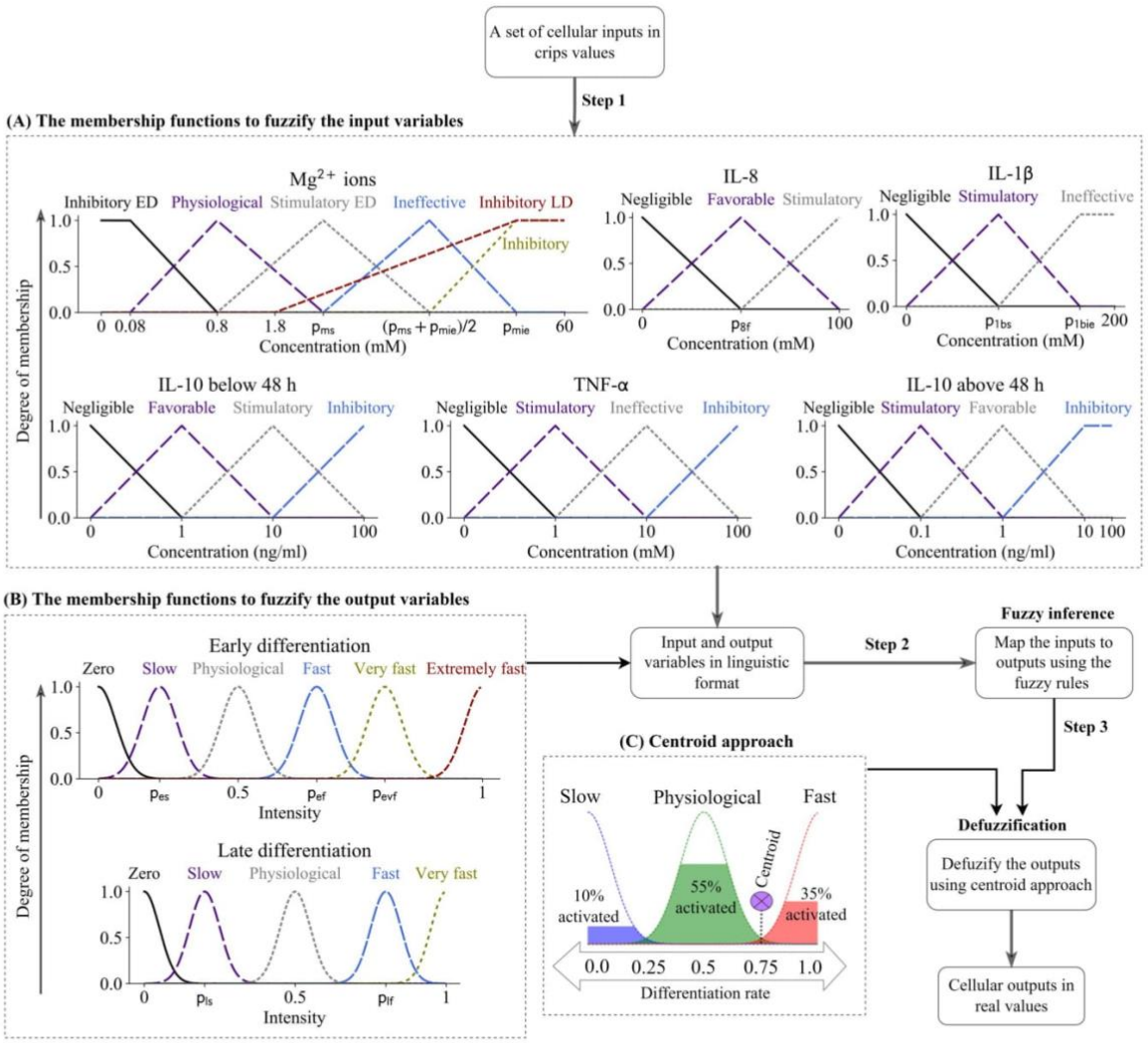

Fig 10. The complete flow of the implemented FL controller in this study. In step 1, the cellular inputs are transformed to linguistic variables using the membership functions given in (A). A set of triangular and trapezoid memberships functions are used during this fuzzification process. Similarly, cellular outputs of early and late differentiation rates are defined in linguistic formats using the membership functions given in (B). A set of Gaussian membership functions are used for this purpose. In step 2, the FL controller receives the cellular inputs and calculates the cellular outputs, both in linguistic form. In step 3, the outputs are defuzzified and converted into crisp, real values using the centroid approach (C). The terms 'ED' and 'LD' stand for early differentiation and late differentiation, respectively.

https://doi.org/10.1371/journal.pcbi.1010482.g010

viability [47–49]. To account for these observations, we create six membership functions to define the cellular input of Mg^{2+} ions as shown in Fig 10A. The parameter of p_{ms} is defined to mark the peak occurrence of the *Stimulatory* effect. The parameter of p_{md} marks the beginning of the *Inhibitory* effect. The membership function of *Ineffective* is defined as the transition state from *Stimulatory* to *Inhibitory* state.

IL-10 is a key anti-inflammatory cytokine in the bone regenerative process including osteogenic differentiation [33]. The mediatory effects of IL-10 are shown to significantly depend on

the applied concentration as well as the length of application [13], [33][50]. Chen et al. [33] showed that IL-10 has a dual effect on osteogenic activities; IL 10 in low concentration activates p38/MAPK signaling pathway and stimulates osteogenic activities, while higher concentrations of IL-10 inhibit p38/MAPK signaling by activating NF-kB and consequently downregulating osteogenesis. They found that IL-10 has the highest stimulatory effect at the concentration of 0.1 ng/ml, while the concentration of 10 ng/ml showed a significantly inhibitory effect on osteogenesis [33]. However, Valles et al. [13] showed an increasing stimulatory effect of IL-10 on osteogenesis by increasing the concentration from 0.1 to 10 ng/ml. They also experimented the importance of application time and concluded that while IL-10 can be pro-osteogenic after short-term treatment (48 hours), its continuous application can produce inhibitory effects [13]. Therefore, in the definition of the FL controller, we set the application time of 48 hours to differentiate short- and long- term treatment periods. Accordingly, we define two separate sets of functions to fuzzify the cellular input of IL-10 depending on the application time. In the controller that simulates IL-10 for the application of less or equal to 48 hours, we define a constant increase in the stimulatory effect of IL-10 from 0 to 10 ng/ml (see Fig 10A). However, for the case where the application time exceeds 48 hours, the promotory effect of IL-10 decreases by exceeding 0.1 ng/ml (see Fig 10A), in compliance with the findings of Chen et al. [33].

TNF-α is a primary cytokine in the inflammatory reaction which plays an important role in osteogenic differentiation [51]. The regulatory effects of TNF-α on osteogenesis have been shown to be concentration-dependent; while low concentration of TNF-α is assumed stimulatory, its high concentration has an inhibitory effect on osteoblastic differentiation [13], [52]. According to the results of Valles et al. [13] and Glass et al. [52], we define the stimulatory concentration of TNF-α as 1 ng/ml and the inhibitory concentration as 100 ng/ml [52]. TNF-α at a concentration of 10 ng/ml is shown to have neither stimulatory nor inhibitory effect on osteogenesis [13], [52]. Thus, the concentration of 10 ng/ml is defined as the neutral state with an ineffective role in osteogenesis (see Fig 10A).

IL-8 is traditionally classified as a pro-inflammatory cytokine with the main role of recruiting the inflammatory cells to the injury site [17][53]. In addition, IL-8 is shown to play an important role in the commitment of MSCs to bone cells [54][55]. Qiao et al. [17] showed that IL-8 is especially important when the inflammatory response is mediated by Mg^{2+} ions; IL-8 is the primary player in promoting osteogenesis when macrophages are treated by Mg^{2+} ions [17]. They also showed that the regulatory effect of IL-8 on osteogenesis is dose-dependent and substantially increases within the concentration of 0 to 100 ng/ml [17]. To account for these observations, we define three membership functions to fuzzify the cellular input of IL-8 (see Fig 10A), where the stimulatory role of IL-8 rapidly increases by an increase in its concentration. The parameter of p_{8f} marks the peak occurrence of *Favorable* condition which is an intermediate state toward *Stimulatory* level.

IL-1β is a major pro-inflammatory cytokine with an important role in the simulation of osteoclastogenesis [56]. IL-1β is also shown to increase osteogenic activities of MSCs, especially when it is administrated in a low concentration within 1 to 10 ng/ml [17]. To account for these observations, we define three membership functions to fuzzify IL-1β (see Fig 10A), where two parameters of p_{1bs} and p_{1bie} mark the peak and end of the stimulatory effect. In addition, IL-1β is reported to be an antagonizer of IL-8 osteogenic effects [17]; Qiao et al. [17] showed that IL-1β substantially reduces the secretion of the osteogenic biomarkers stimulated by IL-8. Thus, in the present FL controller, IL-1β has a dual role in osteogenetic response; on the one hand, it stimulates osteogenesis; on the other hand, it hampers the stimulatory role of IL-8.

4.2 Cellular outputs and fuzzification process

The outputs of the fuzzy controller are early and late differentiation rates. These values are defined in linguistic formats using the set of membership functions given in Fig 10B. The early differentiation process is assumed to occur in six different rates within the range of 0 and 1, with 0.5 representing the physiological rate. The parameters of p_{es}, p_{ef}, and p_{evf} are defined to mark the intensities of *Slow*, *Fast*, and *Very fast* levels, accordingly. The late differentiation process is fuzzified using five membership functions shown in Fig 10B, with 0.5 representing the physiological rate (see Fig 10B). The parameter of p_{ls} and p_{lf} are defined to mark the *Slow* and *Fast* membership levels. Gaussian membership functions (GMFs) with the activation value of 1 and the sigma value of 0.05 are employed for the fuzzification of the output variables. GMFs offer multiple advantageous such as smoothness and concise notation as well as superior reliability and robustness of the system [57][58].

4.3 Fuzzy inference and defuzzification process

The set of rules given in Table 1 is used to determine the differentiation rates in response to the cellular inputs. A Mamdani-type FL controller is used for the calculations. Since multiple rules can be triggered simultaneously, the centroid technique is used to determine the final output of the controller. In this technique, the area bound by the activation degree is summed over different fuzzy sets, and the center of the sums is calculated to represent the final outcome (see Fig 10C) [59].

4.4 Simulation of the differentiation process

Similar to our previous study [31], we define the factor of *maturity* to mark the degree of progression along the line of osteogenic differentiation. *Maturity* holds a value in the range of 0 and 1 and is calculated for a given time (T) using early and late differentiation rates (r_e and r_l, respectively) as,

$$Maturity = \begin{cases} T \cdot r_e, & T \leq T_e \\ T_e \cdot r_e + (T - T_e) \cdot r_l, & T > T_e \end{cases} \quad (1)$$

where T_e is time required for the early maturation process.

$$T_e = \mathrm{M}_t \cdot T_d \quad (2)$$

where M_t is the early maturation threshold, and T_d is the time required for MSC to fully differentiate to osteoblast. M_t is a value between 0 and 1, marking the end of early differentiation process.

In Eq (1), r_e and r_l are the scaled versions of f_e and f_l (fuzzy outputs), respectively,

$$\mathrm{r}_e = \mathrm{r}_0 \cdot S(f_e) \quad (3)$$

$$\mathrm{r}_l = \mathrm{r}_0 \cdot S(f_l) \quad (4)$$

where r_0 is the physiological rate of osteogenic differentiation, calculated as $1/T_d$, where S is a function that scales the outputs of fuzzy controller, which are initially between 0 and 1,

$$S(x) = \begin{cases} 2 \cdot \alpha_{s,k} \cdot (\mathrm{x} - 0.5) + 1, & x \leq 0.5 \\ 2 \cdot \alpha_{i,k} \cdot (\mathrm{x} - 0.5) + 1, & x > 0.5 \end{cases} \quad (5)$$

where x is the input from the FL controller. $\alpha_{s,k}$ and $\alpha_{i,k}$ are the scaling coefficients for the stimulatory and inhibitory effects, respectively, $k \in \{e, f\}$.

4.5 Empirical data

The empirical data obtained from 5 sets of published experiments are used to estimate the free parameters of the present model (see S1 Table for the summary of the experiments). These experiments evaluate the bioregulatory effect of different Mg^{2+} ions as well as different inflammatory cytokines on the osteogenic differentiation of MSCs. Three markers of ALP, OC, and ARS are used to study the differentiation process. ALP is commonly used as an early differentiation marker, while OC and ARS are recognized as the markers of the late differentiation phase [40], [60]. These factors are correlated with *maturity*, which is the simulated indicator of differentiation progress in the present study,

$$y_i(\mathrm{x}) = (x + \beta_i)^{n_i} \cdot k_{i,j} \tag{6}$$

where x is the conditioned value of maturity, y_i is the quantity of the biomarker with $\mathrm{i} \in \{ALP, OC, ARS\}$, β_i is the baseline of the marker, n_i is the degree of nonlinearity, and $k_{i,j}$ is the correction factor applied for each experiment with $j \in 1{:}5$. For ALP, x is calculated as,

$$x = \begin{cases} maturity, & maturity \leq M_t \\ M_t, & maturity > M_t \end{cases} \tag{7}$$

In Eq (7), we assume that ALP correlates with maturity until the early maturation threshold and stays constant afterward, accounting for the fact that ALP is the early differentiation marker. OC and ARS, as the late marker of differentiation, correlate with maturity in its whole range, i.e. x = maturity. In Eq (6), β_i takes into account that the differentiation markers can be detected even at the beginning of an experiment where the simulated maturity is zero [33]. The parameter of n_i is defined to catch the non-linear correlation between maturity and the differentiation markers. Lastly, $k_{i,j}$ takes into account the variations in the measurements of the markers across different experiments, e.g. differences in the reported units.

4.6 Calibration process and sensitivity analysis

The overview of the calibration process is given in Fig 11A. DE is a metaheuristic stochastic search algorithm based on an evolutionary process which improves the candidate solution by an iterative approach [61]. Although DE is considered a global optimization algorithm, the estimated parameter values can be different at each run. To overcome this issue, we execute multiple DE runs and use the posterior distributions to infer the parameter values (see Fig 11A).

The overview of the sensitivity analysis is given in Fig 11B. Two approaches of LSSP and SSIP are employed to study the sensitivity of the model to its parameters. In LSSP, one or several parameters are simultaneously perturbed with a magnitude of 50 percent around the inferred values. Fractional factorial design (FFD) and the analysis of variance (ANOVA) are used for sampling and analysis of this approach, which are explained in detail in our previous publication [31]. In SSIP, the parameters of the model are perturbed one at a time, with a magnitude of 15 percent around the inferred values.

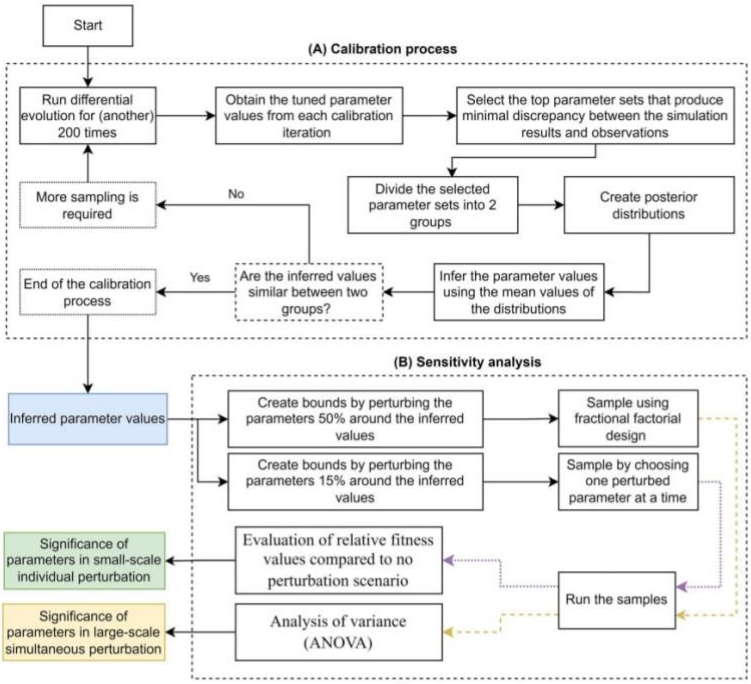

Fig 11. The complete flow of the calibration process and the sensitivity analysis implemenetd in this study.

https://doi.org/10.1371/journal.pcbi.1010482.g011

Supporting information

S1 Fig. Dispersity of the parameter values obtained during the calibration process for different calibration scenarios of C1, C2, C3, C4, C5 and C1-5. Individual runs are the results of each calibration process; All samples represent the mean of combined individual runs; First (1st) and second (2nd) halfs of samples indicate the means of the frist half and second half of combined individual runs, respectively. The values were scaled by dividing by the length of the priors.
(TIFF)

S1 Table. The summary of the specifications of the cell culture experiments used to estimate the model's free parameters.
(DOCX)

S2 Table. The fuzzy logic rules in IF/THEN format. The words in green are the cellular inputs while those in red are cellular outputs.
(DOCX)

S3 Table. The list of the free parameters in the present model, and the inferred values during different calibration schemes. Those marked by '-'were not inferred during that particular calibrations scenario.
(DOCX)

S1 Text. Specification of the software used in this study.
(DOCX)

Acknowledgments

Maxwell computational resources operated at Deutsches Elektronen-Synchrotron (DESY), Hamburg, Germany were used in the computational tasks.

Author Contributions

Conceptualization: Jalil Nourisa, Berit Zeller-Plumhoff, Regine Willumeit-Römer.

Data curation: Jalil Nourisa.

Formal analysis: Jalil Nourisa.

Funding acquisition: Regine Willumeit-Römer.

Investigation: Jalil Nourisa.

Methodology: Jalil Nourisa.

Project administration: Berit Zeller-Plumhoff.

Resources: Berit Zeller-Plumhoff.

Software: Jalil Nourisa.

Supervision: Regine Willumeit-Römer.

Validation: Jalil Nourisa.

Visualization: Jalil Nourisa.

Writing – original draft: Jalil Nourisa.

Writing – review & editing: Berit Zeller-Plumhoff, Regine Willumeit-Römer.

References

1. Willumeit-Römer R. The Interface Between Degradable Mg and Tissue. Jom. 2019; 71(4):1447–55.
2. Rahmati M, Silva EA, Reseland JE, Heyward CA., Haugen HJ. Biological responses to physicochemical properties of biomaterial surface. Chem Soc Rev. 2020; 49(15):5178–224. https://doi.org/10.1039/d0cs00103a PMID: 32642749
3. Zhang J, Ma X, Lin D, Shi H, Yuan Y, Tang W, et al. Magnesium modification of a calcium phosphate cement alters bone marrow stromal cell behavior via an integrin-mediated mechanism. Biomaterials. 2015; 53:251–64. https://doi.org/10.1016/j.biomaterials.2015.02.097 PMID: 25890724
4. Qi T, Weng J, Yu F, Zhang W, Li G, Qin H, et al. Insights into the Role of Magnesium Ions in Affecting Osteogenic Differentiation of Mesenchymal Stem Cells. Biol Trace Elem Res. 2021; 199(2):559–67. https://doi.org/10.1007/s12011-020-02183-y PMID: 32449009
5. Lin S, Yang G, Jiang F, Zhou M, Yin S, Tang Y, et al. A magnesium-enriched 3D culture system that mimics the bone development microenvironment for vascularized bone regeneration. Adv Sci. 2019; 6(12):1900209. https://doi.org/10.1002/advs.201900209 PMID: 31380166
6. Luthringer BJC, Willumeit-Römer R. Effects of magnesium degradation products on mesenchymal stem cell fate and osteoblastogenesis. Gene [Internet]. 2016; 575(1):9–20. Available from: https://doi.org/10.1016/j.gene.2015.08.028 PMID: 26283150
7. Wang Y, Geng Z, Huang Y, Jia Z, Cui Z, Li Z, et al. Unraveling the osteogenesis of magnesium by the activity of osteoblasts in vitro. J Mater Chem B. 2018; 6(41):6615–21. https://doi.org/10.1039/c8tb01746h PMID: 32254870
8. Li RW, Kirkland NT, Truong J, Wang J, Smith PN, Birbilis N, et al. The influence of biodegradable magnesium alloys on the osteogenic differentiation of human mesenchymal stem cells. J Biomed Mater Res Part A. 2014; 102(12):4346–57. https://doi.org/10.1002/jbm.a.35111 PMID: 24677428
9. Zhang X, Chen Q, Mao X. Magnesium Enhances Osteogenesis of BMSCs by Tuning Osteoimmunomodulation. Biomed Res Int. 2019; 2019. https://doi.org/10.1155/2019/7908205 PMID: 31828131

10. Díez-Tercero L, Delgado LM, Bosch-Rué E, Perez RA. Evaluation of the immunomodulatory effects of cobalt, copper and magnesium ions in a pro inflammatory environment. Sci Rep [Internet]. 2021; 11(1):1–13. Available from: https://doi.org/10.1038/s41598-021-91070-0 PMID: 34083604
11. Zhang Y, Böse T, Unger RE, Jansen JA, Kirkpatrick CJ, van den Beucken JJJP. Macrophage type modulates osteogenic differentiation of adipose tissue MSCs. Cell Tissue Res. 2017; 369(2):273–86. https://doi.org/10.1007/s00441-017-2598-8 PMID: 28361303
12. Carty F, Mahon BP, English K. The influence of macrophages on mesenchymal stromal cell therapy: Passive or aggressive agents. Clin Exp Immunol. 2017; 188(1):1–11. https://doi.org/10.1111/cei.12929 PMID: 28108980
13. Valles G, Bensiamar F, Maestro-Paramio L, García-Rey E, Vilaboa N, Saldaña L. Influence of inflammatory conditions provided by macrophages on osteogenic ability of mesenchymal stem cells. Stem Cell Res Ther. 2020; 11(1):1–15.
14. Gong L, Zhao Y, Zhang Y, Ruan Z. The macrophage polarization regulates MSC osteoblast differentiation in vitro. Ann Clin Lab Sci. 2016; 46(1):65–71. PMID: 26927345
15. Romero-López M, Li Z, Rhee C, Maruyama M, Pajarinen J, O'Donnell B, et al. Macrophage effects on mesenchymal stem cell osteogenesis in a three-dimensional in vitro bone model. Tissue Eng—Part A. 2020; 26(19–20):1099–111. https://doi.org/10.1089/ten.TEA.2020.0041 PMID: 32312178
16. Mazur A, Maier JAM, Rock E, Gueux E, Nowacki W, Rayssiguier Y. Magnesium and the inflammatory response: potential physiopathological implications. Arch Biochem Biophys. 2007; 458(1):48–56. https://doi.org/10.1016/j.abb.2006.03.031 PMID: 16712775
17. Qiao W, Wong KHM, Shen J, Wang W, Wu J, Li J, et al. TRPM7 kinase-mediated immunomodulation in macrophage plays a central role in magnesium ion- induced bone regeneration. Nat Commun [Internet]. 2021; 12(2885). Available from: https://doi.org/10.1038/s41467-021-23005-2 PMID: 34001887
18. Leidi M, Dellera F, Mariotti M, Maier JAM. High magnesium inhibits human osteoblast differentiation in vitro. Magnes Res. 2011; 24(1):1–6. https://doi.org/10.1684/mrh.2011.0271 PMID: 21421455
19. Zhou H, Liang B, Jiang H, Deng Z, Yu K. Magnesium-based biomaterials as emerging agents for bone repair and regeneration: from mechanism to application. J Magnes Alloy. 2021;(xxxx).
20. da Silva Lima F, da Rocha Romero AB, Hastreiter A, Nogueira-Pedro A, Makiyama E, Colli C, et al. An insight into the role of magnesium in the immunomodulatory properties of mesenchymal stem cells. J Nutr Biochem [Internet]. 2018; 55:200–8. Available from: https://doi.org/10.1016/j.jnutbio.2018.02.006 PMID: 29554498
21. Metzcar J, Wang Y, Heiland R, Macklin P. A Review of Cell-Based Computational Modeling in Cancer Biology. JCO Clin Cancer Informatics. 2019 Feb;(3):1–13. https://doi.org/10.1200/CCI.18.00069 PMID: 30715927
22. Prasad A, Alizadeh E. Cell Form and Function: Interpreting and Controlling the Shape of Adherent Cells. Vol. 37, Trends in Biotechnology. Elsevier Ltd; 2019. p. 347–57.
23. Nourisa J, Rouhi G. Prediction of the trend of bone fracture healing based on the results of the early stages simulations: a finite element study. J Mech Med Biol. 2019; 19(5).
24. Nourisa J, Rouhi G. Biomechanical evaluation of intramedullary nail and bone plate for the fixation of distal metaphyseal fractures. J Mech Behav Biomed Mater. 2016; 56. https://doi.org/10.1016/j.jmbbm.2015.10.029 PMID: 26655955
25. Zhao C, Medeiros TX, Sové RJ, Annex BH, Popel AS. A data-driven computational model enables integrative and mechanistic characterization of dynamic macrophage polarization. iScience. 2021;102112. https://doi.org/10.1016/j.isci.2021.102112 PMID: 33659877
26. Bordon J, Moskon M, Zimic N, Mraz M. Fuzzy Logic as a Computational Tool for Quantitative Modelling of Biological Systems with Uncertain Kinetic Data. IEEE/ACM Trans Comput Biol Bioinforma. 2015; 12 (5):1199–205. https://doi.org/10.1109/TCBB.2015.2424424 PMID: 26451831
27. Nobile MS, Votta G, Palorini R, Spolaor S, De Vitto H, Cazzaniga P, et al. Fuzzy modeling and global optimization to predict novel therapeutic targets in cancer cells. Bioinformatics [Internet]. 2019; 36(7):2181–8. Available from: https://doi.org/10.1093/bioinformatics/btz868 PMID: 31750879
28. Aldridge BB, Saez-Rodriguez J, Muhlich JL, Sorger PK, Lauffenburger DA. Fuzzy Logic Analysis of Kinase Pathway Crosstalk in TNF/EGF/Insulin-Induced Signaling. PLoS Comput Biol. 2009; 5(4). https://doi.org/10.1371/journal.pcbi.1000340 PMID: 19343194
29. Wang M, Yang N. Three-dimensional computational model simulating the fracture healing process with both biphasic poroelastic finite element analysis and fuzzy logic control. Sci Rep [Internet]. 2018; 8(1):1–13. Available from: https://doi.org/10.1038/s41598-018-25229-7 PMID: 29712979
30. Niemeyer F, Claes L, Ignatius A, Meyers N, Simon U. Simulating lateral distraction osteogenesis. PLoS One. 2018; 13(3):e0194500. https://doi.org/10.1371/journal.pone.0194500 PMID: 29543908

31. Nourisa J, Zeller-Plumhoff B, Helmholz H, Luthringer-Feyerabend B, Ivannikov V, Willumeit-Römer R. Magnesium ions regulate mesenchymal stem cells population and osteogenic differentiation: a fuzzy agent-based modeling approach. Comput Struct Biotechnol J [Internet]. 2021; 19:4110–22. Available from: https://doi.org/10.1016/j.csbj.2021.07.005 PMID: 34527185

32. Price K V. Differential evolution. In: Handbook of optimization. Springer; 2013. p. 187–214.

33. Chen E, Liu G, Zhou X, Zhang W, Wang C, Hu D, et al. Concentration-dependent, dual roles of IL-10 in the osteogenesis of human BMSCs via P38/MAPK and NF-kB signaling pathways. FASEB J. 2018; 32(9):4917–29.

34. Sarugaser R, Lickorish D, Baksh D, Hosseini MM, Davies JE. Human umbilical cord perivascular (HUCPV) cells: a source of mesenchymal progenitors. Stem Cells. 2005 Feb; 23(2):220–9. https://doi.org/10.1634/stemcells.2004-0166 PMID: 15671145

35. Spolaor S, Gribaudo M, Iacono M, Kadavy T, Oplatková ZK, Mauri G, et al. Towards human cell simulation. In: Lecture Notes in Computer Science (including subseries Lecture Notes in Artificial Intelligence and Lecture Notes in Bioinformatics). Springer Verlag; 2019. p. 221–49.

36. Esteva A, Robicquet A, Ramsundar B, Kuleshov V, DePristo M, Chou K, et al. A guide to deep learning in healthcare. Vol. 25, Nature Medicine. Nature Publishing Group; 2019. p. 24–9.

37. Geris L, Gerisch A, Vander Sloten J, Weiner R, Van Oosterwyck H. Angiogenesis in bone fracture healing: A bioregulatory model. J Theor Biol. 2008; 251(1):137–58. https://doi.org/10.1016/j.jtbi.2007.11.008 PMID: 18155732

38. Zhao C, Mirando AC, Sové RJ, Medeiros TX, Annex BH, Popel AS. A mechanistic integrative computational model of macrophage polarization: Implications in human pathophysiology. PLoS Comput Biol. 2019; 15(11):1–28. https://doi.org/10.1371/journal.pcbi.1007468 PMID: 31738746

39. Kuhn C, Checa S. Computational modeling to quantify the contributions of VEGFR1, VEGFR2, and lateral inhibition in sprouting angiogenesis. Front Physiol. 2019; 10(MAR):1–14.

40. Bahney CS, Zondervan RL, Allison P, Theologis A, Ashley JW, Ahn J, et al. Cellular biology of fracture healing. J Orthop Res. 2019; 37(1):35–50. https://doi.org/10.1002/jor.24170 PMID: 30370699

41. Nourisa J. janursa/MSC_OB_Mg_ICs: [Internet]. Zenodo; 2022.

42. Wu L, Feyerabend F, Schilling AF, Willumeit-Romer R, Luthringer BJ. Effects of extracellular magnesium extract on the proliferation and differentiation of human osteoblasts and osteoclasts in coculture. Acta Biomater. 2015; 27(294–304). https://doi.org/10.1016/j.actbio.2015.08.042 PMID: 26318802

43. Yoshizawa S, Brown A, Barchowsky A, Sfeir C. Magnesium ion stimulation of bone marrow stromal cells enhances osteogenic activity, simulating the effect of magnesium alloy degradation. Acta Biomater. 2014; 10(6):2834–42. https://doi.org/10.1016/j.actbio.2014.02.002 PMID: 24512978

44. Cecchinato F, Agha NA, Martinez-Sanchez AH, Luthringer BJC, Feyerabend F, Jimbo R, et al. Influence of magnesium alloy degradation on undifferentiated human cells. PLoS One. 2015; 10(11):1–18. https://doi.org/10.1371/journal.pone.0142117 PMID: 26600388

45. Leem Yea-Hyun and Lee Kang-Sik and Kim Jung-Hwa and Seok Hyun-Kwang and Chang Jae-Suk and Lee D-H. Magnesium ions facilitate integrin alpha 2-and alpha 3-mediated proliferation and enhance alkaline phosphatase expression and activity in hBMSCs. J Tissue Eng Regen Med. 2016; 10:527–36.

46. Maradze D, Musson D, Zheng Y, Cornish J, Lewis M, Liu Y. High Magnesium Corrosion Rate has an Effect on Osteoclast and Mesenchymal Stem Cell Role during Bone Remodelling. Sci Rep [Internet]. 2018; 8(1):1–15. Available from: https://doi.org/10.1038/s41598-018-28476-w PMID: 29968794

47. Zhang X, Zu H, Zhao D, Yang K, Tian S, Yu X, et al. Ion channel functional protein kinase TRPM7 regulates Mg ions to promote the osteoinduction of human osteoblast via PI3K pathway: In vitro simulation of the bone-repairing effect of Mg-based alloy implant. Acta Biomater [Internet]. 2017; 63(6):369–82. Available from: https://doi.org/10.1016/j.actbio.2017.08.051 PMID: 28882757

48. Burmester A, Willumeit-Römer R, Feyerabend F. Behavior of bone cells in contact with magnesium implant material. J Biomed Mater Res—Part B Appl Biomater. 2015; 105(1):165–79. https://doi.org/10.1002/jbm.b.33542 PMID: 26448207

49. Wang J, Witte F, Xi T, Zheng Y, Yang K, Yang Y, et al. Recommendation for modifying current cytotoxicity testing standards for biodegradable magnesium-based materials. Acta Biomater. 2015; 21:237–49. https://doi.org/10.1016/j.actbio.2015.04.011 PMID: 25890098

50. Saldaña L, Bensiamar F, Vallés G, Mancebo FJ, García-Rey E, Vilaboa N. Immunoregulatory potential of mesenchymal stem cells following activation by macrophage-derived soluble factors. Stem Cell Res Ther. 2019; 10(1):1–15.

51. Karnes JM, Daffner SD, Watkins CM. Multiple roles of tumor necrosis factor-alpha in fracture healing. Bone. 2015; 78:87–93. https://doi.org/10.1016/j.bone.2015.05.001 PMID: 25959413

52. Glass GE, Chan JK, Freidin A, Feldmann M, Horwood NJ, Nanchahal J. TNF-$α$ promotes fracture repair by augmenting the recruitment and differentiation of muscle-derived stromal cells. Proc Natl Acad Sci. 2011; 108(4):1585–90.

53. Koch AE, Polverini PJ, Kunkel SL, Harlow LA, DiPietro LA, Elner VM, et al. Interleukin-8 as a macrophage-derived mediator of angiogenesis. Science (80-). 1992; 258(5089):1798–801. https://doi.org/10.1126/science.1281554 PMID: 1281554

54. Yang A, Lu Y, Xing J, Li Z, Yin X, Dou C, et al. IL-8 enhances therapeutic effects of BMSCs on bone regeneration via CXCR2-mediated PI3k/Akt signaling pathway. Cell Physiol Biochem. 2018; 48(1):361–70. https://doi.org/10.1159/000491742 PMID: 30016780

55. Yoon DS, Lee K-M, Kim S-H, Kim SH, Jung Y, Kim SH, et al. Synergistic action of IL-8 and bone marrow concentrate on cartilage regeneration through upregulation of chondrogenic transcription factors. Tissue Eng Part A. 2016; 22(3–4):363–74. https://doi.org/10.1089/ten.tea.2015.0425 PMID: 26871861

56. Mondagas SC, Jilka RL. Bone marrow cytokines, and bone remodeling. N Engl J Med. 1995; 332:305–11.

57. Hameed IA. Using Gaussian membership functions for improving the reliability and robustness of students' evaluation systems. Expert Syst Appl [Internet]. 2011; 38(6):7135–42. Available from: https://doi.org/10.1016/j.eswa.2010.12.048

58. Sadollah A. Introductory Chapter: Which Membership Function is Appropriate in Fuzzy System? In: Sadollah A, editor. Fuzzy Logic Based in Optimization Methods and Control Systems and Its Applications [Internet]. Rijeka: IntechOpen; 2018.

59. Iancu I. A Mamdani type fuzzy logic controller. Fuzzy Log Control Concepts, Theor Appl. 2012;325–50.

60. Romani AM. Cellular magnesium homeostasis. Arch Biochem Biophys [Internet]. 2011; 512(1):1–23. Available from: https://www.ncbi.nlm.nih.gov/pmc/articles/PMC3624763/pdf/nihms412728.pdf. PMID: 21640700

61. Mezura-Montes E, Velázquez-Reyes J, Coello Coello CA. A comparative study of differential evolution variants for global optimization. In: Proceedings of the 8th annual conference on Genetic and evolutionary computation. 2006. p. 485–92.

Part IV. Summary and outlook

The contribution of this dissertation to the field of computational biomodeling are twofold. First, the methodological advancement. We developed CppyABM, an open-source general-purpose ABM library, to improve on the state-of-the-art techniques in multiple aspects. CppyABM combines merits of two languages of C++ and Python in one platform. The computational efficiency of C++ offers scalability, while Python provides rapid prototyping with rich data analysis and visualization tools. In addition, CppyABM provides many built-in functions to ease the model development and reduce the possible implementation mistakes and memory mismanagement (see Section III.1).

In addition, the content of this dissertation contributes to the methodological advancement in the simulation of cellular responses to signaling factors. Firstly, the proposed parameter analysis can shed light on the fundamental differences amongst experiments and guide the integration of heterogeneous data from different sources. In Sections III.2III.3, we have showed the importance of this matter in the biological characterization of Mg degradation products, where MSCs cultured in different experiments showed diverse sensitivity to Mg^{2+} ions. In addition, a novel iteration-based calibration approach based on approximate Bayesian calculation (ABC) was proposed in III.2. We showed that this iterative approach has superior performance compared to the single-round ABC widely used in the literature.

Furthermore, the content of this dissertation provides several advancements in the biological characterization of Mg-based materials. Firstly, we compiled the sparse knowledge regarding the regulation of multiple processes involved in osteogenesis such as MSC proliferation, osteoblastic differentiation, and mortality from over 50 different empirical reports in one platform (see III.2 and III.3). This contains not only the regulatory role of Mg^{2+} ions, but also several other regulatory factors which are associated with the Mg degradation products such as pH change, important growth factors and cytokines. Using this information and the implemented calibration process, the model could successfully reproduce empirical data of the eight sets of in vitro cell cultures, in terms of cell population, cell mortality, and osteoblastic differentiation (see III.2 and III.3). In addition, the simulation results, in agreement with the empirical data, have suggested optimal concentration of Mg^{2+} ions for osteogenesis. We showed that Mg^{2+} ions within the concentration of 3-6 mM results in the highest MSC population, and within 6-8 mM is the most effective in stimulating osteoblastic differentiation process (see III.2 and III.3).

Future steps in characterizing bone tissue response to Mg degradation products include the following. Firstly, the interaction of MSC and macrophage, as a crucial process in bone regeneration, is double-sided; macrophage influences MSC and vice versa. Mg products influence both cell types and the quality of their interactions (see section II.2.4). So far, we have solely studied the bio-regulatory effect of macrophage on MSC and the role of Mg^{2+} ions in this process. Next step should be the extension of this model by including the regulatory effects of

MSC on macrophage, as an attempt to present a more realistic biological model. Second, we have so far solely studied the biological role of Mg^{2+} ions, while Mg-based bone implant releases several other materials into the micro surroundings such as alloy materials, e.g. Gladinium and silver. A more comprehensive study of Mg alloys is essential for the successful use of Mg-based implants. Thirdly, we have so far studied the phenotypic cellular response to Mg^{2+} ions such as proliferation and differentiation. However, phenotypic response can be heterogeneous across different cell culture experiments. This implies the importance of understanding the intracellular pathways associated with Mg^{2+} ions to shed light on the underlying regulatory mechanism. To this end, further studies by a focus on intracellular processes such as different OMICs analyses is crucial in the study of Mg-based implants. In these approaches, high throughput measurements, including thousands of genes and proteins, can be analyzed using different techniques such as target gene detection, enrichment analysis, and gene regulatory network analysis.